ABSTRACT

Title of Thesis: CHARACTERIZATION AND COMPARISON OF STRESS HISTORY IN VARIOUS SIZED TWIN-SCREW EXTRUDERS USING RESIDENCE-STRESS DISTRIBUTIONS

William Lawrence Pappas, Master of Science, 2011

Directed By: Associate Professor David I. Bigio,
Department of Mechanical Engineering

Extrusion is used in production across a broad spectrum of industries, including piping and tubing, food, plastics and pharmaceutical. Because some applications involve stress-sensitive ingredients, it is important to be able to predict the amount of stress exerted on the material. Unfortunately, characterization of the stress magnitudes within a twin-screw extruder is extremely difficult due to its complexity.

This thesis presents an approach to characterizing the stress history through the use of residence-stress distributions. Stress beads are used to determine the percentage of polymer that is exposed to a particular magnitude of stress at each location along the residence distribution. A comparison of various mixing geometries on three different sized extruders is performed for a wide range of operating conditions. An extensive DOE analysis of the results yields characteristic equations that are capable of predicting the amount of stress bead breakup for any given operating parameters.

CHARACTERIZATION AND COMPARISON OF STRESS HISTORY IN VARIOUS SIZED TWIN-SCREW EXTRUDERS USING RESIDENCE-STRESS DISTRIBUTIONS

By

William Lawrence Pappas

Thesis submitted to the Faculty of the Graduate School of the
University of Maryland, College Park, in partial fulfillment
of the requirements for the degree of
Master of Science
2011

Advisory Committee:
Associate Professor David I. Bigio, Chair/Advisor
Professor Hugh A. Bruck
Senior Lecturer Chandrasekhar Thamire

Acknowledgements

I would first like to express my sincerest gratitude to my advisor, Dr. Bigio, for his constant support during my time as his student. His guidance and motivation not only helped me with carrying out my research, but also helped me grow and develop as a person. His ideals on completion and intentionality have provided a new mentality and approach which has made my research and other experiences much more fulfilling. I would also like to thank Dr. Bruck and Dr. Thamire for serving on my thesis committee.

This research could not have been done without the help of my undergraduate research assistants, Graeme, Roba, Beserat and Nate. Their devotion to running the experiments and willingness to help out whenever called upon is truly appreciated. I owe a special thank you to my right-hand man, Harry, for his commitment to helping me complete this research. I cannot count the number of late nights he spent in the lab with me running an experiment or helping me with a calculation. For that, I am truly grateful for his dedication.

I would also like to thank Mark Wetzel and Paul Andersen from DuPont and Coperion for allowing me to perform my experiments on their twin-screw extruders. Their experience and insights were extremely helpful in obtaining a full understanding of the mixing mechanisms during extrusion. Additionally, I owe my gratitude to Jim Lochary and Viorel Amariei from Adell Plastics. They were always willing to clean the extruder screws at any time and constantly offered suggestions to make my processes more efficient.

I owe special thanks to thank my good friends, Mike, for helping me with the MATLAB modeling program, and Tom, for keeping me company all those late nights in the lab while we were both writing our theses.

Last but not least, I would like to my family for their never-ending support throughout my work at the University of Maryland. This work is dedicated to you, Mom and Dad.

Table of Contents

List of Tables

List of Figures

Chapter 1 Introduction

1.1 Extrusion and Polymer Processing

Extrusion is any process in which a material is forced through a shaped orifice, such as a die [1]. Extrusion processes come in a variety of types and are carried out on various types of machinery. Extrusion can be classified into two types of processes: discontinuous and continuous. Discontinuous processes typically use ram or reciprocating motions. For continuous processes, there are single-screw extruders, multi-screw extruders, such as the twin-screw extruder and the tri-screw extruder, and continuous disc and drum extruders [2]. This process is continuous in nature as long as the feed material supply is maintained and is capable of very large throughputs. Some common products created via extrusion include certain metals, polymers, ceramics, explosives, food and pharmaceutical products. For the context of this study, polymer extrusion will be the main focus.

The importance of polymer processing comes from the fact that the processing technology plays a dominant role in the cost and properties of the polymer product [3]. In polymer processing, the main goal is taking raw polymeric materials and through chemical reactions, inclusion of additives, and shaping to produce a final, finished product. A typical polymer process involves feeding solid polymer pellets or powder into an extruder where the material is heated to its melting point, any desired fillers or pigments are added to the polymer melt, and the material is then forced out of a shaped die to provide the extrudate with its shape. The melted, extruded polymer is then allowed to cool to form its final state. Through extrusion processes, such as single or twin-screw extrusion, raw polymers can be transformed into countless numbers of final products that have orders of magnitude more value than the original states.

1.2 Types of Screw Extruders

As mentioned in the previous section, there are different types of extrusion machinery utilized in industry. The most common type of extruder is the screw extruder. Screw extruders have played an important role in the polymer industries and today could be the most important unit operation in polymer processing [3], [4]. The two most popular types of screw extruders are the single-screw extruder and the twin-screw extruder. The following sections go into more detail about these two extruders.

1.2.1 Single-Screw Extruders

The single-screw extruder is the most important type of extruder used in the polymer industry. Its advantages are its relatively low cost, straightforward design, ruggedness and reliability. Single-screw extruders are very simple machines capable of producing thousands of pounds of pressure, and as the name suggests, only use one screw for extrusion [5], [6]. This type of extruder comes in a variety of diameters, ranging from 6 mm to over 250 mm. There are numerous screw configurations that have been designed for specific applications and processes, but each screw design typically consists of three main sections: the feeding or conveying section, the melting or compression section, and the melt pumping (metering) section, as seen in Figure 1.1.

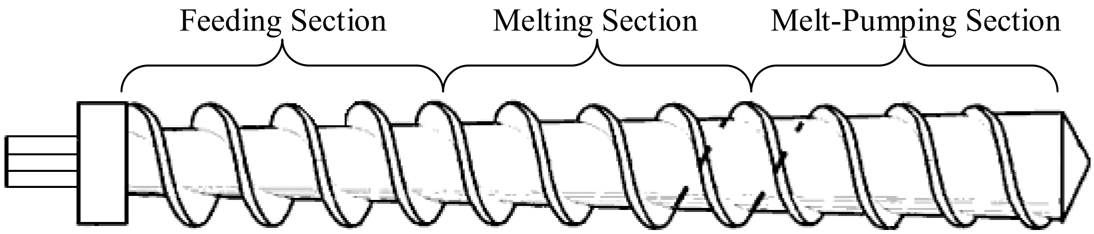

Figure 1.1 - Single-screw extruder screw [3]

The conveying section conveys the material fed into the extruder at the feed throat to the melting section. To maximize conveying capacity, the screw channels for this section are deeper to push more material forward. Although melting of the material begins before the melting section, the melting section is designed with a compression region which has a shallower channel depth. This increases the size of the melted polymer pool and increases the velocity of the melt to the next section of the screw. The melt pumping section pumps the polymer melt out of the extruder and through the die.

Due to the simple design of the single-screw extruder, complex products that may require high degrees of mixing cannot be easily produced. However, single-screw extrusion is ideal for relatively simple products that only need to be shaped and require minimal mixing. Such products include pipes, medical tubing, different types of structural foam, electrical wiring and cables, soaps, and food products, such as pasta.

Single-screw extruders were the first type of extruders to be used in manufacturing. The success and downfalls of these machines led to the design of more complex extruders.

1.2.2 Twin-Screw Extruders

Some downfalls of the single screw extruder are that it is not self cleaning and that the conveying mechanism is dependent on the properties of the extruded material. In an attempt to overcome these issues, the multi-screw extruder was created. A twin-screw extruder (TSE) consists of two single extruder screws. The two main classes of twin-screw extruders are categorized by the relative rotation of the two screws: counter-rotating and co-rotating.

Counter-rotating twin-screw extruders consist of two screws which rotate in opposite directions. This classification of extruder can be further categorized by either being intermeshing or non-intermeshing, as seen in Figure 1.2.

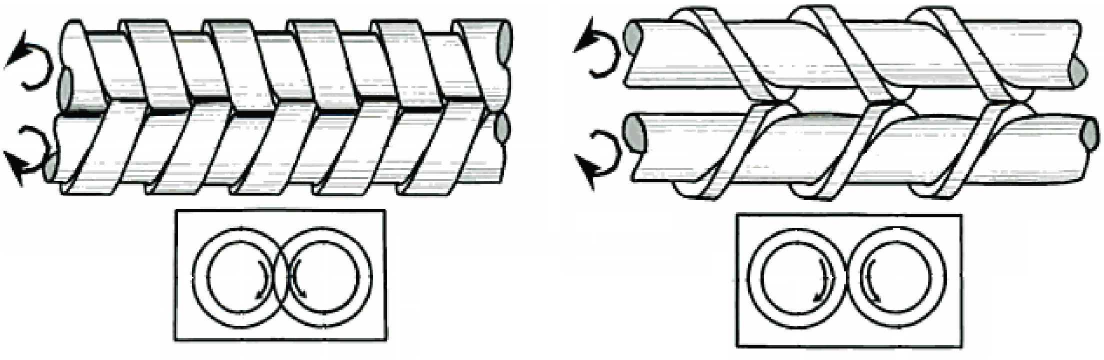

(a) (b)

Figure 1.2 - Counter-rotating twin-screw extruders: (a) fully-intermeshing; (b) non-intermeshing [3]

Intermeshing counter-rotating twin-screw extruders (Figure 1.2 (a)) are designed to have the channel edges of one screw in between the channel edges of the opposing screw. This type of extruder has the best positive conveying capability, but tends to produce very high pressure, which puts a restriction on the screw speed. The other type of counter-rotating twin-screw extruder is the non-intermeshing extruder (Figure 1.2(b)). Non-intermeshing counter-rotating twin screw extruders are designed to have the channels edges of one screw aligned with the channel edges of the other screw, or they can be staggered. They are capable of high degrees of mixing and conveying capacity due to the profile of the polymer melt. Both flows from each screw are being driven into the gap between the screws, causing the melt to either flow into the other screw's melt, or continue its path on the same screw. The calendaring flow between the screws produces high degrees of mixing. However, due to the fact that the channel edges are lined up, this type of extruder is not capable of self-cleaning [3], [7].

The second class of twin-screw extruders is the co-rotating, fully-intermeshing twin-screw extruder, as seen in Figure 1.3.

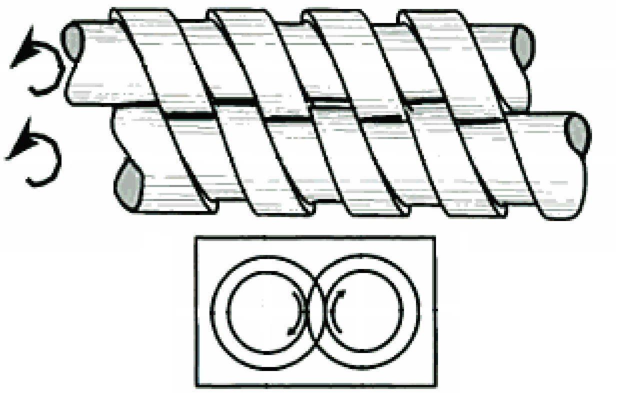

Figure 1.3 – Fully-intermeshing co-rotating twin screw extruder [3]

As the name implies, both screws rotate in the same direction. This induces a high degree of mixing due to the fact that the polymer melt from one screw may flow to the next screw, or continue its motion on the same screw. This promotes constant interfacial interaction, which is important to achieving good mixing. Additionally, because the screws are also fully-intermeshing, the screws are self-cleaning [3], [7], [8]. This type of extruder is the most common type of twin-screw extruder today.

Popularity of twin-screw extruders has steadily grown over the past two decades because of its capability of achieving a high degree of mixing. More complex products that require addition and good distribution of multiple components can now be made in extremely large quantities. These products include snack foods, military propellants, piping, tubing, pharmaceutical products, and more advanced polymer composites, such as micro- and nano-composites.

1.3 Screw Elements

Extruder screw elements come in a variety of types and sizes for each type of extruder. For the purpose of this study, only elements used in the fully-intermeshing co-rotating twin-screw extruders will be discussed, mainly conveying and mixing elements.

It is important to first distinguish between the different types of screw profiles. Screw profiles are classified as having one, two, or three flights (or single, bi-, and tri-lobes, respectively). The three profiles can be seen in Figure 1.4.

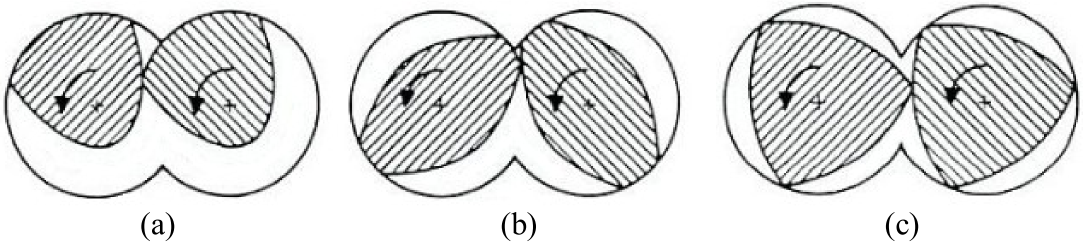
(a) (b) (c)

Figure 1.4 - Cross-sections of co-rotating screws: (a) single flight; (b) two-flight; (c) three-flight [9]

The single-flight element (Figure 1.4(a)) is ideal for operating where maximum conveying capacity of solid materials is required. Due to the large twist and large crests, single-flight elements increases feed intake, degree of conveying, and reduce the effective length; however, does not provide good mixing or shear stress due to the large channels [9]. The two-flight screws, as seen in Figure 1.4(b), have deep channels that allow high volume conveying capacity, but low shear stress (higher shear stress than single-lobe though). Bi-lobed elements are good candidates for shear-sensitive materials and when added ingredients do not require high shear [7]. The tri-lobe screw elements (Figure 1.4(c)) have shallower channels than the two-flight elements, producing low volume conveying capacity. However, three-flight elements induce higher levels of shear stress than the single or two-lobed at identical operating conditions, and thus have better mixing capability.

1.3.1 Conveying Elements

Right-handed or forward conveying elements are used to convey polymer and other ingredients from the feed throat of the extruder to the die. Conveying elements are classified by the pitch of the flights. The pitch of these elements influences the degree of fill within the element. A wide or large screw pitch is used to reduce built up pressure under a vent port, as well as increase conveying capacity. A wide-pitched element also decreases the degree of fill. To build up pressure and increase the degree of fill, a narrow or small screw pitch is used.

Left-handed or reverse conveying elements are used to generate backpressure. These elements consist of channels that are in the opposite direction, causing the polymer melt to flow backwards. These elements are typically used where a melt seal is required and are used to increase the degree of fill to 100%. Reverse elements are also often used behind a mixing element, such as a kneading block, to enhance mixing [3], [9], [10].

1.3.2 Mixing Elements

A mixing element is used to achieve different levels of mixing. In co-rotating twin-screw extruders, a kneading block is typically used to accomplish this. Kneading blocks are elements that consist of staggered, flat paddles that impart shear stress on the polymer melt. Most kneading elements contain five of these paddles. The stagger angle of the paddles influences the conveying capability of these elements. Kneading blocks are capable of achieving two types of mixing: distributive and dispersive mixing (discussed further in Section 1.4.1), depending on the size of the kneading paddles.

Kneading blocks come in a variety of sizes and staggers. The kneading paddles come in three relative sizes: narrow, medium, and wide. Narrow kneading blocks, especially in a tri-lobe profile, provides good mixing and excellent conveying capabilities, but induce very low shear. Medium-sized paddles provide less mixing and conveying capabilities than the narrow kneading blocks, but induce more shear stress to the polymer. Wide kneading blocks induce very high shear stresses because of the large paddles. This magnifies the elongational stress and increases the percentage of the polymer melt that experiences stagnation. However, due to the wider paddles, the conveying and mixing capabilities are significantly reduced.

Kneading elements also come in three different kinds of staggers: forward, reverse, and neutral. Forward-conveying kneading blocks convey material forward from the feed throat to the die, but also allow back-mixing through the gaps in between paddles. Reverse-conveying kneading blocks increase backpressure, similar to reverse-conveying elements, but do not have as high of pressure because some material pushes forward through the gaps in the paddles. Neutral kneading blocks have neither forward nor reverse stagger. These elements rely on the pressure and forward motion of preceding element to convey the polymer melt through the element [3], [9], [11].

Different combinations of the kneading blocks can be used to produce different types of mixing. For more intense mixing, wide kneading blocks and neutral kneading blocks are used in conjunction to induce high shear stress to the material. Narrow kneading blocks produce a less intense mixing section and are typically used for shear-sensitive materials. Almost any desired degree of mixing can be achieved as long as the right combination of kneading elements and conveying elements are used.

1.4 Mixing

Mixing is defined as the intermingling by mechanical action of two or more differentiated components within a continuum [12]. It is a process that increases compositional uniformity throughout a mixture. The goal of mixing is to reduce the specific concentration of these components by blending them together, yielding a minimal combined concentration. The minimum gradient of concentration of the components is achieved when the mixture can be sampled at any location and has the same composition from location to location [13]. Mixing is achieved by inducing motion of the components and having their interfaces interact with one another.

Mixing machinery is categorized into two categories: batch mixers and continuous mixers.

Batch mixers are the more versatile type of mixers. They allow for the most flexibility of mixtures produced and traceability of mixtures. The length of time of mixing can easily be monitored and controlled, as well. However, they are not capable of continuous operation and become expensive and unpractical when large amounts of materials need to be mixed.

Continuous mixing machinery, such as an extruder, is advantageous as it allows for continuous operation and high throughput of product as long as the feed supply is maintained. Additionally, it has reduced operation and labor costs due to automation. Some disadvantages of continuous mixers are the reduced flexibility in changes made to products, such as the inclusion of new additives or a different polymer base, as this may call for new operating and processing conditions. The quality of mixing is also sacrificed in extruders. There is a correlation with time and how well individual components are mixed together. An extruder imparts an axial velocity on the ingredients that are fed into it, which allows material to exit the extruder; however, this also reduces the amount of time the ingredients have to mix. This magnifies the importance of having the appropriate screw geometry that is designed for the specific desired operation (i.e. the type of mixing to be achieved).

1.4.1 Types of Mixing

Mixing in an extruder can be distinguished by two types: distributive and dispersive, which will be described in the following sections.

1.4.1.1 Distributive Mixing

Distributive, or extensive, mixing induces low magnitudes of shear to the polymer melt and any components. This type of mixing produces a uniform distribution of the components within the extruded material. Mixing of this nature can be identified by the history of deformation induced on the extrusion material (strain) [12]. Due to the low shear, distributive mixing is only capable of breaking and recombining the polymer melt, not the components. This produces the uniform distribution. The extruder elements that produce distributive mixing are narrow kneading blocks. Narrow kneading blocks allow the polymer melt to flow around the kneading paddles, but not necessarily between the barrel and the paddles. Due to the narrow width of the paddles, elongational stress, caused by the squeezing of material between two opposing paddles, magnitudes are not high enough to induce component breakage.

Distributive mixing is useful in applications where low shear stress is desired. For instance, adding fibers with very high aspect ratios in which breakage of the filler is not desirable. Mixing of very shear-sensitive materials is also well suited for distributive mixing [14].

1.4.1.2 Dispersive Mixing

Dispersive, or intensive, mixing induces high magnitudes of shear stress to the extruded material and additives. While distributive mixing is produced by strain, dispersive mixing is produced by the induced stress on the material. Dispersive mixing is the reduction in size or scale of a component (agglomerates or droplets) within a material [15]. Due to the high shear, agglomerates are broken down and dispersed within the polymer melt. To produce dispersive mixing, wide kneading blocks are used within an extruder screw geometry. Wide kneading blocks allow the material to flow over the tips of the paddles, which squeezes the flow between the paddle and the barrel. Additionally, due to the wider width of the kneading block paddles, the magnitude of stress caused by the squeezing of opposing paddles (elongational stress) is large enough to break down components into smaller sizes [14].

Applications of dispersive mixing include the use of dispersing pigments or color concentrates, as well as liquid additives, into a polymer melt, as seen in Figure 1.5.

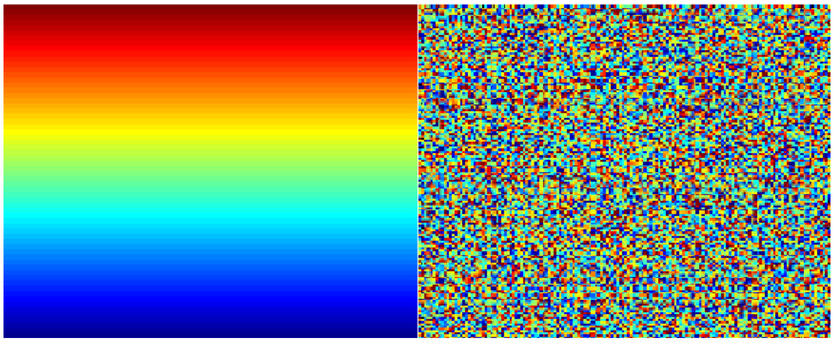

(a) (b)

Figure 1.5 – (a) Poorly dispersed color pigments and (b) well-dispersed color pigments

When adding solid particles or other ingredients to a rubber matrix, the magnitude of induced stress must be great enough to overcome the high viscosity of the matrix, making dispersive mixing through the use of wide kneading blocks an excellent candidate [16].

1.5 Residence-Time Distribution

The paths taken by fluid elements in an extruder are not always the same and may require different amounts of time to move through it. The distribution of these different lengths of time makes up what is called a residence-time distribution (RTD) [17]. To measure an RTD, a nonreactive, passive tracer is injected into the system and the concentration of the tracer is measured through the use of an optical probe. Residence-time distributions have been used to monitor numerous features of extruders, such as consistency, polymer degradation, and the degree of mixing [18]. The RTD function can be expressed by:

$$e(t) = \frac{c(t)}{\int_0^\infty |c(t)|dt} \tag{1.1}$$

Where e(t) is the normalized RTD function and c(t) is the probe response (i.e. tracer concentration). RTDs are very useful in extrusion processes, such as reactive mixing, where the amount of time materials spend in the extruder is an important variable to the quality of the product. In cases where time is unimportant to the extrusion process, a residence-time distribution may not be as useful or insightful to the process. The shape of the RTD curve is dependent on the operating conditions of the extruder. An increase in screw speed or flow rate (or both) decreases the amount of time a tracer is in an extruder, which yields a sharpening of the RTD curve (i.e. taller and narrower). This sharpening of the curve indicates that the concentration came out nearly at the same time, as it did not have time to distribute and disperse within the flow. A wider and shallower curve indicates that the tracer dispersed within the melt and its concentration was well spread out through the extruder. The shapes of the

RTD curves for this study will be of importance when combined with other distributions.

1.6 Motivation for Research

Mixing is an important step in the processing of polymers. It impacts not only mechanical properties, but also the physical and chemical properties of the material [19]. In the case of reinforcing a polymer through the addition of fillers, (i.e. carbon or glass fibers, particles, clay, etc.) achieving a good degree of mixing will enhance the properties of the composite [20]. Additionally, a well-mixed composite will have reduced anisotropy due to the uniform distribution of the reinforcing filler and reduced agglomerates. Mixing can also affect the appearance of the material. With the addition of color concentrates or additives, the amount of induced mixing can produce polymer composites with completely different color schemes, as seen previously in Figure 1.5. In reactive mixing, the appropriate degree of mixing is crucial to producing high quality materials. In energetic and some chemical reactions, if the mixing is insufficient or too great, the product may be unable to perform its appointed task. Additionally, the mixture could become highly unstable, potentially causing damage to the equipment and any operators.

Achieving efficient and an appropriate degree of mixing in extrusion are of critical importance when trying to produce a consistent, high quality product [21]. As discussed previously, dispersive mixing is related to the imparted stress on the polymer and additives. The ability to characterize the stress induced by different screw configurations is necessary to be able to predict the degree of mixing that will be achieved by that particle design. This is extremely important in applications where stress has an impact on the quality of the product. For instance, in pharmaceutical applications, where the additives are shear-sensitive, it is important to identify the amount of stress the screw design is imparting. If the proper screw configuration is not used, ingredient degradation may occur, yielding bad product. Additionally, with the use of fiber-reinforcements in polymer systems, distribution of the fibers is all that is required. Too much stress may cause the fibers to break, making the composite incapable of performing its intended tasks.

The ability of characterizing the stress induced by different screw configurations will have a substantial impact on the extrusion industry. With the correct screw geometry, the quality of product will increase and the amount of scrapped product will be reduced, yielding higher profits for extrusion industries.

1.7 Goals of Thesis

The goals of this thesis are to establish a methodology to measure the residence-stress distribution and characterize the stress history in a fully-intermeshing co-rotating twin-screw extruder. Using stress-sensitive sensor beads, the magnitudes of stress induced by various mixing geometries inside of an extruder can be determined. Using generated residence-time distributions and residence-stress distributions, further insights regarding the shear-stress mechanisms and flow paths inside the mixing sections were obtained. This will be the first time stress data as a function of the residence distribution to be recorded. Finally, through the use of special statistical analysis, a single equation will be generated that correlates stress induced in a mixing section to operating conditions and other important variables.

1.8 Structure of Thesis

In the following chapters, the methodology and results from this study will be presented. Chapter 2 presents the work that has been performed in the past by other researchers in attempts to characterize and predict mixing within an extruder. Chapter 3 contains all theoretical calculations used for analysis. Chapter 4 discusses the experimental setup, as well as all materials, tools, screw geometries, and other twin-screw extruders used in this study. Chapter 5 presents the results from this work, including the percentage of sensor bead breakup, residence distributions (time, stress, volume, and revolution), and finally the correlation equations that relate stress to the operating conditions. Chapter 6 summarizes the results obtained from this study and future work for this approach.

Chapter 2 Literature Review

There has been extensive work performed in the past to try to determine the mixing performance inside an extruder. Primarily, studies have focused on factors that affect distributive and dispersive mixing within single and multi-screw extruders. These factors include throughputs, screw speeds, different combinations of screw elements, the addition of ingredients, and other methodologies to amplify mixing performance. Due to the widespread work that has been done across the field, this literature review will focus on experiments and studies performed on only co-rotating twin-screw extruders.

The methodologies of determining mixing capabilities in twin-screw extruders can be separated into three main categories:

- Stress distributions
- 3-D simulations of mixing
- Experimentally determined residence distributions

The following sections discuss each of these methodologies with the advances and limitations that each have made in determining mixing.

2.1 Stress Distributions

In this category of work, through the use of stress sensitive materials or beads, a stress distribution within an extruder was generated. There were a limited number of direct experiments found in the literature. Curry et al [22], [23] used hollow glass spheres to determine the stress in a twin-screw extruder. Two experiments were carried out on a ZSK-40 twin-screw extruder that was modified as a high stress compounder. Two different screw geometries were tested. The first screw design (#1) utilized numerous kneading blocks and the second screw design (#2) consisted of different combinations of forward and reverse conveying elements with various pitches. The screw geometry with the kneading blocks was predicted to generate higher stresses due to the presence of numerous kneading blocks. The selected extrusion material was polybutene in liquid form to eliminate any bead breakage during melting and other extrusion mechanisms needed to melt solid pellets.

In the first experiment, only one type of bead was used. The glass spheres had a rated failure pressure of 4.5 kpsi for 10% rupture. However, these beads were found to fail in the shear mode at 32.35 kpsi ± 9.14 kpsi at a 67% confidence interval. The beads were fed separately from the polybutene at a concentration of 12.8 volume %. The throughputs and screw speeds were varied for both screw configurations. The extruded polybutene-glass sphere composites were extruded and collected. To determine the percentages of bead breakage, ASTM D792 method A-1 was used to measure the density of the samples, as well as burning the polymer away from the glass beads to count the number of broken beads. The results from that experiment can be seen in Table 2.1.

Table 2.1 - Sphere rupture in twin-screw extruder

Condition #	Test Screw	Rate (lb/hr)	RPM	% Broken Bubbles
1	1	49.2	75	2
2	1	44.3	347	2
3	1	90.3	200	5
4	2	46.7	152	9
5	2	49.5	298	15
6	2	21.1	154	14

From the first experiment, Curry reported that a higher percentage of glass beads broke using the purely conveying element geometry than the screw design with the kneading blocks.

The second experiment that was performed studied the effects of viscosity and bead strength. Two grades of the polybutene were studied, the first grade was H300 and the second was H-1500 with viscosities of 709 and 87 Pa-s 10 s^{-1} 25^{o}C, respectively. Three glass beads with different critical stress levels were tested and are presented in Table 2.2.

Table 2.2 - Critical non-compressive failure stresses of glass spheres

Sphere Type	Mean (kPa)	St. Dev (kPa) ±
A16	51	10.5
A20	138	11.7
D32	259	39.5

The purpose of this experiment was to investigate the effects of screw configuration and screw speed. The same two screw configurations from the previous experiment were used. The flow rate was kept at a constant 50 lb/hr and the screw speed was run at 80, 150, and 350 rpm. The beads were fed at a concentration of 10 volume% within both grades of polybutene. The results from this experiment can be seen in Figure 2.1

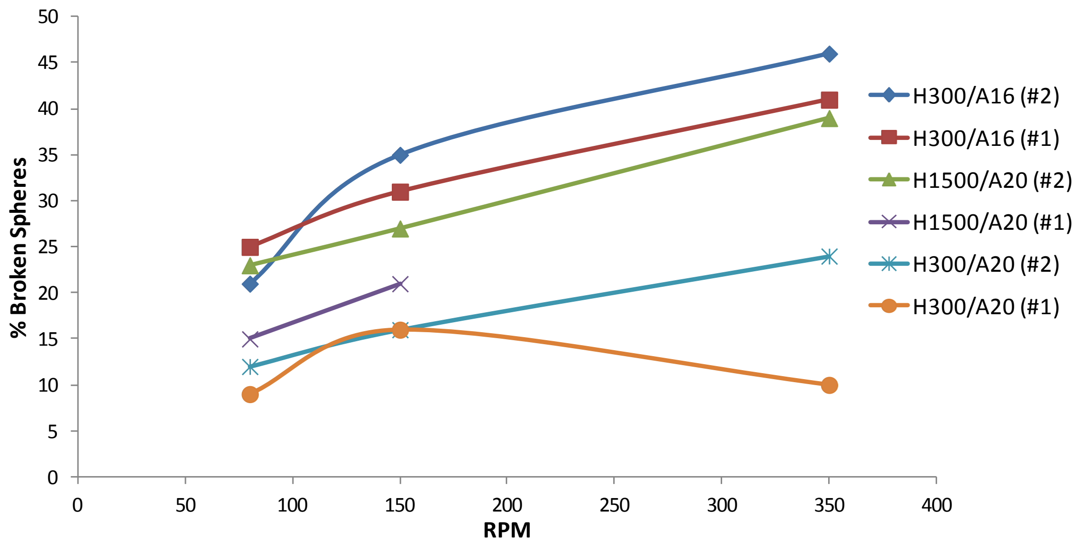

Figure 2.1 - Glass sphere breakage as a function of screw speed

From these results, it was evident that as screw speed increase, the percent breakup of glass beads also increased, with the exception of one data point. As seen in the first experiment, the screw design that utilized the forward and reverse conveying elements (#2) produced the higher percentage of glass bead breakup. This was the case for each strength of glass bead used and for each grade of material. The figure above also shows that the more viscous grade of polybutene produced higher percentages of glass bead breakup.

Due to the numerous and time consuming steps required to obtain results, there were limitations to this approach. One limitation is that the results were not obtained in real time. Once the polybutene-glass bead composites were extruded, the polybutene was burned off and the number of broken beads was then counted by hand. This introduces human error and also limits the number of positions that were sampled due to the time required to analyze the results. The stress distributions were therefore generated using only a few samples.

Others have also used stress distributions to quantify the stress induced on the extruded material. Manas-Zloczower et al [24] and Canedo et al [25] introduced and applied the pass distribution (i.e. number of passes) to model agglomerate breakup and screw geometries in mixers. Szydlowski et al [26] used stress distributions and applied them to numerical simulations in co-rotating, intermeshing extruders. However, these stress distributions were applied in models or simulations, not in actual experimentation.

2.2 3-D Simulations

With technological breakthroughs in computing capacity, the use of three-dimensional simulations to analyze the flow field has grown over the past decade. Numerous researchers have used 3-D simulations to predict and quantify the quality of mixing using a specified screw geometry. The majority of this type of work has been to study the mixing performance of either conveying elements or kneading blocks.

Researchers have studied the effects of single, double, and triple-flighted conveying screws on mixing. Rios et al [27] and others [28], [29] concluded that the two-lobe conveying element provided good distributive and dispersive mixing, and increasing screw speed enhanced mixing performance. To the contrary, Cheng et al [30] found that three-lobed conveying elements were ideal for distributive mixing and also found that increasing screw speed enhances the mixing performance for these elements.

Others have simulated kneading blocks and their performance in distributive and dispersive mixing. Ishikawa et al [31],[32] and numerous others [33–38] used finite element modeling and particle tracking on a two-lobed co-rotating twin screw extruder and applied it to mixing performance. Ishikawa performed pressure and temperature simulations on these elements because the results could be checked experimentally. After verifying that the simulations were in fact accurate, the simulations were then applied to characterize mixing performance. Ishikawa's study, through the use of particle markers, found that wide kneading blocks in conjunction with neutral and left-handed kneading blocks, enhanced dispersive mixing. Additionally, using narrow kneading blocks, as well as neutral and left-handed kneading blocks enhanced distributive mixing. Both Lawal and Ishikawa concluded that due to the random distributions of the particles, good mixing was achieved using bi-lobed kneading blocks in a co-rotating TSE.

Yoshinaga et al [39] and Manas-Zloczower [40] simulated the effects of tri-lobed kneading blocks on mixing performance. Yoshinaga proposed numerous mixing indices for screw elements as a method of quantifying the quality of mixing. Through this technique, it was found that the neutral kneading block was superior to the left-handed and right-handed kneading blocks in distributive mixing. Manas-Zloczower compared a 53-mm tri-lobe to a 30-mm bi-lobe twin-screw extruder. She found that the three-lobed extruder produced better dispersive mixing characteristics than the bi-lobed extruder through the use of the marker tracking.

Although 3-D simulations have become extremely powerful and accurate, there are still numerous inherent limitations. The mechanism that governs mixing in extruders is extremely complex and has yet to be fully determined. 3-D simulations are only as accurate as the code and governing equations used; if mixing mechanisms have yet to be fully understood, then there is going to be error in any mixing simulations. In addition, the assumption of fully-filled mixing sections was required to proceed with the analysis, which is not always achieved. Assumptions are often required and used for simulation methods. For example, in marker particle tracking, one assumption is that there are no interactions between the marker particles. However, in a real flow field inside an extruder, fluid particles are constantly interacting with each other. Therefore, the simulation models an unrealistic flow, further reducing the accuracy of the model.

2.3 Experimentally determined residence distributions

2.3.1 Residence-Time Distributions

The most commonly performed experiment to quantify mixing performance is through the use of the residence-time distribution. Through the use of a tracer and an optical probe, the RTD can be determined within an extruder.

Shearer and Tzoganakis [41–43] used the residence-time distribution and reactive polymer tracers to measure distributive mixing. By introducing two reactive chemical tracers (5 wt. %), and measuring the RTD in both the conveying and mixing zone, the degree of mixing could be measured. They concluded that the degree of mixing increased as the residence time increased within the conveying zone, for a given flow rate. For the same residence time, a higher flow rate significantly increased mixing. However, their results also indicated that the there was no correlation between residence time within the mixing section and degree of mixing.

Numerous other methods have been used to try to correlate residence-time distributions to imply mixing. Cheng et al [44] used the residence-time distribution and dye intensity (i.e. concentration) as a means of characterizing mixing performance within the mixing section using kneading blocks. He found that the residence time through kneading blocks was a function of percent drag flow, and that a critical drag flow existed around 30%. At this value, the fill length of the kneading blocks does not change significantly. This shows that mixing performance is enhanced by having a fully-filled system versus a partially-filled system. The more filled a kneading block system is, the higher the shear rate elongational deformation, which produce better distributive mixing. Todd [45] and Tadmor et al [46] relate residence distributions to the Peclet number as a measure of axial mixing. By decreasing the Peclet number, which can be achieved by using elements with high helix angles, the quality of axial mixing can be increased. Other experiments using the residence-time distributions are discussed in [18], [47–52].

Although the residence-time distribution within an extruder for a set of given operating conditions has been found to be an important parameters for other mechanisms, it does not correlate well with mixing. The primary reason for this is that typical residence distributions only provide an axial history of the flow within an extruder. It presents no information regarding the degree of mixing or stress history.

2.3.2 Residence-Revolution and Residence-Volume Distributions

In processes where time is a key parameter, such as reactive extrusion, the corresponding residence-time distribution is important. In some processes, however, time may not be an important variable. The number of passes through an extruder (i.e. cumulative screw revolutions) or volumes of extrudate may be more appropriate for certain applications. Through simple transformations, using screw speed (N) and flow rate (Q), residence-revolution distributions (RRD) and residence-volume distributions (RVD) can be obtained, as seen in Equations 2.1 and 2.2, respectively.

$$f(n) = \frac{c\left(\frac{n}{N}\right)}{\int_0^\infty \left|\left(\frac{n}{N}\right)\right| dn} \tag{2.1}$$

$$g(v) = \frac{c\left(\frac{v}{Q}\right)}{\int_0^\infty \left|\left(\frac{v}{Q}\right)\right| dv} \tag{2.2}$$

Where *f(n)* is the RRD function and *g(v)* is the RVD function. Additionally, *n* is the accumulated screw revolutions and *v* is the accumulated volumes of extruded material. Using these distributions, further insights in the mixing behaviors can be gained.

Gao et al [53], [54] and later Zhang et al [55] performed RTD experiments using tracer concentrates with different screw geometries and operating conditions. Using the transformations stated above, the RVD and RRD curves were obtained. Gao showed that specific throughput (Q/N), an estimate of the degree of fill, was a key variable in determining the flow characteristics. For operating conditions with the same specific throughput, the RRD and RVD were the same. Another observation was that specific throughput impacted the delay in both the RVD and RRD domains. A larger Q/N yielded a shorter revolution delay in the RRD domain and a larger extrudate volume delay in the RVD domain. Additionally, in the RVD domain, it was found that all of the generated RVD curves are nearly identical. This showed that the operating conditions had no impact on the axial distribution of the tracer, for a given screw design. The results from this study indicate that only by changing screw designs can the quality of mixing be affected.

Chapter 3 Experimental Methods

The equipment, materials, and procedures that were used for generating and characterizing the stress history in extruders are introduced and explained in the following sections.

3.1 Equipment

The equipment used for this experiment consists of three different sized twin-screw extruders with different screw geometries utilized for each extruder.

3.1.1 Twin Screw Extruders

3.1.1.1 28-mm TSE

The primary extruder used in this study was a Coperion ZDSK-28 co-rotating, fully-intermeshing twin-screw extruder located in the Advanced Manufacturing Laboratory at the University of Maryland. The screws have three flights and their diameter was 28-mm. The length to diameter ratio (L/D) was 32. The experimental setup using the 28-mm TSE can be seen in Figure 3.1.

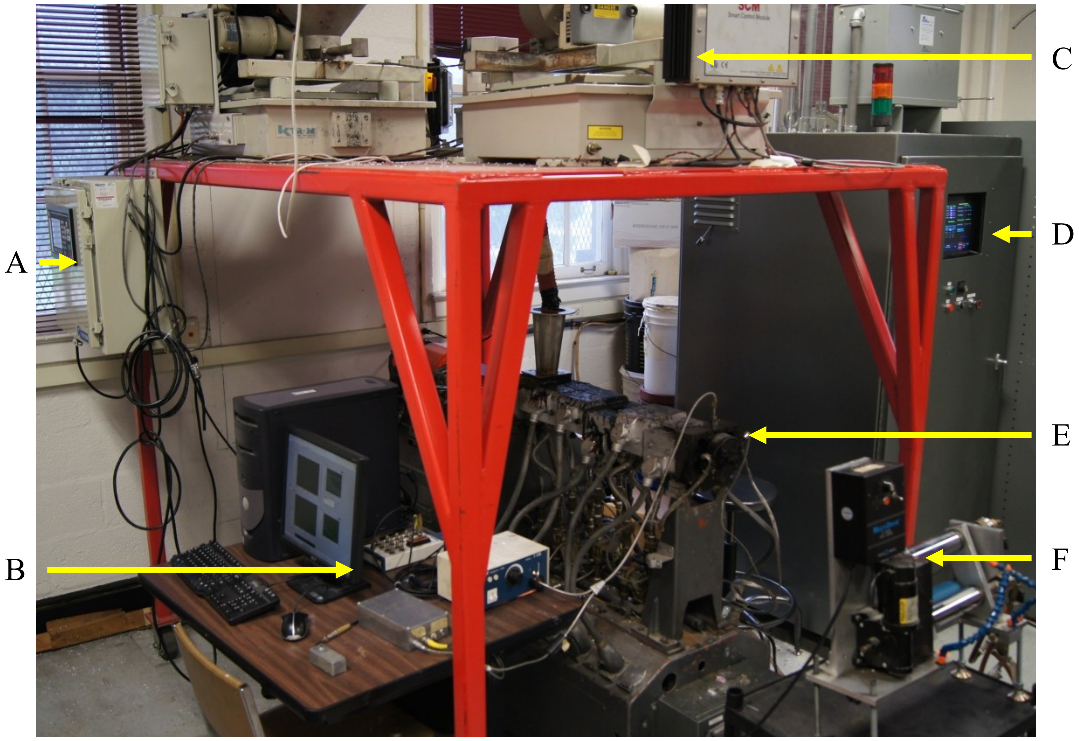

Figure 3.1 - Experimental set up for 28-mm twin screw extruder

The 28-mm extruder setup consisted of a 28-mm twin screw extruder (E) with a control panel (D), polymer feeder (C) with control panel (A), data acquisition system (B), and a chill roller (F) used for sample collection.

The extruder was made up of eight main sections. The first was the feed port. This section was used for polymer feeding into the extruder. The next five sections, also known as “barrel zones,” were used to heat the material to its melting point so mixing of the material and any additives can be performed more easily than in their solid states. The seventh section was a metal block that was used to house data acquisition instruments, as well as connected the eighth section to the extruder. The block had two ports where instruments could be inserted into the flow. Only one of the ports was used for this experiment, which held the fiber optic probe. The block also had four screw holes threaded into it to connect the last section, the “die zone” to the extruder. The die zone was the section where the melted material was formed by the shape of the die and left the extruder. The shape of the die was a thin slit that was 25 mm wide and 1 mm thick.

The eight sections together were used to feed material into the extruder, melt the material, hold instrumentation to acquire data from the polymer flow, and then shape the extrudate so that it could be easily collected. Figure 3.2 below shows the arrangement of the eight sections of the 28-mm extruder, with the flow of the polymer moving from left to right.

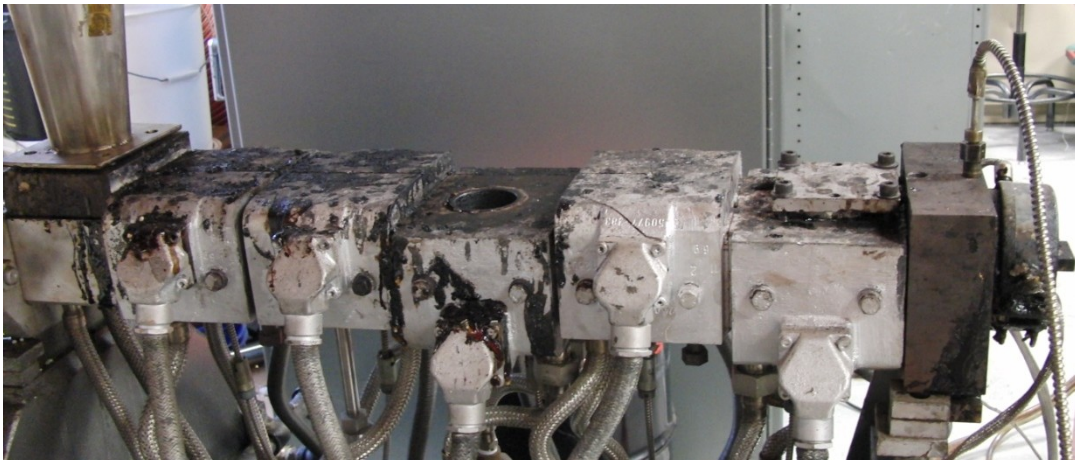

Figure 3.2 - Arrangement of barrels and die zone

As seen in the above figure, the third barrel zone had a hole in the barrel, or referred to as "mixing port," where additives could be added into extruder. For these experiments, that port was used to insert the stress sensors inside the extruder.

The 28-mm extruder was controlled by a FACTS MI – 101 control system with a digital touch-screen control panel. Figure 3.3 below shows an image of the controller.

Figure 3.3 - FACTS MI-101 control system

The FACTS control system was used to control the temperature of the barrel zones and die zone, as well as control the rotation speed of the extruder screws, which had a maximum value of 300 RPM. The controller had both digital and manual controls. The manual controls were located on the outside of the control cabinet. These included a dial to control screw speed, on/off switches, as well as an emergency stop button. The digital control panel also enabled the user to turn the extruder on and off, as well as designate the screw speed, however, it also controlled the temperature of the barrel and die zones

To feed the extruder with material, a laboratory scale K-TRON loss-in weight twin screw pellet feeder (Figure 3.4) was used. The feeder was suspended above the extruder on a platform and a flexible tube was used to direct the polymer pellets into the feed port of the extruder.

Figure 3.4 - K-TRON loss-in weight pellet feeder

The feeder was controlled by a KCM control system which was used to control the feed rate of the K-TRON feeder. The maximum feed rate of the K-TRON was approximately 10 lb/hr. The KCM could also be used to control more than one K-TRON feeder as it had the capability to switch between any connected feeders and operate them. Figure 3.5 below shows an image of the control panel.

Figure 3.5 - KCM control system for K-TRON pellet feeder

As the melted polymer left the extruder, attempting to collect samples was very difficult due to the temperature of the material. To cool the extrudate, as well as flatten it into a clean strip, a chill roller was utilized (Figure 3.6).

Figure 3.6 - Chill roller

The chill roller contained three rollers, one on top and two on the bottom. The extruded polymer passed over the top roller and was then flattened in between the two bottom rollers. The rollers were controlled by a motor and the speed of the rollers was adjusted to match the speed of the extrudate. Attached to the two steel rollers is a water line that is connected to a water source. Upon turning on the water source, water flowed through the rollers and cooled them, which cooled the polymer melt when it came in contact with the rollers. Additionally, two sprinklers were also available for further cooling if necessary. The chill roller enabled the user the neatly and safely collect sample strips of the polymer.

3.1.1.2 26-mm TSE

Another set of experiments was performed at the Coperion headquarters, in Ramsey, NJ. The extruder used at that facility was a ZSK-26 MC fully-intermeshing, co-rotating twin-screw extruder. The screw diameter was 26-mm and had a length to diameter ratio 37. The screws in this machine were bi-lobed. The extruder consisted of nine barrels which were all heated to 200^{o}C and a die which was also heated to 200^{o}C. The mixing port of this extruder was used as the injection site. The light probe was inserted into the extruder via an open instrumentation slot just before the die, similar to that of the 28-mm extruder.

3.1.1.3 18-mm TSE

The last set of experiments was carried out using a Coperion ZSK-18 MegaLab fully intermeshing, co-rotating twin screw extruder located at the DuPont Research Station in Wilmington, DE. This extruder had a diameter of 18-mm and an L/D ratio of 40. The screws from this machine also had two flights, similar to the 26-mm. The 18-mm extruder consisted of 9 barrel sections, heated to different temperatures. The first two barrels were heated to 120^{o}C, barrels 3 and 4 were heated to 190^{o}C, the next four barrels were heated to 180^{o}C, and the final barrel, as well as the die, was heated to 200^{o}C. An open port located just before the mixing section was used as the location for the injections. The optical probe for this setup was inserted into the extruder directly after the mixing section, as opposed to after the pumping section for the 26-mm and 28-mm extruders.

3.1.2 Screw Geometries

The design of the screw geometry is extremely important in achieving low or high degrees of mixing. Mixing is related to the amount of stress induced on the material flowing through the extruder. If a high magnitude of stress is achieved, then it would be expected that the degree of mixing would also be high. The geometries used for this study contained three primary regions: a melting region, a conveying region, and a mixing region.

The melting region was used to transform the solid polymer pellets into a melt where the material could flow through the extruder. The polymer melt in this phase made mixing much easier. The function of the conveying region was to move the polymer melt from the melting region to the mixing region. The conveying regions consisted of different sized and pitched conveying elements for polymer relaxation and decompression. The mixing region, for this study, was the region of interest and as the name implies, was used to mix the polymer melt. This region consisted of different combinations of various sized kneading blocks in an attempt to achieve different degrees of mixing. After the kneading blocks, forward conveying elements were used to push the material to the die and out of the extruder. This section of conveying elements is known as the "pumping section." These three regions made up the screw geometries used in this work.

The following sections give the specific screw designs for each extruder used.

3.1.2.1 28-mm TSE

For the 28-mm extruder, four different geometries were investigated. Each geometry consisted of the same melting region and conveying region. The melting region of the screws consisted of various sized conveying elements, a medium kneading block element (3.0 cm) and a left-handed narrow kneading block element (1.5 cm). The conveying region consisted on only two different-sized conveying elements. One of elements was 4.5 cm long with an axial pitch of 1.5 cm. This element was used right after the melting region and directly under the mixing port because of its large size and ability to move the maximum amount of material. The other that was used was a 3.0 cm long conveying element with a pitch of 1.0 cm. The design of these regions can be seen in Figure 3.7.

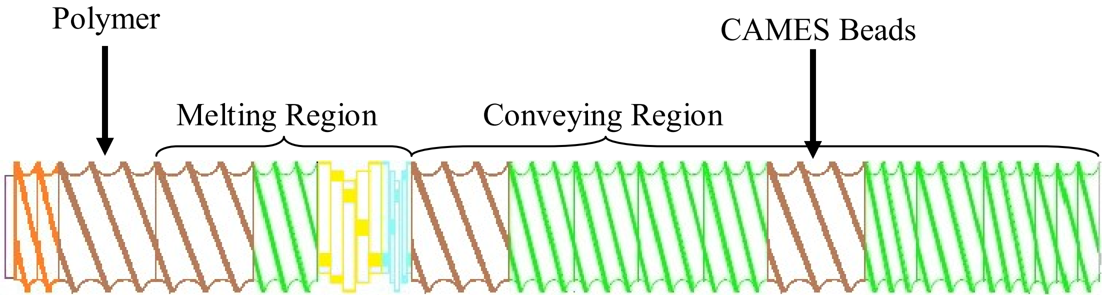

Element	Axial Length (cm)	Axial Pitch (cm)
RH Conveying	1.0	1.0
RH Conveying	4.5	1.5
RH Conveying	3.0	1.0
RH Kneading Block	3.0	0.6
LH Kneading Block	1.5	0.3

Figure 3.7 - Melting and conveying regions for all 28-mm screw designs

These two regions remained unchanged throughout the experiments performed using the 28-mm extruder. The polymer is fed into the 4.5 cm long conveying element just before the melting region, and the stress measuring devices were inserted into the extruder via the mixing port, which fell into the second 4.5 cm long conveying element in the conveying region.

The mixing region of the first screw design (Figure 3.8) that was studied consisted of four narrow kneading blocks, one neutral kneading block, and a left-headed narrow kneading block.

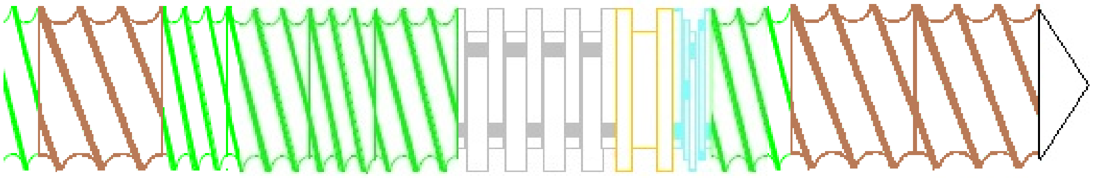

Element	Axial Length (cm)	Axial Pitch (cm)
RH Conveying	4.5	1.5
RH Conveying	3.0	1.0
RH Kneading Blocks	1.5	0.3
Neutral Kneading Block	2.0	0.5, 1.0, 0.5
LH Kneading Block	1.5	0.3
End Cap	2.5	--

Figure 3.8 – 28-mm screw design #1

The mixing section of the second screw design was modified in that three narrow kneading blocks were removed and replaced with a wide kneading block element of comparable length. This design can be seen in Figure 3.9.

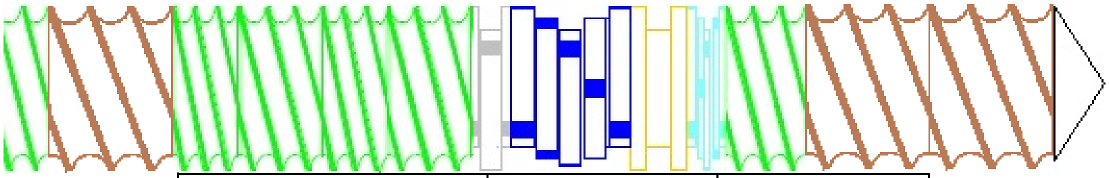

Element	Axial Length (cm)	Axial Pitch (cm)
RH Conveying	4.5	1.5
RH Conveying	3.0	1.0
RH Kneading Blocks	1.5	0.3
RH Kneading Blocks	4.5	0.9
Neutral Kneading Block	2.0	0.5, 1.0, 0.5
LH Kneading Block	1.5	0.3
End Cap	2.5	--

Figure 3.9 – 28-mm screw design #2

The next two screw geometries utilized a left-handed conveying element at the end of the mixing region rather than a neutral kneading block and a left-handed kneading block. The third geometry studied is displayed in Figure 3.10.

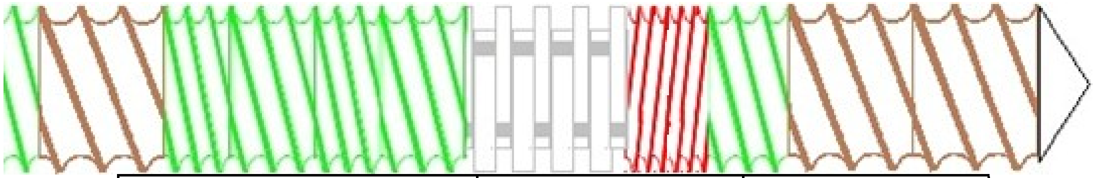

Element	Axial Length (cm)	Axial Pitch (cm)
RH Conveying	4.5	1.5
RH Conveying	3.0	1.0
RH Kneading Blocks	1.5	0.3
LH Conveying	3.0	1.0
End Cap	2.5	--

Figure 3.10 – 28-mm screw design #3

The geometry above utilized the left-handed conveying element behind four narrow kneading blocks. The reverse element causes more back pressure in the mixing region, ensuring that the channels of the kneading blocks are full.

The fourth screw design for the 28-mm TSE again removed three narrow kneading blocks and replaced it with a wide kneading block, as shown in Figure 3.11.

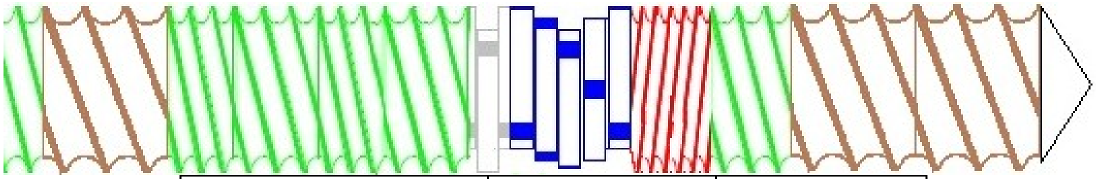

Element	Axial Length (cm)	Axial Pitch (cm)
RH Conveying	4.5	1.5
RH Conveying	3.0	1.0
RH Kneading Blocks	1.5	0.3
RH Kneading Blocks	4.5	0.9
LH Conveying	3.0	1.0
End Cap	2.5	--

Figure 3.11 - 28-mm screw design #4

3.1.2.2 26-mm TSE

Three screw geometries were investigated on Coperion's 26-mm twin screw extruder. Similar to the 28-mm screw designs, the melting and conveying regions did not change for the three designs. The melting zone consisted of various sized conveying elements and neutral kneading blocks, which can be seen in Figure 3.12. The polymer was fed into the 3.6 cm long conveying element (yellow element) where it was then moved into special conveying elements (pink elements) that were designed to push maximum amounts of material into the kneading block section. The melted polymer is then conveyed to the mixing section.

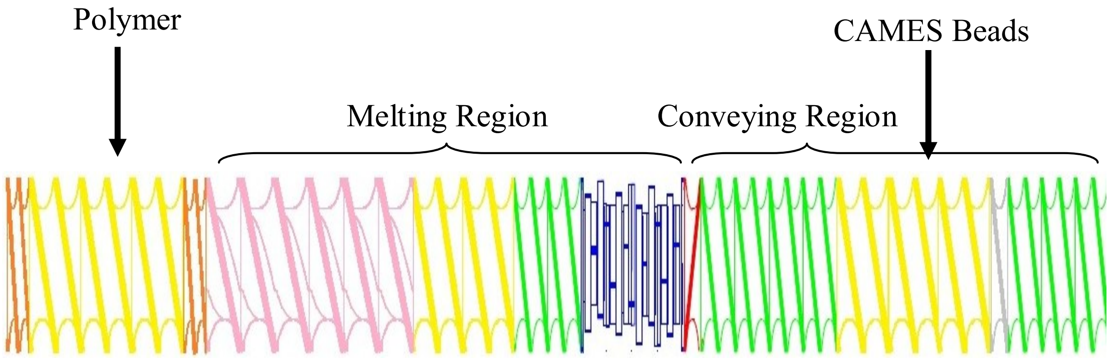

Element	Axial Length (cm)	Axial Pitch (cm)
RH Conveying	1.6	1.6
RH Conveying	3.6	3.6
RH Conveying	2.4	4.8
RH Conveying	2.4	2.4
Neutral Kneading Blocks	1.8	0.36
LH Conveying	1.2	2.4
RH Conveying	1.2	2.4
End Cap	2	----

Figure 3.12 - Melting and conveying regions for all 26-mm screw designs

The mixing region of first screw design used for the 26-mm extruder is shown in Figure 3.13. This region consisted of six narrow kneading blocks and two left-handed conveying elements.

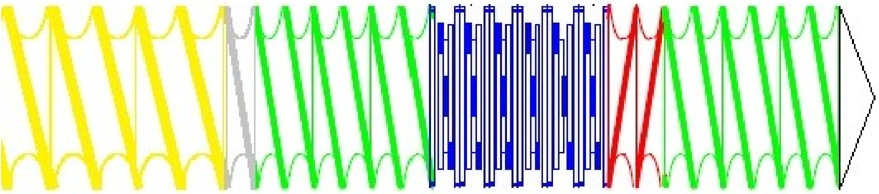

Element	Axial Length (cm)	Axial Pitch (cm)
RH Conveying	3.6	3.6
RH Conveying	1.2	2.4
RH Conveying	2.4	2.4
RH Kneading Block	1.2	0.24
LH Conveying	1.2	2.4
End Cap	2.0	--

Figure 3.13 - 26-mm screw design #1

The geometry for the second screw design removed all the narrow kneading blocks and replaced them with three medium kneading blocks, of comparable length. The mixing region geometry can be seen in Figure 3.14.

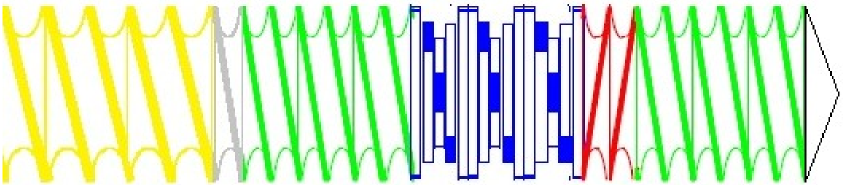

Element	Axial Length (cm)	Axial Pitch (cm)
RH Conveying	3.6	3.6
RH Conveying	1.2	2.4
RH Conveying	2.4	2.4
RH Kneading Block	2.4	0.48
LH Conveying	1.2	2.4
End Cap	2.0	--

Figure 3.14 - 26-mm screw design #2

The last screw design (#3) used on Coperion's 26-mm extruder can be seen in Figure 3.15. The medium kneading blocks were removed and were replaced with a two wide kneading blocks, again keeping the total length of the kneading blocks the same in the mixing region.

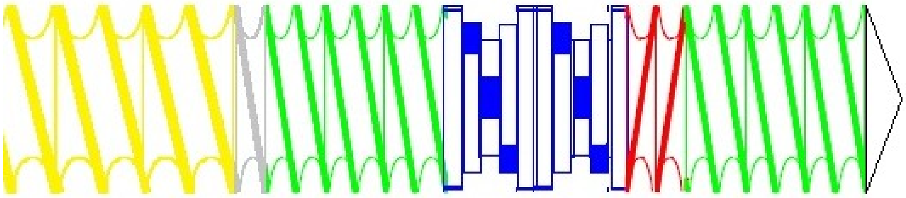

Element	Axial Length (cm)	Axial Pitch (cm)
RH Conveying	3.6	3.6
RH Conveying	1.2	2.4
RH Conveying	2.4	2.4
RH Kneading Block	3.6	0.72
LH Conveying	1.2	2.4
End Cap	2.0	--

Figure 3.15 - 26-mm screw design #3

3.1.2.3 18-mm TSE

The experiment performed on DuPont's 18-mm TSE consisted of two screw designs. The melting and conveying regions can be seen in Figure 3.16.

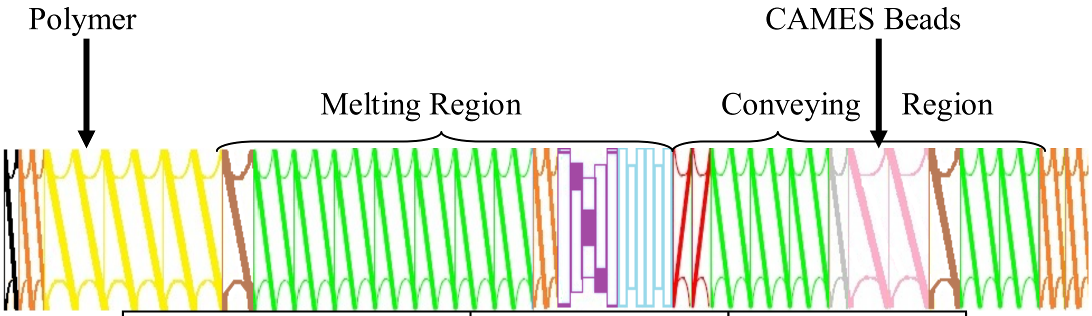

Element	Axial Length (cm)	Axial Pitch (cm)
RH Conveying	1.2	1.2
RH Conveying	1.6	1.6
RH Conveying	1.8	3.6
RH Conveying	1.2	2.4
RH Conveying	2.4	2.4
RH Kneading Blocks	2.4	0.48
Neutrual Kneading Blocks	1.6	0.32
LH Conveying	1.6	0.8
RH Conveying	1.2	2.4
RH Conveying	2.4	2.4

Figure 3.16 – Melting and conveying regions for all 18-mm TSE screw designs

The melting section of the 18-mm TSE was slightly more complicated than the other melting sections, consisting of five different sized conveying elements, one wide kneading block, and two neutral kneading blocks, which were backed by a two reverse conveying elements. The conveying region also consisted of five different sized conveying elements with a 2.4 cm long conveying element (pink element) used to receive the CAMES and ink injections. Similar to the 26-mm and 28-mm extruders, these two regions remained unchanged for the duration of the experiment.

The first screw design using the 18-mm extruder is seen in Figure 3.17. The mixing section on the first screw design consisted of four narrow kneading blocks and two reverse conveying elements.

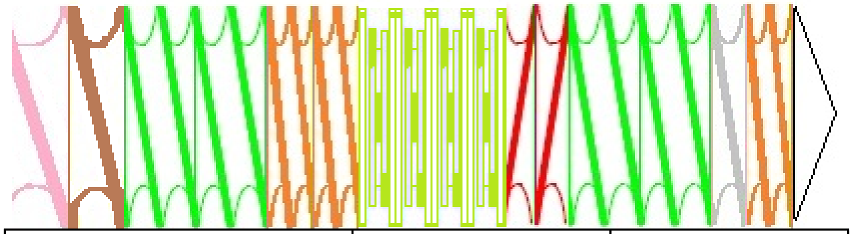

Element	Axial Length (cm)	Axial Pitch (cm)
RH Conveying	2.4	2.4
RH Conveying	1.2	2.4
RH Conveying	2.4	2.4
RH Conveying	1.6	1.6
RH Kneading Blocks	0.8	0.16
LH Conveying	1.6	0.8
RH Conveying	1.2	2.4
End Cap	1.6	--

Figure 3.17 - 18-mm TSE screw design #1

The four narrow kneading blocks were removed and replaced with two medium kneading blocks, as shown in Figure 3.18, for screw design #2.

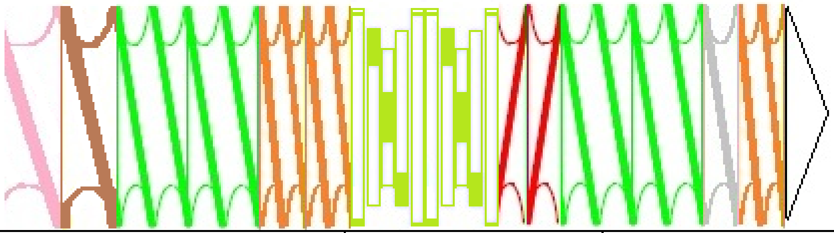

Element	Axial Length (cm)	Axial Pitch (cm)
RH Conveying	2.4	2.4
RH Conveying	1.2	2.4
RH Conveying	2.4	2.4
RH Conveying	1.6	1.6
RH Kneading Blocks	1.6	0.32
LH Conveying	1.6	0.8
RH Conveying	1.2	2.4
End Cap	1.6	--

Figure 3.18 - 18-mm TSE screw design #2

3.1.3 Data Acquisition Equipment

To collect the data produced by the extruder, a data acquisition system was set up, as seen in Figure 3.19.

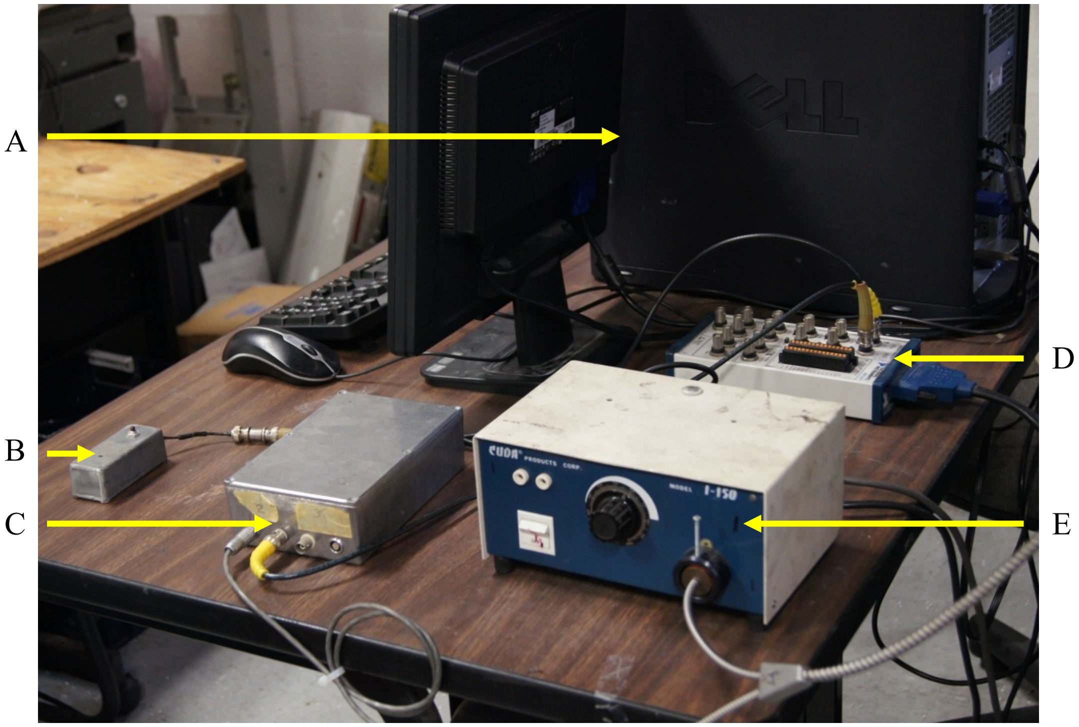

Figure 3.19 - Data acquisition system set up

The system consisted of a CPU (A), light source with reflective optical probe (E), amplifier (C), spike generator (B), and connector block (D).

The program used to analyze and collect the data was National Instruments' (NI) LabVIEW. The interface of the program used to acquire the data is seen in Figure 3.20.

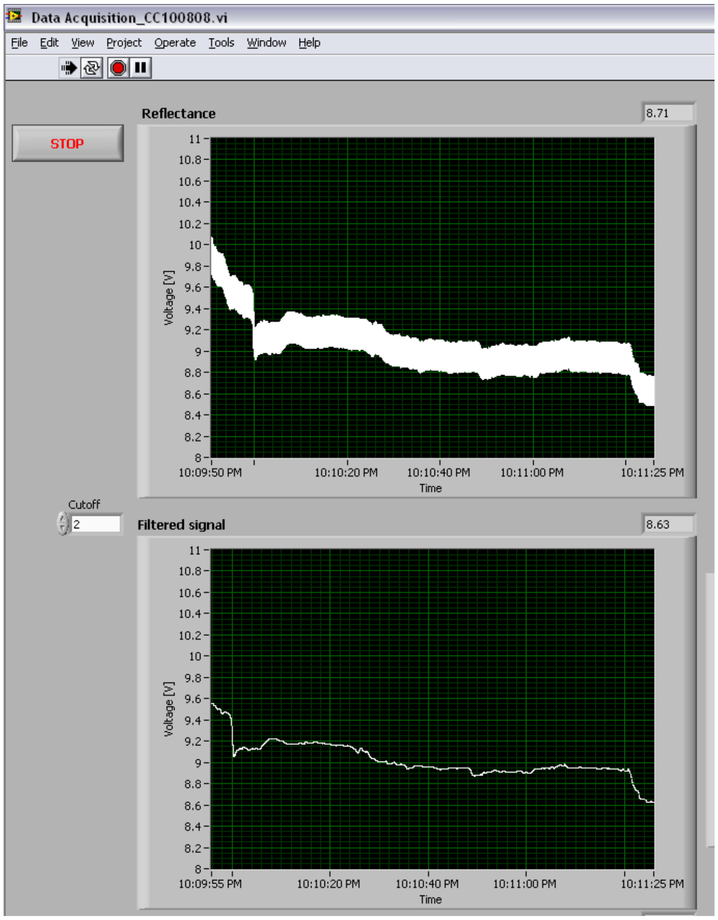

Figure 3.20 - Data acquisition program interface

The collected data was displayed unfiltered in the reflectance grid of Figure 3.20. The data was sampled at a frequency of 120 Hz. To eliminate the variation in the data as seen in the reflectance plot, a Butterworth filter was added to reduce interference and noise from the data. It was found that a cutoff value of 2 produced the clearest results, as seen in the bottom (Filtered signal) plot of the figure.

The data was generated using a Cuda I-150 reflective optical probe inserted into the extruder via one of the available probe slots in the metal block before the die, as seen previously in Figure 3.2. The probe consisted of a split fiber-optic bundle, where light, powered by a light source, was transmitted from one fiber bundle. The light was then scattered and then collected by the other fiber bundle, where it was then converted into a voltage. The probe provided a maximum output voltage of 1 V DC. To increase this maximum value so small changes in the data could be seen, an amplifier was added into the system. The signals from the amplifier were then sent to a NI BNC-2110 connector block which was connected to the CPU. Additionally, a spike generating device was added for timing purposes. As the experiment was performed, an operator pressed the button which sent a spike signal to the LabVIEW program signaling it to erase all previous recorded data and begin sampling at that instant. This device was also connected to the connector block. The connector block then converted the signals and allowed visualization of the data on the LabVIEW program interface. Once the experiment was complete, the program was stopped, and the data was then converted into a spreadsheet and the entire process repeated for the next experiment.

3.2 Materials

3.2.1 High-Density Polyethylene

The extrusion polymer for this research study was high-density polyethylene (HDPE) Alathon H6018 in pellet form from Equistar Chemicals in Houston, TX. This grade of HDPE is a medium molecular weight high density homo-polymer and is typically used for food wrapping and extrusion coating. The melt index for this material was 18.0 g/10 min, had a density of 0.960 g/cc, and a melt temperature of 199^{o}C [56].

3.2.2 "CAMES" Beads

Calibrated microencapsulated sensor, or "CAMES", beads from Mach I, Inc. in King of Prussia, PA were utilized as the method to measure the stress history in the extruders. The beads are designed to detect shear stresses during mixing and indicate the magnitude of the stress via the release of encapsulated dye [57]. Figure 3.21 below shows an image of the CAMES beads under a microscope.

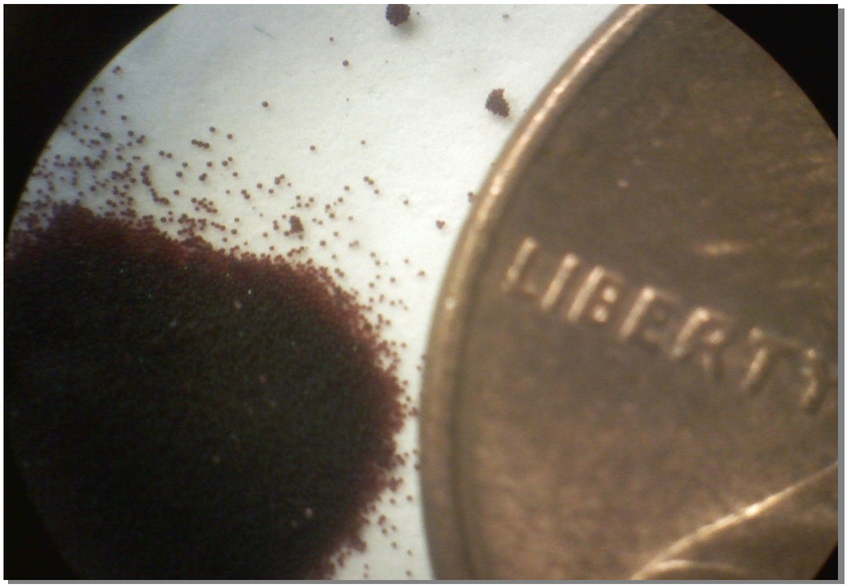

Figure 3.21 - Calibrated microencapsulated sensor (CAMES) beads

These sensor beads are calibrated to rupture at specific critical stress levels as a function of the bead diameter and bead wall thickness. The sensors are synthesized and processed by controlled procedures to select a range of particle diameters and wall thicknesses that establish the preferred shear stress rupture sensitivity [58]. When the shear stress induced by the extruder exceeded the bead threshold, the microcapsules rupture. This caused the dye contained within the bead to be released into the extruder and stain the polymer melt. For the experiments performed, a total of four different levels of CAMES beads were used, two of which were red and the other two were blue, as seen in Figure 3.22.

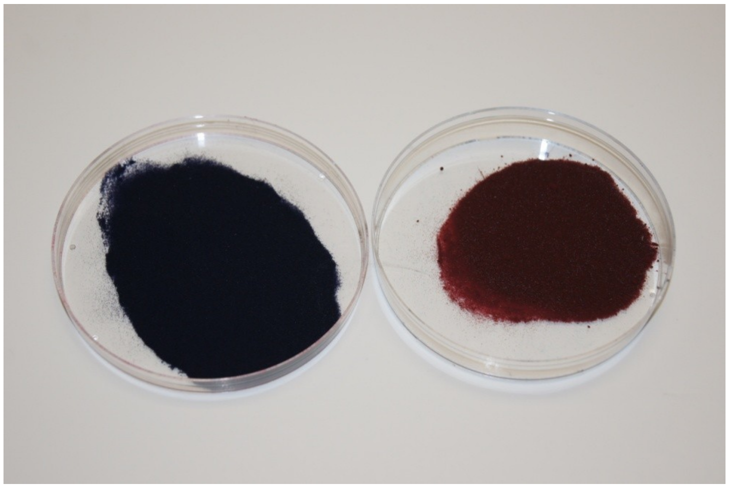

Figure 3.22 - Blue and Red CAMES beads used during experimentation

The specific dye that was released by the CAMES beads that were red was Red B Disazo dye and the beads that were blue contained AUTOMATE Blue 8A dye. Table 3.1 below provides information on the CAMES beads used for this research investigation.

Table 3.1 - CAMES beads information including diameters, critical shear stresses, color of encapsulated dyes, and location where beads were used

Bead Diameter (µm)	**Critical Shear Stress (kPa)**	**Dye Color**	**Locations Used**
X > 90	119 ± 24	Red	UMD (28-mm)
X < 44	223 ± 27	Red	Coperion (26-mm)
X > 75	92 ± 14	Blue	Coperion (26-mm) UMD (28-mm)
45 < X < 75	158 ± 21	Blue	DuPont (18-mm)

3.2.3 Reference Shots

Using the same dye that was encapsulated by the two colors of CAMES beads, Red B Disazo for the red beads and AUTOMATE Blue 8A for blue beads from Rhom & Haas Co., in Philadelphia, PA, “reference” dye shots were produced. The purpose of these shots was to provide reference RTD curves that represented 100% breakup of the CAMES beads. These shots were prepared using super high impact polystyrene (Super HIPS) 935E in pellet form from Total Petrochemicals in Houston, TX as the base material. 6.57 grams of Super HIPS were dissolved in 55 mL of Xylene while being mixed on a hotplate-stirrer. Once the pellets completely dissolved, 0.73 mL of dye (either Red B Disazo or AUTOMATE 8A) was added and continuously mixed in until uniformly distributed. The solution was then placed under the fume hood until the remaining xylene evaporated, producing a batch of solidified dye, as seen in Figure 3.23.

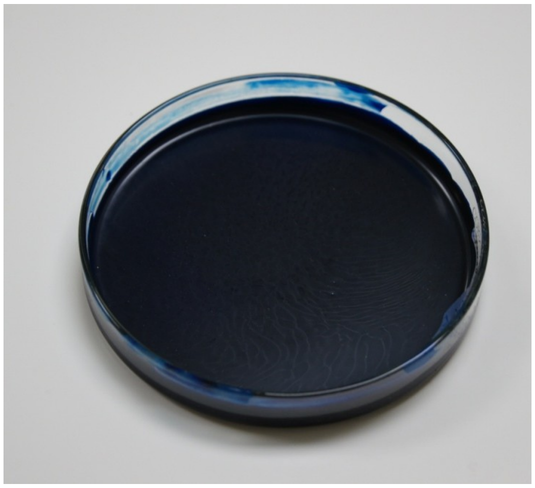

Figure 3.23 - Solidified blue ink batch

The solid dye was then cut and weighed to match that of the CAMES beads shots that were injected into the extruder.

3.2.4 Titanium Dioxide

Due to the transparent nature of HDPE when melted, the light from the optical probe would pass through the polymer melt and only record the reflectance of the extruder screws. As the screws rotated, large signal spikes were produced as a result of the reflection off the edges of the channels of the conveying elements making data analysis very difficult. To resolve the problem, Ti-Pure R-105 Titanium Dioxide (TiO_2) in pellet form (Figure 3.24) from DuPont in Wilmington, DE was fed into the extruder with the HDPE pellets.

Figure 3.24 - Titanium dioxide

The Ti-Pure R-105 is a titanium dioxide pigment that produces bright TiO_2, which when added to the HDPE melt, created a bright white color [59]. The white background did not allow the light from the light probe to completely penetrate through the polymer melt and reflect off the screws. The TiO2 reduced the signal spikes and boosted the fiber optics' performance due to the larger contrast between the white background and the red and blue dyes.

3.3 Central Composite Design of Experiment Grids

To perform statistical analysis on the data that was collected, a central composite design (CCD) of experiment grid was used. A CCD grid was chosen for analysis because of the expected non-linear relationship of the input variables. This grid was useful in laying out the data to visually show relationships between percent breakup of CAMES beads and different operating conditions. Additionally, a statistical analysis could be performed to generate the correlation equations between bead breakup and the operating conditions. The ranges of the operating conditions were determined by the capabilities of the three extruders used in this experiment. The first number of an experimental condition represents the throughput, Q, measured in lb/hr. The second number corresponds to the screw speed, N, measured in RPM. The axes for each grid were screw speed (N) along the horizontal axis and specific throughput (Q/N) for the vertical axis. Q/N was chosen because RTDs scale with both Q and N. In a previous study, Gao et al [53] found that specific throughput was a key variable in determining the characteristics of residence-volume distributions (RVD) and residence-revolution distributions (RRD). To properly reproduce those results and investigate trends of CAMES breakup in the RVD and RRD domains, Q/N was used as one of the primary variables.

3.3.1 28-mm CCD Grid

The central composite design of experiment grid used for experiments with the 28-mm extruder is shown below in Figure 3.25.

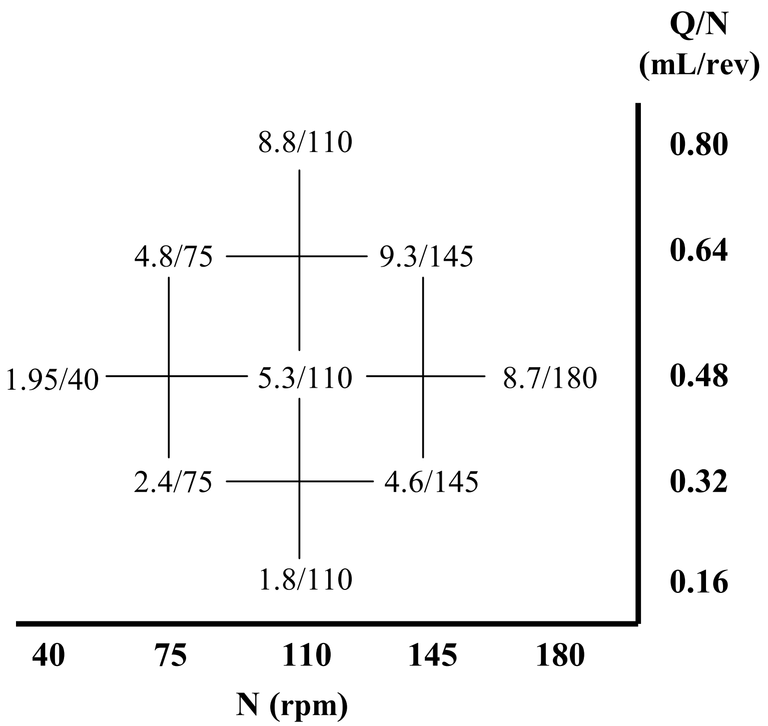

Figure 3.25 - CCD grid for 28-mm TSE with operating conditions

The range of screw speeds investigated was between 40 and 180 rpm in 35 rpm intervals, and the range of throughputs was between 1.8 and 8.8 lb/hr. Flow rates and screw speeds were used in conjunction to produce conditions with the same specific throughput values (Q/N). The range of Q/N values investigated was between 0.16 and 0.80 mL/rev. Another thing to note about this CCD grid is the left to right downward diagonals, which have the same flow rates, within some error in the accuracy of the pellet feeders, as demonstrated in Figure 3.26.

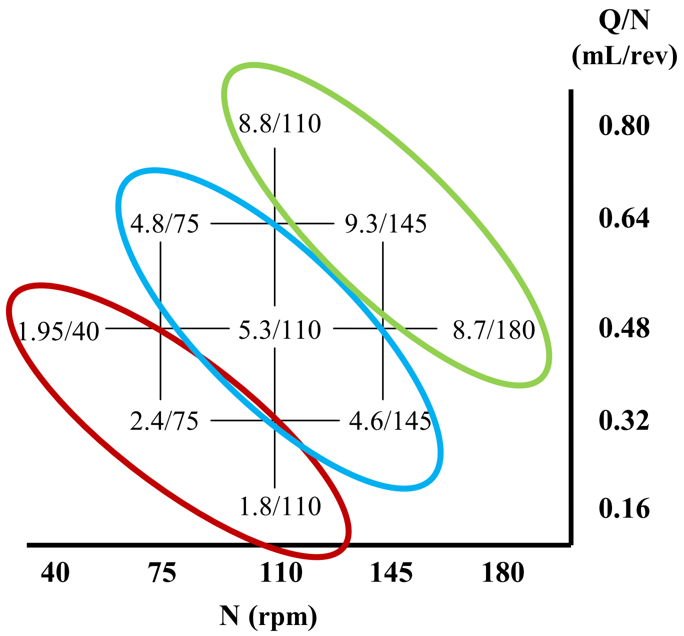

Figure 3.26 - Illustration of constant flow rate diagonals on CCD experimental grid

The three circles in the figure above show the constant flow rate diagonals on the CCD grid. The lowest diagonal (red circle) is referred to as “diagonal 1.” The middle diagonal (blue circle) is referred to as “diagonal 2,” and the highest diagonal (green circle) is known as “diagonal 3.” This experimental grid was used for every experiment on the 28-mm extruder.

3.3.2 26-mm CCD Grid

The central composite design grid used for the 26-mm twin screw extruder at Coperion is shown in Figure 3.27.

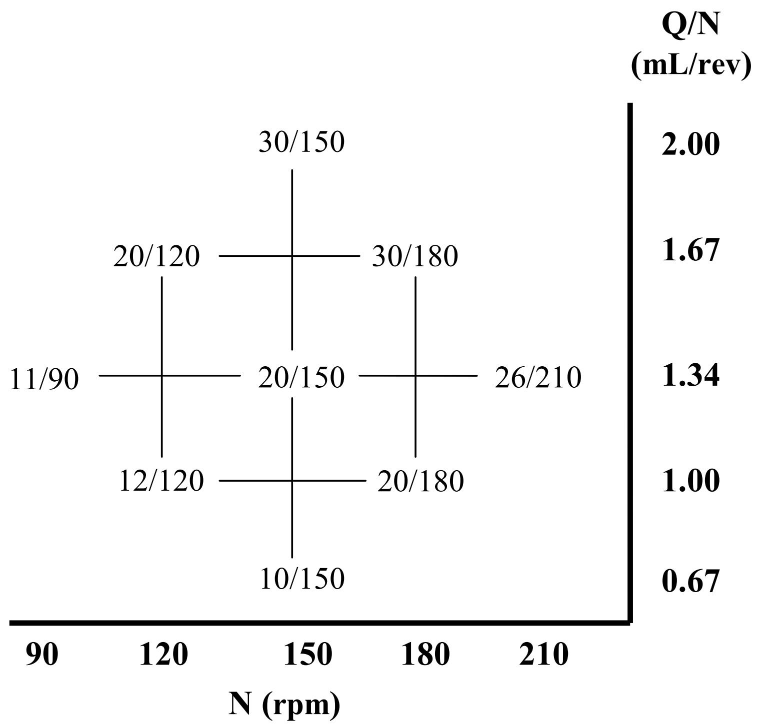

Figure 3.27 - CCD grid for 26-mm with operating conditions

The capabilities of the 26-mm extruder were much higher than that of the 28-mm extruder due to the more powerful machine. The range of flow rates was between 10 and 30 lb/hr, and the screw speeds were between 90 and 210 rpm. With a more powerful machine, a wider range of specific throughputs could also be achieved, ranging between 0.67 and 2.00 mL/rev. Additionally, the three constant diagonals (mentioned in the previous section) were also present in this CCD grid. The figure above shows the operating conditions run using the narrow, medium, and wide kneading blocks for the 26-mm extruder.

3.3.3 18-mm CCD Grid

The central composite design of experiment grid used for the 18-mm twin screw extruder at DuPont's Research Station is shown in Figure 3.28.

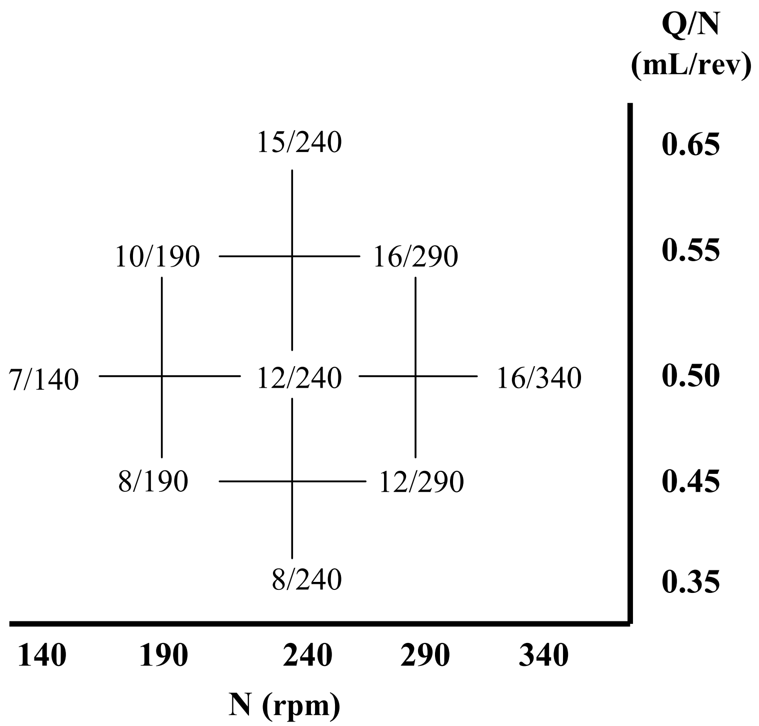

Figure 3.28 - CCD grid for 18-mm TSE with operating conditions

Figure 3.28 above shows the operating conditions for the experiments using the 18-mm twin screw extruder for narrow and medium kneading blocks. Due to its small size, the 18-mm was not capable of handing throughputs as high as the 26-mm extruder; however, it was able to achieve much higher screw speeds. The range of screw speeds studied with this machine was between 140 and 340 rpm, with flow rates ranging between 7 and 16 lb/hr. The range of specific throughputs was between 0.35 and 0.65 mL/rev. Additionally, this CCD grid also had the three constant flow rate diagonals

3.4 Procedures

3.4.1 Experimental Procedure

To begin the experiments, the extruder was first turned on and the five extruder barrels were allowed to heat up to their set temperatures of 200°C and the die zone was heated to 190°C using the FACTS MI – 101 control panel. Once these temperatures were achieved, the desired operating screw speed was set. Using the K-TRON loss-in weigh feeder, the operating flow rate was set and the polymer flowed into the feed port of the extruder. The drawn motor amperage was monitored once the operating conditions were set, as they fluctuated while the extruder was adjusting to the new inputs. Once the fluctuations were minimal, this ensured that steady state had been reached. Additionally, the extrudate from the die was looked at until it came out completely transparent. This indicated that any remaining material (typically brown or black from being burnt) from previous day's experiments were purged from the extruder so that it would not cause erroneous data when passing underneath the optical probe. After these startup procedures were completed, the extruder was now prepared and ready to carry out experimentation.

The next step was to prepare the data acquisition equipment. The light for the fiber optic probe was turned on and the bulb brightness was set to its highest setting. The voltage converter and amplifier were turned on as well. The data acquisition program in LabVIEW was then initialized and the data file to be written was set up.

As the color of the melted HDPE came out clear, Titanium Dioxide was dropped into the feed port of the extruder at a constant rate of 2 pellets every 10 seconds continuously for the duration of the experiment. Before the CAMES beads or ink could be injected into the extruder, it was important to have a start point for the curve to begin. To accomplish this, the data acquisition program collected data for at least 15 seconds to establish a clear start line or "baseline." An example of a clear baseline is shown in Figure 3.29.

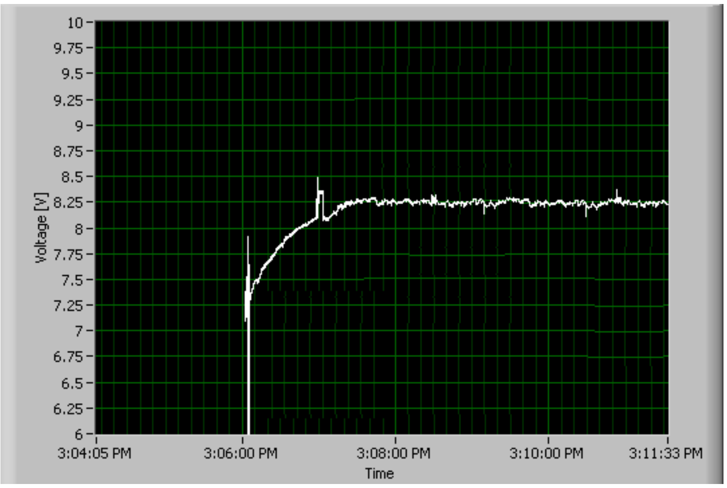

Figure 3.29 - Straight baseline required before experiment can begin

When the baseline had been established, the experiment was performed. The injection system was then set up over the mixing port of the extruder. The first injection in the order of the experiment was the ink shot. The injection was carried out using a modified syringe. The tip was removed and covered with a very thin piece of lens paper. This provided a platform for the ink or CAMES shots to be loaded on to. A sharp rod was added to the tip of the plunger, enabling the plunger to pierce the lens paper and inject the shot into the extruder quickly. The syringe can be Figure 3.30.

Figure 3.30 - Modified syringe used for injection

The syringe was filled with 0.63 grams of the solid pieces of ink and injected into the channels of the conveying element. As the operator injected the contents of the syringe, another operator simultaneously pushed the button on the spike generator. This spike was received by the LabVIEW program and deleted any previously recorded data for that file up until the instant the spike was sent. After the ink was injected into the extruder, the extrudate from the die was cut and fed through the chill roller to flatten and cool the sample so that it could be collected.

While in the extruder, the solid pieces of ink melted and stained the HDPE. The polymer then moved through the mixing section, where it became further mixed by the kneading blocks. Once through the mixing section, the polymer melt was then pushed forward towards the die by the pumping section. At the end of the pumping section was where the optical probe was located. The probe then recorded the reflectance of the stained polymer. Figure 3.31 and Figure 3.32 below display the outputs of the optical probe at two different times during one experiment.

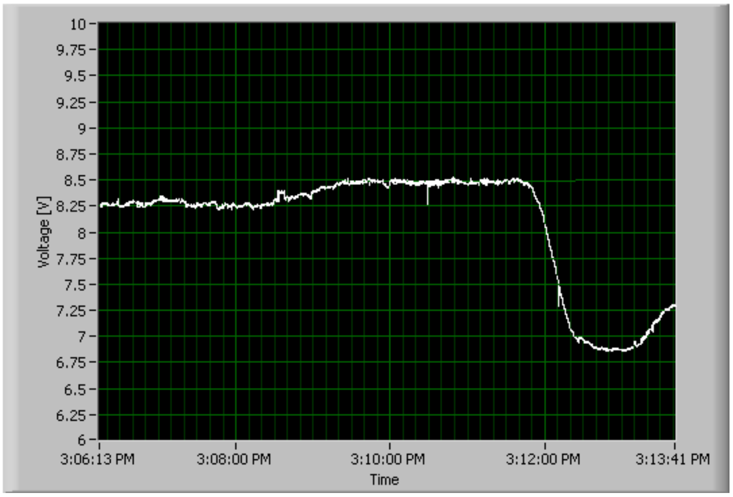

Figure 3.31 - Optical response as high concentration passed under probe

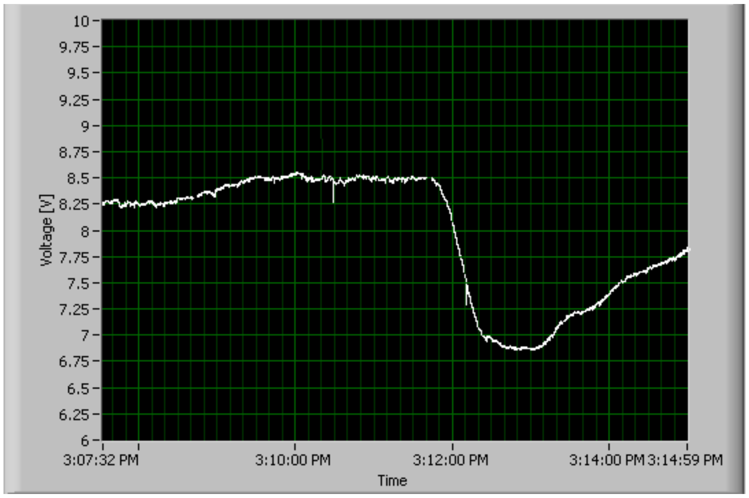

Figure 3.32 - Optical response after high concentration passed under probe

Figure 3.31 above shows that as the stained polymer moved underneath the light probe, the recorded voltage signal dropped very steeply. This is a result of the polymer melt being stained by the ink. The darkened polymer absorbed a percentage of the light from the optical probe, which decreased the amount of reflectance off the polymer. As the stained melt continued to pass underneath the light probe, the concentration of the ink is reduced and the voltage signal begins to increase again, as seen in Figure 3.32**.** The reduction in concentration was due to the inherent back mixing during extrusion. As the majority of the stained polymer moves through the channels of the mixing section, a percentage of the melt hits the paddles of the kneading blocks, causing a stagnation point. This caused some material to halt its forward progress or even more backwards slightly through the flow. The slowed motion of the melt leads to reduced concentration of stained polymer over time, as again seen in Figure 3.32. Once the voltage signal reached the initial established baseline and the collected extrudate from the die returned to its original pure white color (all ink was removed), the data acquisition program was then stopped. Figure 3.33 below shows an example of a completed experimental run that reached the starting baseline.

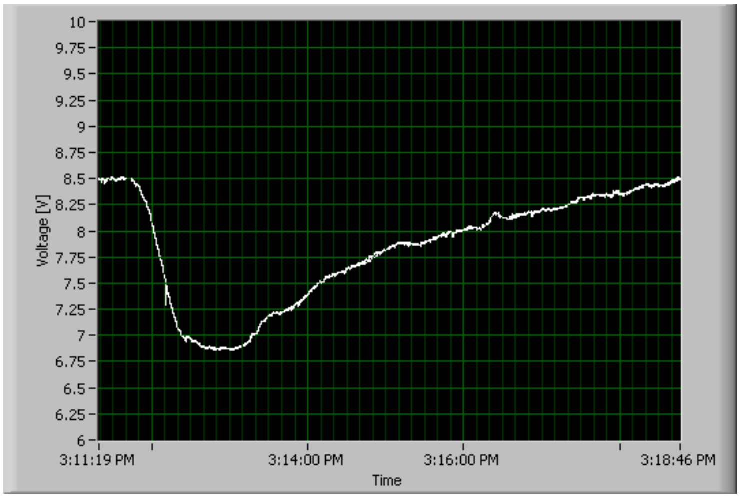

Figure 3.33 - Completed experimental run

The result from the experiment was a generated residence-time distribution curve using a concentrated amount of die, as seen in Figure 3.33.

After all the ink was removed from the extruder, the experiment was then set up for the next experimental run using the CAMES beads. To prepare for the next experiment, the data acquisition was reinitiated and the syringe was filled with a comparable amount of sensors beads to that of the ink shot, which was 0.51 grams. Before the beads were injected, a baseline was again established for at least 15 seconds. The beads were then injected and the procedure was repeated. When the voltage signal reached the initial baseline after dropping due to the concentration of the beads, the end result of an experiment using the CAMES sensors was a residence-stress distribution curve. A residence-stress distribution is similar to that of a residence time distribution except that the amplitude of the curve (concentration) is a function of the stress exerted onto the polymer melt. The higher the magnitude of stress, the higher the amplitude of the residence-stress distribution curve because as more CAMES beads rupture, the concentration of dye released into the flow increased.

For an operating condition, four experiments were run, two replicas of ink injections yielded residence time distributions and two replicas of CAMES beads injections produced residence stress distributions. This was performed for all nine operating conditions on the experimental CCD grid for a given screw geometry.

3.4.2 Analytical Procedures

3.4.2.1 Percent Breakup Calculation

Once a full experiment was performed on an operating condition, analysis of the data was the next step. To do so, a LabVIEW program was developed to generate traditional RTD curves and extract important information from them. Traditional RTD curves have a positive area, i.e. they typically have values greater than the initial baseline; however, the curves generated by the light probe (Figure 3.33) are pointed downward (measured voltages are less than the baseline value), so this had to be corrected. The LabVIEW program that was used for analysis consisted of three main parts of the program. The first part was to read the data file generated by the light probe, as seen in Figure 3.34. The two files that were read were an ink RTD curve (top) and a CAMES RSD curve (bottom).

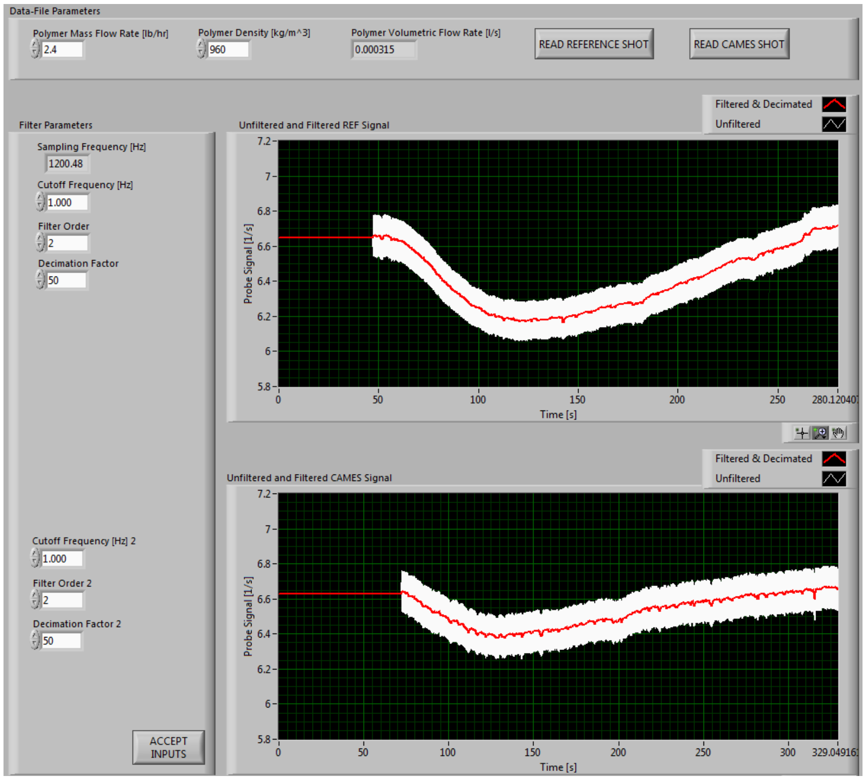

Data-File Parameters

Polymer Mass Flow Rate [lb/hr]: 2.4

Polymer Density [kg/m^3]: 960

Polymer Volumetric Flow Rate [l/s]: 0.000315

Filter Parameters

Sampling Frequency [Hz]: 1200.48

Cutoff Frequency [Hz]: 1.000

Filter Order: 2

Decimation Factor: 50

Cutoff Frequency [Hz] 2: 1.000

Filter Order 2: 2

Decimation Factor 2: 50

Figure 3.34 - First part of LabVIEW analysis program

It is important to note the differences in the beginning of the two curves compared to the rest of the curves. To simplify the analysis, a single value was inserted before the curve begins to drop down. This ensured that the calculated area underneath the curves did not vary if a different delay point was selected. The delay point was the point in the curve in which the data would “flip itself over.” That is, whichever value was selected as the delay point, the following points in the curve subtracted their voltage value from the delay point. This flipped the curve over the x-axis, as shown in Figure 3.35.

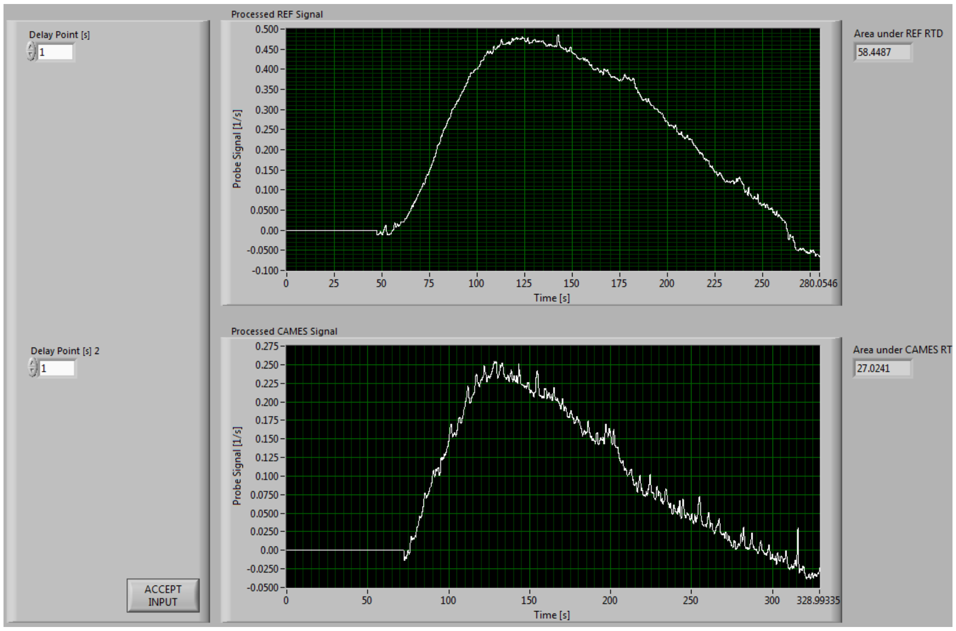

Delay Point [s]: 1

Area under REF RTD: 58.4487

Delay Point [s] 2: 1

Area under CAMES RT: 27.0241

Figure 3.35 - "Flipped" ink and CAMES curves with corresponding areas underneath the curves

After the curves were flipped, the areas underneath each were calculated and were displayed next to the respective RTD or RSD curve. When the areas were calculated, the percentage of CAMES beads that were broken was determined using the following equation:

$$\%\,Breakup = \frac{A_C}{A_R} x100\% \tag{3.1}$$

Where A_C is the area under the CAMES RSD curve and A_R is the area under the ink RTD curve. For a visualization of the two curves together, they were both normalized with respect to the area under the ink RTD curve and plotted, as seen in Figure 3.36.

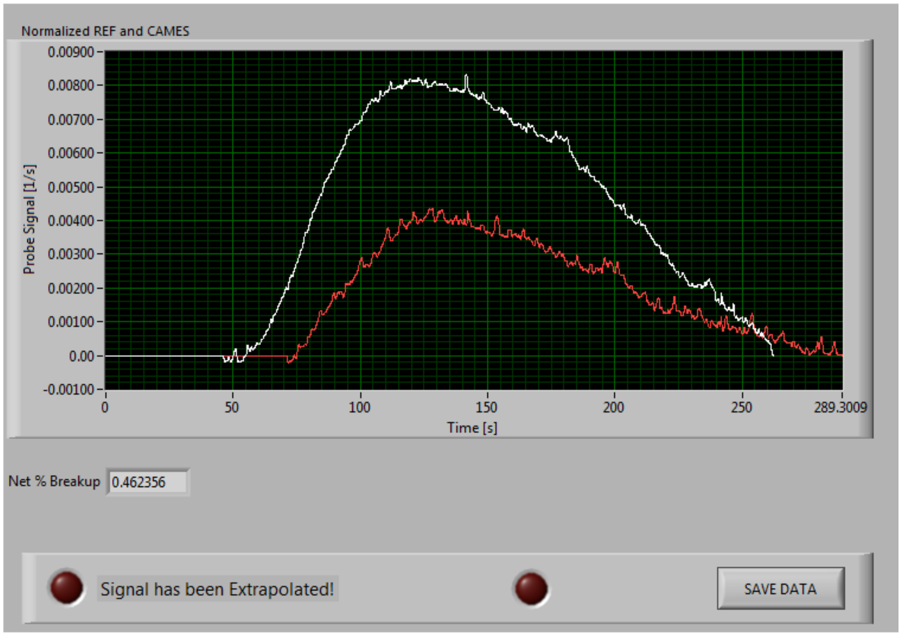

Net % Breakup 0.462356

Signal has been Extrapolated!

Figure 3.36 - Normalized RTD and RSD plotted together

The results are then written to an excel file where plotting and further extraction of data can take place. Additionally, the file size was decimated by a factor of 50 to reduce file size and increase computing capacity. This process was performed for each combination of ink and CAMES to produce an average percent breakup and experimental error for every operating condition on a central composite design grid.

3.4.2.2 Curve Modeling

Looking at the two data curves presented in Figure 3.36, although the curves looked smooth, there were still small spikes and dips in other data that made the curves look visually unpleasing. Additionally, when the data was transformed to other domains, such as RVD and RRD domains, the differences in the shapes of the curves caused problems. By using a model, transformations were performed more easily and the residence distribution curves are more visually appealing. The selected model was a two-parameter Weibull distribution. Due to its versatility in modeling data because of its various parameters [60], it was used to model the RTD and RSD data. The equation for a two-parameter Weibull distribution is given by:

$$f(x; \lambda, k) = \frac{k}{\lambda}\left(\frac{x}{\lambda}\right)^{k-1} e^{-\left(x/\lambda\right)^{k}} \tag{3.2}$$

Where k is the shape parameter (k > 0) and λ is the scale parameter (λ > 0). Using MATLAB, a program was written (See Appendix A) to try various combinations of k and λ, and select the best values of the parameters that reduced the error between the model and the raw data. After the values have been selected, the program produced a model curve that fit the data and exported it to excel where it could be used for plotting and domain transformations. An example of the curve with the raw data is seen in as seen in Figure 3.37.

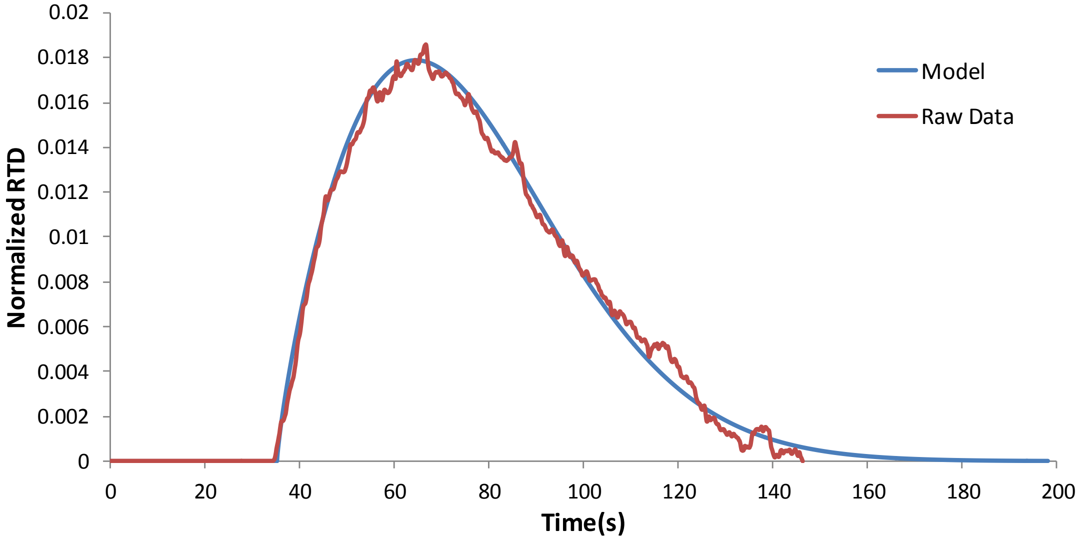

Figure 3.37 - Ink RTD with Weibull model

As the figure above indicates, the Weibull distribution model was a good fit for this data, as it is with all the generated residence-time and residence-stress distribution curves. Using the modeled data, trends in the RVD and RRD domains were more easily observed because the general shapes of the models were the same.

3.4.2.3 Statistical Analysis

The central composite design of experiment grids were selected because special statistical analyses can be performed to generate an equation that predicts the percent breakup for individual or numerous combined grids. Using JMP ® 9.0.0 software, the statistical analyses of these grids was performed quickly and easily. After an analysis had been performed, a report would be generated, providing information such as the coefficient of determination (R^2), values for the parameters, and how statistically significant each parameter was. Only parameters that were statistically significant were included in the prediction equations. An example of a report can be seen in Figure 3.38.

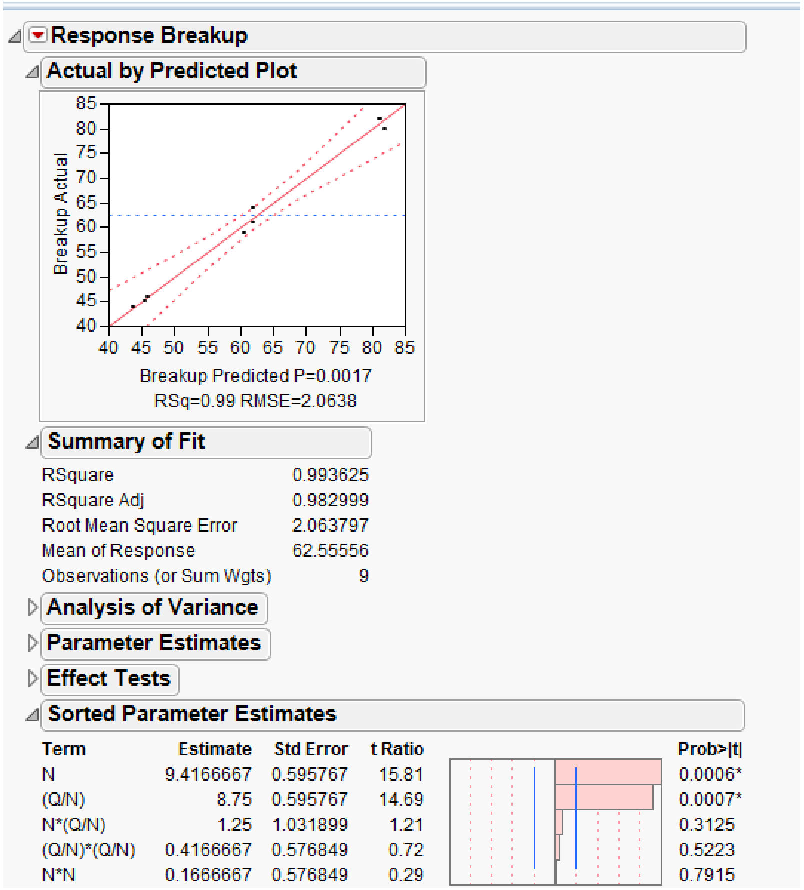

Response Breakup

Actual by Predicted Plot

Breakup Predicted P=0.0017
RSq=0.99 RMSE=2.0638

Summary of Fit

RSquare	0.993625
RSquare Adj	0.982999
Root Mean Square Error	2.063797
Mean of Response	62.55556
Observations (or Sum Wgts)	9

Analysis of Variance

Parameter Estimates

Effect Tests

Sorted Parameter Estimates

Term	Estimate	Std Error	t Ratio	Prob>|t|
N	9.4166667	0.595767	15.81	0.0006*
(Q/N)	8.75	0.595767	14.69	0.0007*
N*(Q/N)	1.25	1.031899	1.21	0.3125
(Q/N)*(Q/N)	0.4166667	0.576849	0.72	0.5223
N*N	0.1666667	0.576849	0.29	0.7915

Figure 3.38 - Report generated from JMP statistical analysis software

Chapter 4 Theoretical Calculations

This chapter reviews the theoretical calculations that were used for this study.

4.1 Percent Drag Flow

The percent drag flow, or percent channel fill, is a very important parameter for designing the extruder screws and optimizing the operating conditions of the machine. Percent drag flow refers to how full a screw element is with polymer melt, with 100% being completely full. Figure 4.1 below shows the geometry of a typical screw, which will be used for the drag flow calculation.

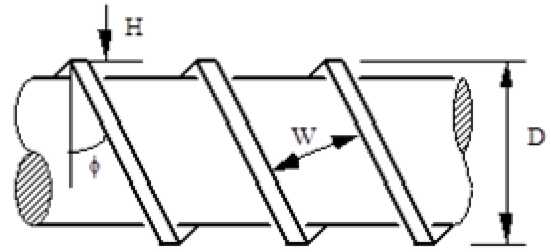

Figure 4.1 - Sketch of a screw

To compute drag flow, one must first consider how to compute the total flow rate. The total flow rate, Q_{total}, is the calculated as the sum of the drag flow rate, Q_{drag}, and the pressure flow rate, $Q_{pressure}$, as seen in Equation 4.1.

$$Q_{total} = Q_{drag} + Q_{pressure} \tag{4.1}$$

To evaluate Q_{drag} and $Q_{pressure}$, (Equations 4.2 and 4.3, respectively) it is first assumed that the flow cross section of the screw channel is rectangular. By applying shape factors (F_d and F_p), the assumption is corrected as the cross section of flow is not actually rectangular.

$$Q_{drag} = \frac{(2\mathrm{n}-1)}{2} v_{bz} W H F_d \tag{4.2}$$

$$Q_{pressure} = \frac{(2n-1)}{12} \frac{WH^3}{\mu} \left(-\frac{\partial P}{\partial z}\right) F_p \tag{4.3}$$

Where:

n = number of flights on the element (2 for a bi-lobe and 3 for a tri-lobe)

W = width of the screw channel (mm)

H = height of the screw channel (mm)

v_{bz} = down channel component of the barrel velocity (m/s)

μ = polymer viscosity (Pa·s)

$(-\partial P/\partial z)$ = down channel pressure gradient (Pa/m)

F_d = drag flow shape factor, which is a function of the ratio of H/W

F_p = pressure flow shape factor, which is also a function of the ratio of H/W

The values of F_d and F_p can be obtained from work performed by Denson and Hwang [61] and Booy [62].

In the absence of a down channel pressure gradient (due to an open discharge or a partially filled channel), $Q_{pressure}$ goes to zero. This yields that the total flow rate is only equal to the drag flow rate (Equation 4.5). Additionally, the down channel barrel velocity, v_{bz}, can be rewritten as:

$$v_{bz} = \pi DNcos(\varphi) \tag{4.4}$$

Where:

D = diameter of the screw (mm)

N = screw rotation speed (rpm)

φ = helical angle of the screw flight (degrees)

$$Q_{total} = Q_{drag} = \frac{(2\mathrm{n}-1)}{2} v_{bz} W H F_d \tag{4.5}$$

Substituting Equation 4.4 into Equation 3.5, the drag flow rate becomes:

$$Q_{drag} = \frac{(2n-1)}{2} \pi D W H N F_d \cos(\varphi) \tag{4.6}$$

The desired specific throughput, an estimate of the degree of fill in the partially filled sections, *(Q/N)*, is determined by the percent channel fill and the specific throughput at 100% drag flow, as calculated in Equation 4.7.

$$\left(\frac{Q}{N}\right)_{desired} = (\%\ Drag\ Flow) \left(\frac{Q}{N}\right)_{100\%\ drag} \tag{4.7}$$

To calculate the specific throughput at 100% drag flow, Equation 4.6 above is to be used, but with slightly different notation.

$$\left(\frac{Q}{N}\right)_{100\%\ drag} = \frac{(2n-1)}{2} \pi D W H N F_d \cos(\varphi) \tag{4.8}$$

To calculate the percent drag flow or percent channel fill, take the ratio of volumetric flow rate of all the materials fed into the extruder, Q_t, and the flow rate at 100% drag flow (Equation 4.8) for the same screw configuration and same screw speed, as seen in Equation 4.9 below.

$$\% \, Drag \; Flow = \left(\frac{Q_t}{Q_{100\% \, drag}} \right) \times 100 \tag{4.9}$$

Using Equation 4.9, the percent drag flows for each experimental operating condition were obtained. Table 4.1 below displays the dimensions and other variables for the 28-mm, 26-mm, and 18-mm twin-screw extruders.

Table 4.1 - Dimensions of kneading blocks used on twin-screw extruders

Dimension	**28-mm Narrow KB**	**28-mm Wide KB**	**26-mm Narrow KB**	**26-mm Medium KB**	**26-mm Wide KB**	**18-mm Narrow KB**	**18-mm Medium KB**
D (mm)	28	28	26	26	26	18	18
W (mm)	10.5	18	9	9.4	14.5	8	8
H (mm)	2.54	2.54	4.55	4.55	4.55	3.2	3.2
φ (^{o})	24	50	25	25	35	15.8	15.8
n	3	3	2	2	2	2	2
F_d	0.758	0.859	0.494	0.515	0.686	0.68	0.68

Using the dimensions of each extruder from the table above and the operating conditions presented in the CCD grids in Sections 3.3.1 – 3.3.3, the corresponding drag flow for each kneading block used can be calculated. Tables 4.2, 4.3, and 4.4 present the calculated percent drag flows for the 28-mm, 26-mm, and 18-mm extruders, respectively.

Table 4.2 - Drag flow calculations for 28-mm TSE

Operating Conditions		$Q_{100\%\ drag}$ (lb/hr)	Narrow KB	Wide KB
Screw Speed (rpm)	Flow Rate (lb/hr)		Drag Flow (%)	Drag Flow (%)
40	1.95	16.1	12	9
75	2.4	30.1	8	6
75	4.8	30.1	16	12
110	1.8	44.2	4	3
110	5.3	44.2	12	9
110	8.8	44.2	20	15
145	4.6	58.3	8	6
145	9.3	58.3	16	12
180	8.7	72.4	12	9

Table 4.3 - Drag flow calculations for 26-mm TSE

Operating Conditions		$Q_{100\%\ drag}$ (lb/hr)	Narrow KB	Medium KB	Wide KB
Screw Speed (rpm)	Flow Rate (lb/hr)		Drag Flow (%)	Drag Flow (%)	Drag Flow (%)
90	11	19.5	60	55	30
120	12	26.1	45	40	25
120	20	26.1	75	70	35
150	10	32.6	30	25	15
150	20	32.6	60	55	30
150	30	32.6	90	85	45
180	20	39.1	45	40	25
180	30	39.1	75	70	35
210	26	45.6	60	55	30

Table 4.4 - Drag flow calculations for 18-mm TSE

Operating Conditions		$Q_{100\%\ drag}$ (lb/hr)	Narrow KB	Medium KB
Screw Speed (rpm)	**Flow Rate (lb/hr)**		**Drag Flow (%)**	**Drag Flow (%)**
140	7	19.7	35	35
190	8	26.7	30	30
190	10	26.7	40	40
240	8	33.7	25	25
240	12	33.7	35	35
240	15	33.7	45	45
290	12	40.8	30	30
290	16	40.8	40	40
340	16	47.8	35	35

As seen in all the drag flow calculation tables for the 28-mm and 26-mm extruders, narrow kneading blocks have the higher percent drag flows than medium and wide kneading blocks. This is due to the smaller channels of the narrow kneading blocks, which increases the percent of the channel that is filled with polymer melt. Wide kneading blocks have the lowest percent drag flows because the channels of these kneading blocks are the widest.

Looking at percent drag flow calculations for the 18-mm extruder, it is observed that the drag flows are the same for the narrow and medium kneading blocks (the dimensions in Table 4.1 for both kneading blocks are also the same). Due to the very small size of the narrow and medium kneading blocks, measuring the dimensions on these elements is very difficult. To overcome this obstacle, the dimensions of the conveying element just before the mixing section were recorded. It was assumed that because the mixing section would be completely full (due in part by the two reverse elements after the kneading blocks), the percent drag flow rate from the preceding conveying element would be the same as the kneading blocks in the mixing section.

The percent drag flow results will be used to help explain certain phenomena inside the extruder. Additionally, it will be used in conjunction with obtained results to possibly making predictions regarding the stress history inside the extruders.

4.2 CAMES Beads Critical Stress Levels

The CAMES beads provided by MACH I Inc, (as discussed in Section 3.2.2) were calibrated using a capillary flow device. The shear stress at the wall was used to correlate with the breakup of the beads; however, under normal laminar flow, the stress distribution in a capillary tube is not uniform. Consequently, the wall shear stress does not represent the actual shear stress experienced by the beads. It is necessary to develop a theoretical model to calculate the critical shear stress (the stress in which the beads will begin to break) [63].

To create the model, first consider the flow inside of a capillary tube, as seen in Figure 4.2. Due to the high viscosity of the fluid inside the very a capillary tube with very small diameter, the flow can be considered laminar.

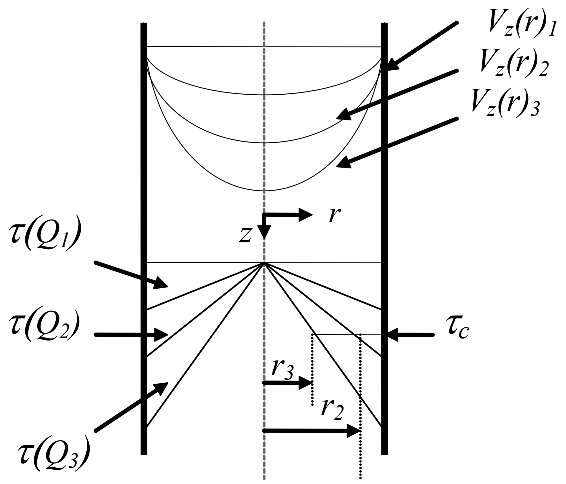

Figure 4.2 - Sketch of flow field and stress distribution inside a capillary tube [63]

Starting from the Navier-Stokes Equation in cylindrical coordinates in the z-direction (Equation 4.10):

$$\rho\left(\frac{\partial u_z}{\partial t}+u_r\frac{\partial u_z}{\partial r}+\frac{u_\varphi}{r}\frac{\partial u_z}{\partial \varphi}+u_z\frac{\partial u_z}{\partial z}\right) = -\frac{\partial P}{\partial z}+\mu\left[\frac{1}{r}\frac{\partial}{\partial r}\left(r\frac{\partial u_z}{\partial r}\right)+\frac{1}{r^2}\frac{\partial^2 u_z}{\partial \varphi^2}+\frac{\partial^2 u_z}{\partial z^2}\right]+\rho g_z \tag{4.10}$$

This equation reduces to, after simplification.

$$\frac{1}{r}\frac{d}{dr}(r\tau_{zr})+\frac{dP}{dz}=0 \tag{4.11}$$

Applying the boundary condition: $\tau_{zr}=0$ at $r=0$, the stress distribution inside the capillary tube becomes:

$$\tau_{zr}=\left(\frac{\Delta P}{L}\right)r \tag{4.12}$$

From Equation 4.12, the shear stress ($\tau(Q_i)$ in Figure 4.2) is related to the pressure difference at a given radial position. By determining the cross-sectional area of the flow that exceeds the critical stress level (τ_c), the percent breakup can then be calculated as a function of the flow rate.

The velocity profile of a Newtonian fluid can be obtained (Equation 4.13) from the Navier-Stokes Equation (4.10).

$$V_z = \left(\frac{\Delta P R^2}{4\mu L}\right)\left[1 - \left(\frac{r}{R}\right)^2\right] \tag{4.13}$$

The flow rate of the fluid between R and r_c (where r_c is the radial position where $\tau_{zr} = \tau_c$) can be calculated using Equation 4.14 and the total flow rate can be calculated using Equation 4.15.

$$Q_c = \int_0^{2\pi} \int_{r_c}^{R} V_z r dr d\theta \tag{4.14}$$

$$Q_T = \int_0^{2\pi} \int_0^{R} V_z r dr d\vartheta \tag{4.15}$$

The percent breakup of the beads can then be calculated by taking the ratio of Q_c/Q_T.

$$Percent\ Breakup = \frac{Q_c}{Q_T} = \left[\left(\frac{r_c}{R}\right)^2 - 1\right]^2 \tag{4.16}$$

Rearranging the terms and solving for r_c (the radial position corresponding to the critical shear stress):

$$r_c = R\sqrt{1 + \sqrt{P}} \tag{4.17}$$

Where P = the percent breakup (%). Plugging Equation 4.17 into Equation4.12, the critical shear stress (τ_c) and shear stress at the wall (τ_w) can now be used in relation to the percent breakup, as seen in Equation 4.18.

$$\sqrt{P} = 1 - \left(\frac{\tau_c}{\tau_w}\right)^2 \tag{4.18}$$

Rearranging the terms above, the critical shear stress of the CAMES beads can be calculated from the given wall shear stress data from Mach I, Inc. in the equation below.

$$\tau_c = \tau_w \sqrt{1 - \sqrt{P}} \tag{4.19}$$

Using Equation 4.19, and the wall shear stress data, the critical stress levels of the beads were calculated, and displayed in the following tables. Since only 10% and 90% rupture data was provided, the wall shear stress values had to be interpolated for intermediate rupture percentages. From this, the critical stress level at each rupture percentage could be calculated. To determine the overall critical stress level, the average of each rupture percentage critical stress level was taken. The critical stresses of the CAMES beads are presented in Table 4.5.

Table 4.5 - Calculation of CAMES beads critical stresses

Diameter of Bead [µm]	τ_w for 10% rupture [kPa]	τ_w for 90% rupture [kPa]	Calculated τ_c [kPa]
X > 90	175	290	119
X < 44	225	700	223
X > 75	120	250	92
45 < X < 75	190	450	158

The calculated values of the critical stress levels are important for determining the relative magnitude of stress the beads are experiencing. Additionally, theoretical calculations of stress can now be performed to inspect the magnitudes of potential mechanisms for bead rupture.

4.3 Shear Stress

Shear stresses induced on the polymer melt and any additives by the conveying elements and kneading blocks play a role in the degree of mixing. For this study, it was important to know the approximate magnitude of the shear stresses.

Shear stress (τ) is given by Equation 4.20:

$$\tau = \mu\dot{\gamma} \tag{4.20}$$

Where:

τ = shear stress (Pa)

μ = viscosity (Pa·s)

$\dot{\gamma}$ = shear rate (sec^{-1})

The shear rate in an extruder screw channel can be calculated using 4.21.

$$\dot{\gamma} = \frac{\pi D N}{60 \times H} \tag{4.21}$$

Plugging Equation 4.21 into 4.20 and determining the viscosity of the polymer for a given shear rate (most polymers are shear thinning, so the viscosity of the polymer decreases as shear rate increases), the induced shear stress can be calculated using the following equation:

$$\tau = \mu\left(\frac{\pi D N}{60 \times H}\right) \tag{4.22}$$

Using Equation 4.22, the theoretical shear stresses induced by a screw element was calculated. Table 4.6 below provides the height and diameter of the conveying elements, as well as the five screw speeds used to calculate the shear stress on the machines used.

Table 4.6 - Screw dimensions and screw speeds for shear stress calculations

	28-mm TSE	26-mm TSE	18-mm TSE
Channel Height [H] (mm)	2.5	4.5	3.2
Screw Diameter [D] (mm)	28	26	18
Screw Speed 1 (rpm)	40	90	140
Screw Speed 2 (rpm)	75	120	190
Screw Speed 3 (rpm)	110	150	240
Screw Speed 4 (rpm)	145	180	290
Screw Speed 5 (rpm)	180	210	340

The three tables below present the calculated shear stresses for each machine using the equations presented in this section. The viscosity values at each shear rate were determined using viscosity data (Figure 4.3) provided by DuPont on the Alathon H6018 HDPE at 200^{o}C.

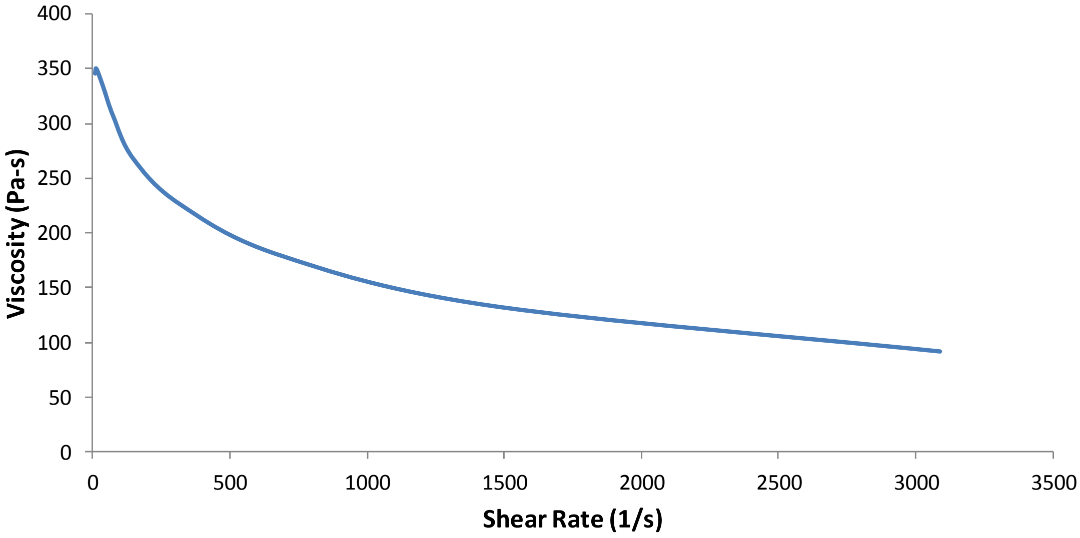

Figure 4.3 - Viscosity of HDPE at 200^{o}C for given shear rates

Table 4.7 displays the shear stress for the 28-mm extruder,

Table 4.8 provides the shear data for the 26-mm extruder, and

Table 4.9 shows the shear stresses for the 18-mm twin-screw extruder.

Table 4.7 - Calculated shear stress for the 28-mm TSE

Screw Speed (rpm)	Shear Rate (sec^{-1})	Viscosity (Pa·s)	Shear Stress (kPa)
40	23.5	341.6	8.0
75	44.0	327.5	14.4
110	64.5	312.5	20.2
145	85.0	299.9	25.5
180	105.6	289.0	30.5

Table 4.8 - Calculated shear stress for the 26-mm TSE

Screw Speed (rpm)	Shear Rate (sec^{-1})	Viscosity (Pa·s)	Shear Stress (kPa)
90	26.9	339.3	9.1
120	35.9	333.4	12.0
150	44.9	326.8	14.7
180	53.9	320.6	17.3
210	62.8	313.7	19.7

Table 4.9 - Calculated shear stress for the 18-mm TSE

Screw Speed (rpm)	Shear Rate (sec^{-1})	Viscosity (Pa·s)	Shear Stress (kPa)
140	41.2	329.5	13.6
190	56.0	318.7	17.8
240	70.7	308.0	21.8
290	85.4	299.7	25.6
340	100.1	291.9	29.2

As seen from the three tables, the highest shear stress is induced by the 28-mm conveying element. The screw speeds run on the 28-mm were slower than those run on the 26-mm extruder and much slower than the 18-mm extruder, yet due to the fact that it is a tri-lobed element (i.e. shallower channels), more shear stress is generated. From these calculations, it is noticeable that the stress levels induced in shear do not match the critical stress levels of the CAMES beads (Table 3.1), indicating that shear stress alone cannot be the cause of achieving large percentages of beads to rupture.

4.4 Elongational Stress

The elongational stress is induced by the squeezing of the polymer melt between kneading block paddles. To calculate the approximate stresses induced on the material, consider the flow between two plates. One of the plates is stationary, and the other is moving towards the plate, as seen in Figure 4.4

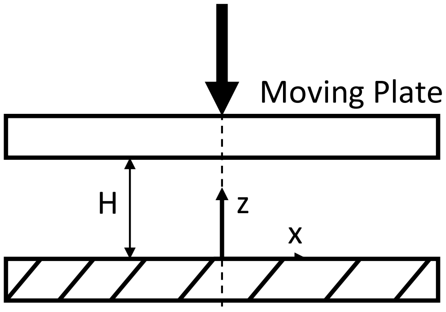

Figure 4.4 - Flow between two plates

As the top plate moves toward the bottom, fixed plate, the material between the plates is squeezed and forced out the sides. Starting with the vorticity equation, as seen in Equation 4.23:

$$\frac{D\vec{\omega}}{Dt} = (\vec{\omega}\cdot\vec{\nabla})\vec{V} - \vec{\omega}(\vec{\nabla}\cdot\vec{V}) + \frac{1}{\rho^2}\vec{\nabla}\rho \times \vec{\nabla}P + \vec{\nabla}\times\left(\frac{\vec{\nabla}\cdot\underline{\underline{\tau}}}{\rho}\right) + \vec{\nabla}\times\vec{B} \quad (4.23)$$

Where:

$\vec{\omega}$ = vorticity

$\vec{V}$ = velocity vector

ρ = density

P = pressure

$\underline{\underline{\tau}}$ = viscous stress tensor

$\vec{B}$ = body force term

Combining with the stream function (Equation 4.24):

$$\nabla^2\psi = -\omega \tag{4.24}$$

Substituting Equation 4.24 into Equation 4.23, and solving for the stream function (which is done so in numerous fluid mechanics text books), the resulting non-dimensional relationship (Equation 4.25) is given by:

$$\psi^* = x\left(\frac{3z^{*2}}{\xi^{*2}} - \frac{2z^{*3}}{\xi^{*3}}\right) \tag{4.25}$$

The dimensionless variables are:

$$\psi^* = \frac{\psi}{VL} \tag{4.26}$$

$$x^* = \frac{x}{L} \tag{4.27}$$

Where V is the velocity of the moving plate and L is the length of the plate.

$$z^* = \frac{z}{H_o} \tag{4.28}$$

$$\xi^* = \frac{H}{H_o} \tag{4.29}$$

Where H_o is the initial height between the two plates and H is the final height of the moving plate. Substituting for the dimensionless terms, the stream function (Equation 4.30) is given by:

$$\psi = Vx\left(3\left(\frac{z}{H}\right)^2 - 2\left(\frac{z}{H}\right)^3\right) \tag{4.30}$$

Using the following equation, the horizontal velocity component (u) can be determined by:

$$u = \frac{\partial \psi}{\partial z} = Vx\left(6\frac{z}{H^2} - 6\frac{z^2}{H^3}\right) \tag{4.31}$$

The term of interest is the extensional shear rate in the horizontal direction $\left(\frac{\partial u}{\partial x}\right)$. To obtain this, Equation 4.31 is differentiated with respect to x, to produce the extensional shear rate, as seen in Equation 4.32.

$$\frac{\partial u}{\partial x} = \frac{6V}{H^2}\left(z - \frac{z^2}{H}\right) \tag{4.32}$$

The z term is the position between the two plates, which is integrated over the height. To account for the different sized paddles of the kneading blocks, a width (w) term has been added. To keep the dimensions of the equation the same, another length scale term has been added on the left side of the equation, being the height between the plates. Additionally, it is believed that flow rate may play a role in the amount of stress produced by the kneading blocks, so a term has been added to account for its contribution. This produces the following relationship (Equation 4.33):

$$\frac{\partial u}{\partial x} = \frac{6Vw}{H^3}\int_{z_o}^{z_f}\left(z - \frac{z^2}{H}\right)dz + \frac{Q}{HwL} \tag{4.33}$$

The elongational stress (τ_e) can now be calculated using Equation 4.34.

$$\tau_e = \mu_e \frac{\partial u}{\partial x} \tag{4.34}$$

The μ_e term is the extensional viscosity, which is given by:

$$\mu_e = 3\mu \tag{4.35}$$

Using Equation 4.33 to calculate the extensional shear rate and applying that to Equation 4.34, the extensional stress induced on the polymer by the kneading blocks can be calculated. Table 4.10 below displays the values used for the calculations.

Table 4.10 - Kneading block dimensions for extensional stress calculations

	w (mm)	**L (mm)**	**H_o (mm)**	**H (mm)**	**z_o (mm)**	**z_f (mm)**
28-mm Narrow KB	2.5	12.1	4.5	1	4.5	1
28-mm Wide KB	8	12.1	4.5	1	4.5	1
26-mm Narrow KB	2.4	14.3	5	1	5	1
26-mm Medium KB	4.8	14.3	5	1	5	1
26-mm Wide KB	7.2	14.3	5	1	5	1
18-mm Narrow KB	1.6	9.9	5	1	5	1
18-mm Medium KB	3.2	9.9	5	1	5	1

Table 4.11 below shows the extensional stress calculations for the 28-mm TSE, Table 4.12 below shows the calculations for the 26-mm TSE, and Table 4.13 shows the extensional stress calculations for the 18-mm TSE.

Table 4.11 - Extensional stress calculations for 28-mm TSE

Operating Condition (lb/hr) / RPM	**28-mm Narrow KB (kPa)**	**28-mm Wide KB (kPa)**
1.95/40	42.56	136.18
2.4/75	76.51	244.79
4.8/75	76.52	244.80

1.8/110	107.07	342.58
5.3/110	107.08	342.59
8.8/110	107.10	342.59
4.6/145	135.45	433.38
9.3/145	135.48	433.39
8.7/180	162.05	518.44

Table 4.12 - Extensional stress calculations for 26-mm TSE

Operating Condition (lb/hr) / RPM	26-mm Narrow KB (kPa)	26-mm Medium KB (kPa)	26-mm Wide KB (kPa)
11/90	96.11	192.13	288.17
12/120	125.90	251.71	377.54
20/120	125.94	251.73	377.55
10/150	154.23	308.40	462.57
20/150	154.28	308.42	462.59
30/150	154.33	308.44	462.61
20/180	181.61	363.07	544.57
30/180	181.65	363.10	544.59
26/210	207.33	414.47	621.66

Table 4.13 - Extensional stress calculations for 18-mm TSE

Operating Condition (lb/hr) / RPM	18-mm Narrow KB (kPa)	18-mm Medium KB (kPa)
7/140	67.06	134.00
8/190	88.01	175.89
10/190	88.03	175.90

8/240	107.41	214.71
12/240	107.45	214.73
15/240	107.48	214.74
12/290	126.32	252.46
16/290	126.35	252.48
16/340	144.26	288.29

From these calculations, it is clear to see that extensional stresses due to the squeezing between the kneading blocks induce the magnitudes of stress required to break the CAMES beads. The calculations show the maximum extensional stresses for each other operating conditions at the boundaries of the paddles. The stresses within the material between the paddles (near the center of the flow) will be great enough to break the beads for certain conditions. This is seen primarily with the wide kneading blocks and higher screw speeds, which is confirmed by the results in the next chapter.

Chapter 5 Results

The results obtained from the experiments are discussed in this chapter. It has been separated into three parts: Constant N – Constant Q Plots, Central Composite Design Grids, and lastly the Residence Distributions.

5.1 Constant-N, Constant-Q Plots

The first set of data that was obtained was to investigate the effects of flow rate and screw speed on the percent breakup of CAMES beads. This data was collected by first selecting a screw speed, running the experiment for four or five different flow rates while keeping this screw speed constant, and plotting the results. This is referred to as a "Constant-N" plot. To investigate the effects of varying screw speed, a flow rate was selected and kept constant while running at four or five different screw speeds. The results were plotted in a "Constant-Q" plot. The following sections discuss the Constant-N and Constant-Q results for the three different machines.

5.1.1 28-mm TSE

The Constant-N and Constant-Q plots were created using screw designs #3 and #4 on the 28-mm twin-screw extruder. The critical stress of the CAMES beads that were used for both experiments was 92 kPa.

The Constant-N plot generated from obtained data using the 28-mm extruder is displayed in Figure 5.1. The screw speed was kept at a constant 110 RPM, while the flow rate was varied between 1.8 and 8.8 lb/hr.

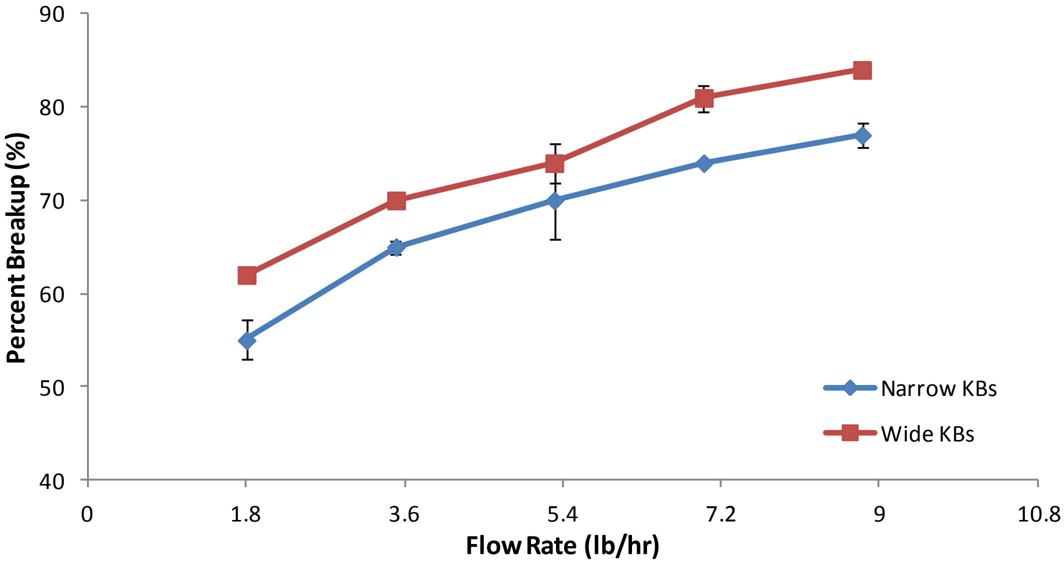

Figure 5.1 - Constant-N plot of narrow and wide KBs on 28-mm TSE

The figure above shows the effects of flow rates and kneading block size on the percentage of CAMES beads breakup. As the flow rate was increased, the percent breakup of beads also increased for both kneading blocks. Wide kneading blocks, as expected, broke a larger percentage of beads for each condition when compared to the narrow kneading blocks. Additionally, within the error, the slopes between data points were nearly identical for both kneading blocks. This indicated that the increase in flow rate produced a consistent increase in percent breakup between the two kneading blocks.

Another variable that was investigated that is related to screw speed and flow rate was the drag flow. The calculated percent drag flow for each operating condition can be seen in

Table 5.1.

Table 5.1 - Calculated percent drag flow per flow rate condition for 28-mm TSE

Flow Rate (lb/hr)	% Drag Flow Narrow KBs	% Drag Flow Wide KBs
1.8	4%	3%
3.5	8%	6%
5.3	12%	9%
7	16%	12%
8.8	20%	15%

As the flow rate increased (keeping screw speed constant), the percent drag flow also increased, as expected from the calculations presented earlier. Due to the very shallow flights and low volume capacity of the tri-lobed elements, the percent drag flows on this machine are much lower than the drag flows for the 26-mm and 18-mm extruders. The calculated drag flow percentages for both narrow and wide kneading blocks are very similar, only differing by a few percent. This similarity could be a factor in the slopes being the same between operating conditions for the different kneading blocks.

The Constant-Q plot using the 28-mm extruder (Figure 5.2) was generated using a constant flow rate of 4 lb/hr and varying the screw speed between 40 and 180 rpm in 35 rpm intervals.

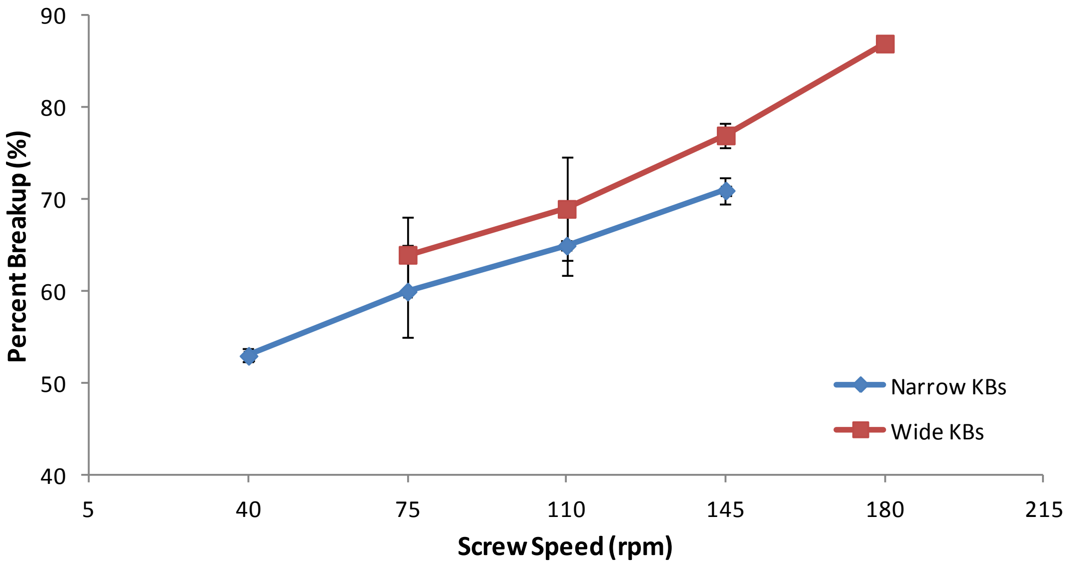

Figure 5.2 - Constant-Q plot of narrow and wide KBs on 28-mm TSE

This plot shows the impact screw speed and kneading block size has on the percent breakup of the sensor beads. Only four operating conditions from each screw design were run due to machine capability and time constraints. As the screw speed was increased for a constant flow rate, the percent breakup also increased for the narrow and wide kneading blocks. Similar to the Constant-N plot, the wide kneading blocks produced a higher percentage of broken beads than the narrow kneading blocks. Another observation similar to the Constant-N plot was the fact that the slopes of the data points were again nearly parallel.

The drag flow percentages for this set of operating conditions were calculated and put in Table 5.2.

Table 5.2 - Calculated percent drag flow per screw speed condition for 28-mm TSE

Screw Speed (rpm)	% Drag Flow Narrow KBs	% Drag Flow Wide KBs
40	25%	-
75	13%	10%
110	9%	7%
145	7%	5%
180	-	4%

As seen from the above table, the percent drag flows decreased as screw speed was increased, while keeping flow rate constant. However, between the two kneading blocks, the percent drag flow for the operating conditions that were run were again nearly identical. This again provided evidence that drag flow could potentially be a factor that impacted the results.

To see if there was any relationship between percent drag flow and percent breakup, an additional experiment was performed. Using the percent drag flows from the Constant-N experiment with a constant 110 rpm, another screw speed was selected, 75 rpm, and kept constant while varying the flow rate to achieve the same percent drag flows. The results from this experiment are displayed in Figure 5.3.

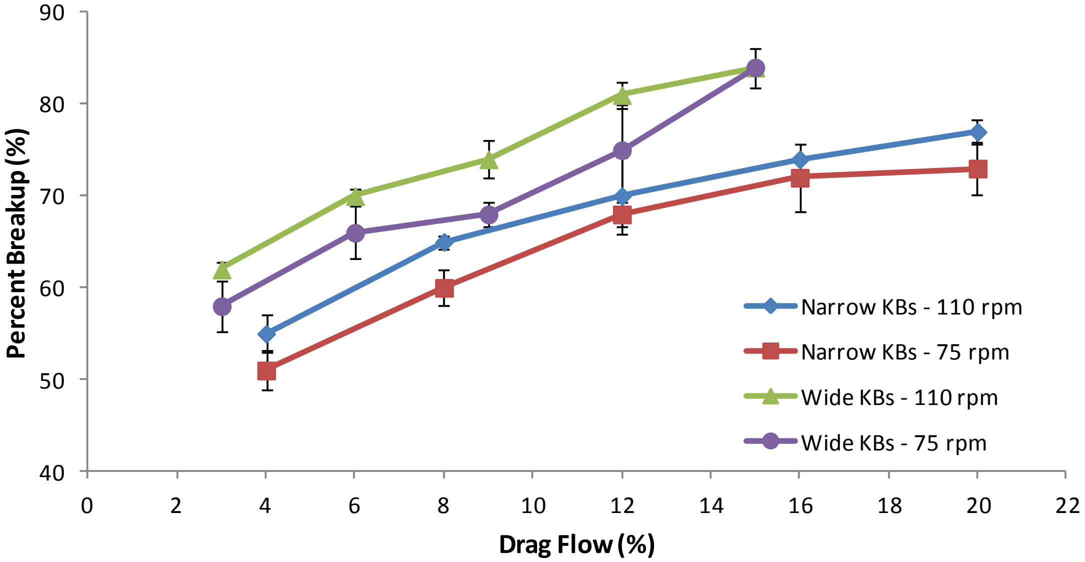

Figure 5.3 - Percent breakup as a function of percent drag flow using narrow and wide KBs on 28-mm TSE

The figure above shows the percent breakup as a function of percent drag flow for two different screw speeds using narrow and wide kneading blocks. For each operating condition and both kneading blocks, as drag flow increased, the percent breakup also increased. Looking at the two different screw speeds for the wide and narrow kneading blocks, within the given error, the trends in the data appear to be the same. The slope of the two wide kneading block curves is only slightly steeper than both narrow kneading block curves. However, looking at the four data curves together, the slopes of all four are very similar, with only two or three data points not quite fitting the rest of the data (i.e. the 75 rpm wide kneading block operating condition with a drag flow of 15%). This figure clearly shows that due to the fact that the percent drag flows are very close, the trends in the data are also the same.

5.1.2 26-mm TSE

Constant-N and Constant-N plots were also generated for the 26-mm twin-screw extruder. The two screw designs that were used were the 26-mm screw design #1 and #3. Screw design #1 was performed using the 92 kPa CAMES beads, and screw design #3 (wide kneading blocks) was performed using the 223 kPa beads.

The Constant-N plot was generated by setting the screw speed at a constant 150 rpm and varying the flow rate between 10 and 30 lb/hr in 5 lb/hr increments. The plot can be seen in Figure 5.4.

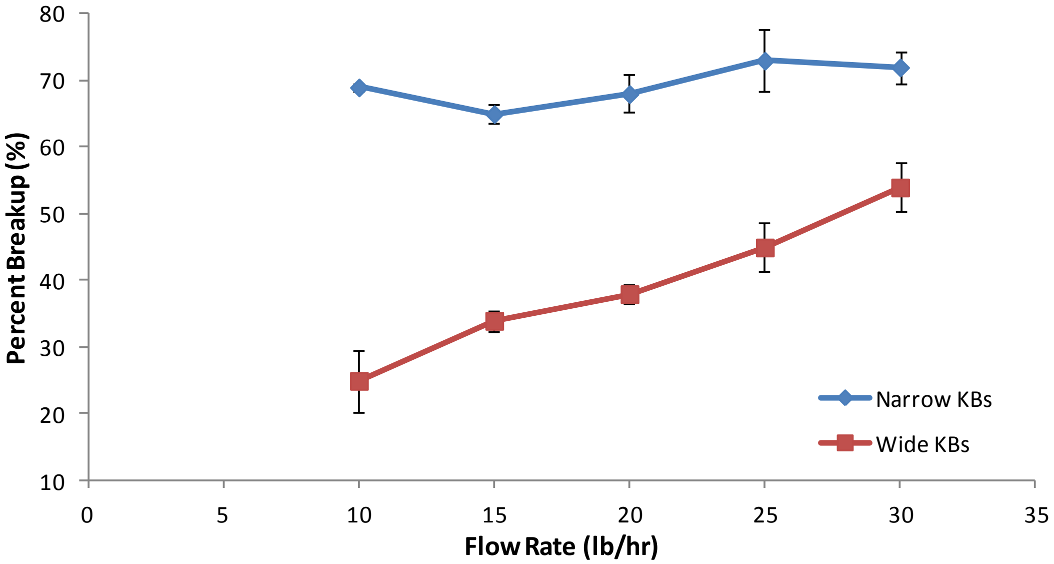

Figure 5.4 - Constant-N plot of narrow and wide KBs on 26-mm TSE

The figure above shows the percent breakup of CAMES beads as a function of flow rate. The figure indicated that the narrow kneading blocks induced a higher percent of bead breakage than the wide kneading blocks, which was not true. The wide kneading blocks used a significantly stronger CAMES bead, which is more than twice the strength of the bead used for the narrow kneading blocks. Although a direct comparison of bead breakup was unable to be done because of the large differences in bead strength, trends in the data, however, can still be observed. From Figure 5.4, it was observed that the two curves do not behave the same. The narrow kneading blocks data appears to have neither an increasing or decreasing trend, but a more level (flat) trend. For the five different flow rates used, the percent breakup is fairly constant (within error) at around 70%. However, this was not the case with the wide kneading blocks. The wide kneading blocks had an increasing trend in percent breakup as flow rate was increased, nearly doubling the percentage of broken beads from the 10 lb/hr condition to the 30 lb/hr.

The percent drag flow for each operating condition was calculated to see if they would provide further insight. The results are shown in Table 5.3.

Table 5.3 - Calculated percent drag flow per flow rate condition for 26-mm TSE

Flow Rate (lb/hr)	% Drag Flow Narrow KBs	% Drag Flow Wide KBs
10	30%	15%
15	45%	25%
20	60%	30%
25	75%	35%
30	90%	45%

As the table above shows, the drag flow percentages are very different between the two kneading blocks. Due to the large differences in size and volume capacity of the two elements, the drag flow percentages for the narrow kneading blocks are almost double that of the wide kneading block for every operating condition. The differences in the data trends as well as the percent drag flow, could again indicate that percent drag flow may be related to percent breakup.

The Constant-Q plot was generated by keeping a constant flow rate of 20 lb/hr and varying the screw speed from 90 to 210 rpm, in 30 rpm intervals. The results from the experiment are shown in Figure 5.5.

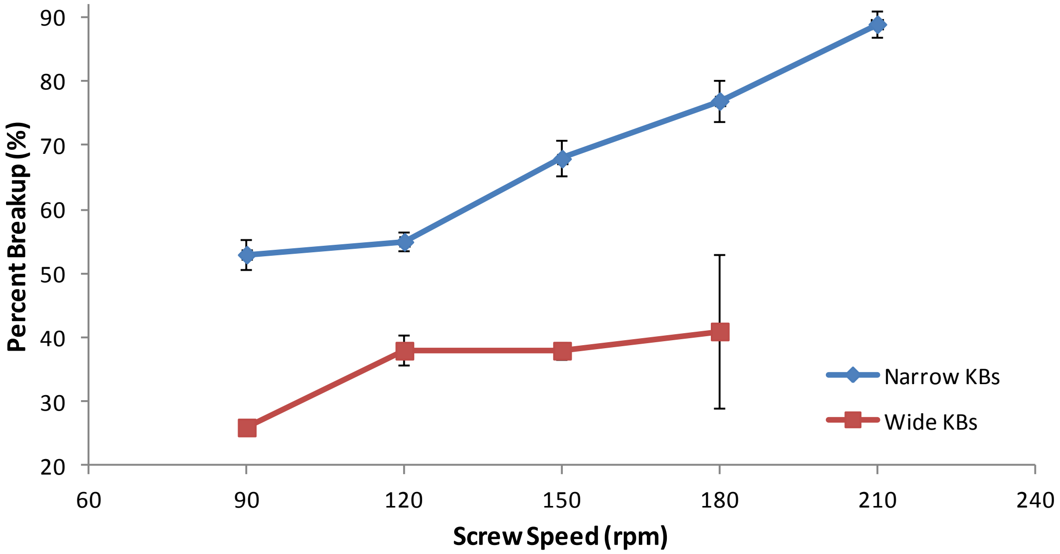

Figure 5.5 - Constant-Q plot of narrow and wide KBs on 26-mm TSE

The figure above shows the percent breakup of CAMES beads as a function of screw speed. Similar to Figure 5.4, the above figure indicates that the trends in the data were not the same between the two kneading blocks. The narrow kneading blocks showed an increase in percent breakup as screw speed also increased. This is expected as shown in the shear stress and elongational stress calculations presented earlier, induced stresses by the extruder increase as the screw speed of the extruder screws are increased. However, this was not the case for the wide kneading blocks. The wide kneading blocks data indicated a relatively flat trend. Although there was an increase in percent breakup from 90 to 120 rpm, the increases in percent breakup for the next two points are not as substantial. Figure 5.5 shows two clearly different trends in the data.

Table 5.4 below shows the calculated drag flow percentages for the performed operating conditions.

Table 5.4 - Calculate percent drag flow per screw speed condition for 26-mm TSE

Screw Speed (rpm)	% Drag Flow Narrow KBs	% Drag Flow Wide KBs
90	100%	50%
120	75%	40%
150	60%	30%
180	50%	25%
210	45%	-

The results from the percent drag flow calculations again indicate that there are large differences in the percent drag flow between the two kneading blocks. The drag flow percentages for the narrow kneading blocks are almost doubled that of the wide kneading blocks for each operating condition. The large differences in drag flow percentages and the different trends in the data from the Constant-Q plot could again be related.

5.1.3 18-mm TSE

The last set of Constant-N and Constant-Q experiments were performed using the 18-mm twin-screw extruder. Using the 18-mm screw designs #1 and #2, as well as 158 kPa CAMES beads, plots of Constant-N and Constant-Q were generated.

The Constant-N plot (Figure 5.6) was generated using a fixed screw speed of 240 rpm, and varying the flow rates between 8 and 15 lb/hr for narrow and medium kneading blocks.

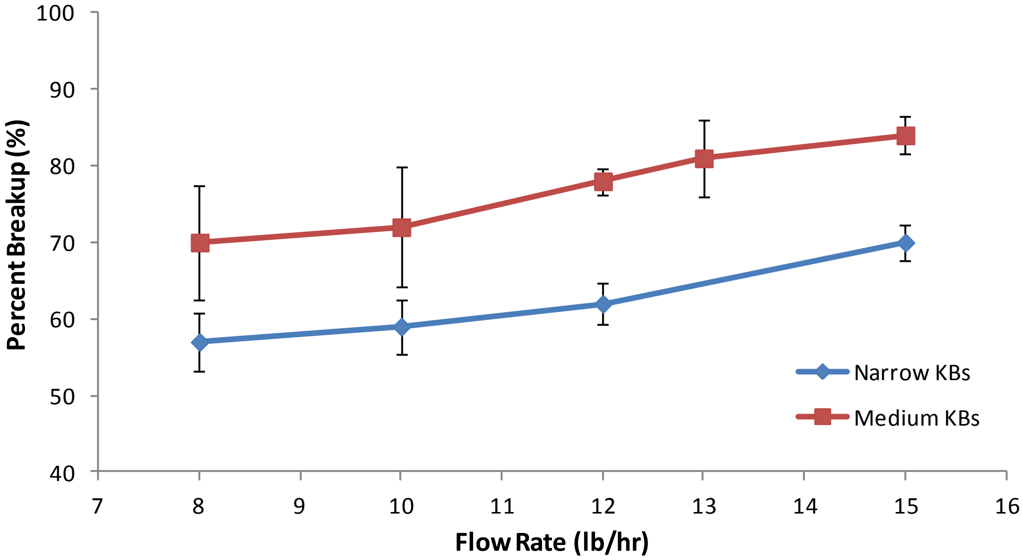

Figure 5.6 - Constant-N plot of narrow and medium KBs on 18-mm TSE

The above figure shows that as flow rate was increased, the percent breakup of CAMES beads also increased. The medium kneading blocks produced a higher percentage of bead breakup than the narrow kneading blocks for every operating condition. Another observation was that for this plot, the trends of the two data curves were nearly identical, with the slopes of the lines between two data points being nearly parallel for the narrow and wide kneading blocks.

The percent drag flow for each operating condition were calculated and displayed in Table 5.5.

Table 5.5 - Calculated percent drag flow per flow rate condition for 18-mm TSE

Flow Rate (lb/hr)	% Drag Flow Narrow KBs	% Drag Flow Medium KBs
8	25%	25%
10	30%	30%
12	35%	35%
13	-	40%
15	45%	45%

As the table above shows, the drag flow percentages are identical for the narrow and medium kneading blocks. As discussed previously in Section 4.1, the percent drag flows for these elements are the same due to the inability to obtain accurate measurements of the narrow kneading blocks because the size was so small. So the conveying element before the mixing section was used to determine the percent drag flow. Similar to the 28-mm Constant-N plot and drag flow calculations, the similar trends in the data were related to the percent drag flows of the two kneading blocks being the same.

The Constant-Q plot was produced by keeping a constant flow rate of 12 lb/hr while varying the screw speed from 190 to 340 rpm, in 50 rpm intervals. The plot can be seen in Figure 5.7.

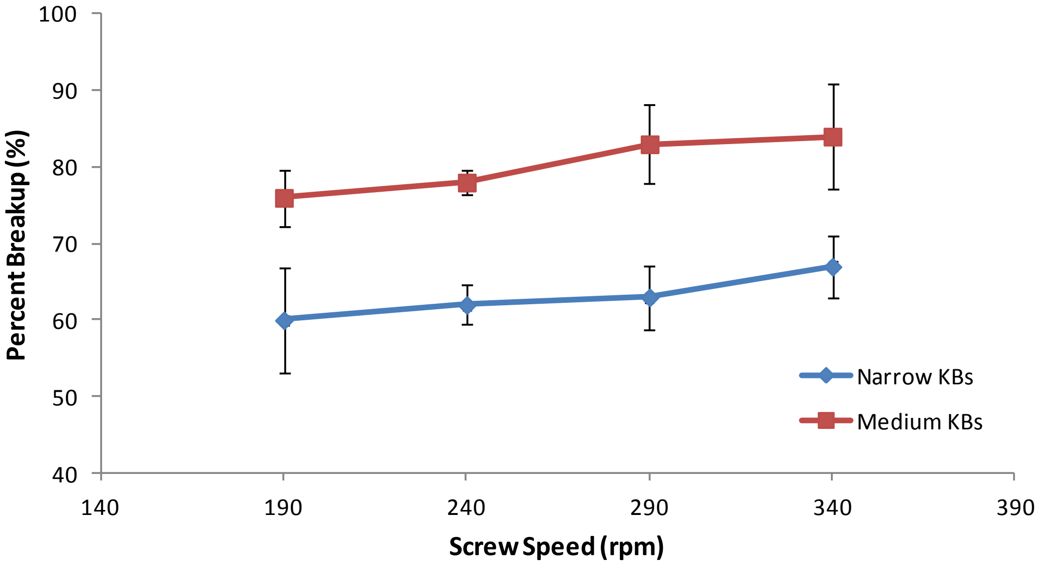

Figure 5.7 - Constant-Q plot using narrow and medium KBs on 18-mm TSE

The figure above displays the percent breakup of beads as a function of the screw speed for four different speeds. Within the given error, it was seen that the percent breakup increased as the screw speed increased, although not very significantly. The slopes of the lines between the data points are again very similar between the two kneading blocks, within the given error.

The percent drag flows for the two kneading blocks were calculated and presented in Table 5.6.

Table 5.6 - Calculated percent drag flow per screw speed condition for 18-mm TSE

Screw Speed (rpm)	% Drag Flow Narrow KBs	% Drag Flow Medium KBs
190	40%	40%
240	35%	35%
290	30%	30%
340	25%	25%

Similar to Table 5.5, the percent drag flows are the same between the two kneading blocks. With the trends in the data being nearly identical and the drag flow percentages being the same between the narrow and wide kneading blocks, this again provided evidence that there was a relationship between the percent drag flow and the trends in the percent breakup data.

5.1.4 Constant-N, Constant-Q Conclusions

From the data generated by the Constant-N and Constant-Q plots for the three different-sized twin-screw extruders, four initial observations/conclusions were made from this small set of data:

1. Percent breakup increased as the screw speed increased, for a constant flow rate

With the exception of one set of data (26-mm wide kneading blocks), this observation is true in all cases. This was an expected result because shear stress and elongational stress are both a function of screw speed. By increasing screw speed, the shear and elongational stresses induced on the material also increase, producing higher percentages of CAMES beads breaking.

2. Percent breakup increased as flow rate increased, for a constant screw speed

With the exception of one set of data (26-mm narrow kneading blocks), this observation was true for each experiment. This result, however, was not an obvious result. As flow rate was increased, the axial velocity component of the extruder (i.e. the velocity component that reduces the residence-time distribution) was also increased, reducing the amount of time the material spent in the extruder. This indicated that the shorter the time spent in the extruder, the more breakup of beads occurred.

3. The percent drag flows can be used to predict trends in the data

When the drag flow percentages were the same or nearly the same (as with the 18-mm and 28-mm experiments), the trends between the different-sized kneading blocks were the same. That is, both data curves had the same behavior and the slopes between data points were nearly parallel. However, with the 26-mm data, the percent drag flows between the kneading blocks were very different, as were the trends in the data.

4. Wide kneading blocks produced higher percentages of bead breakage than narrow kneading blocks

For every experimental operating condition where the critical stress levels of the CAMES beads used for the wide and narrow kneading blocks were the same (excluding the 26-mm data due to the use of different strength beads), wide kneading blocks produced higher breakup percentages than narrow kneading blocks. Due to the larger size of the wide kneading blocks, induced extensional stresses are greater than narrow kneading blocks, producing higher percentages of broken beads.

The conclusions that were made using the Constant-N and Constant-Q plots were initial observations. These insights were looked into further using the more quantitatively detailed central composite design data to see if they could be observed within a much larger set of data.

5.2 CCD Grids

The section discusses the results from the completed central composite design of experiment grids using the operating conditions from Section 3.3. Using these grids, visual observations regarding the trends in the data were made for each screw geometry and machine. Additionally, statistical methods were used to generate a correlation equation relating the percent breakup of CAMES beads and the operating conditions, as well as other variables.

5.2.1 28-mm TSE

The set of experiments performed on the 28-mm twin-screw extruder can be separated into three pairs:

1. Narrow KBs vs. wide KBs with neutral KB using 119 kPa CAMES beads

2. Narrow KBs vs. wide KBs with reverse conveying element using 119 kPa CAMES beads
3. Narrow KBs vs. wide KBs with reverse conveying element using 92 kPa CAMES beads

The operating conditions for all three pairs of experiments were the same and can be seen in Figure 3.25.

5.2.1.1 Narrow KBs vs. Wide KBs with Neutral KB Using 119 kPa CAMES Beads

Narrow and wide kneading blocks, followed by a neutral kneading block and half left-handed kneading block after the mixing section, screw designs #1 and #2 for the 28-mm extruder, respectively, were the first to be investigated. The critical stress of the CAMES beads that were used were 119 kPa. The results of the experiments for this pair can be seen in Figure 5.8.

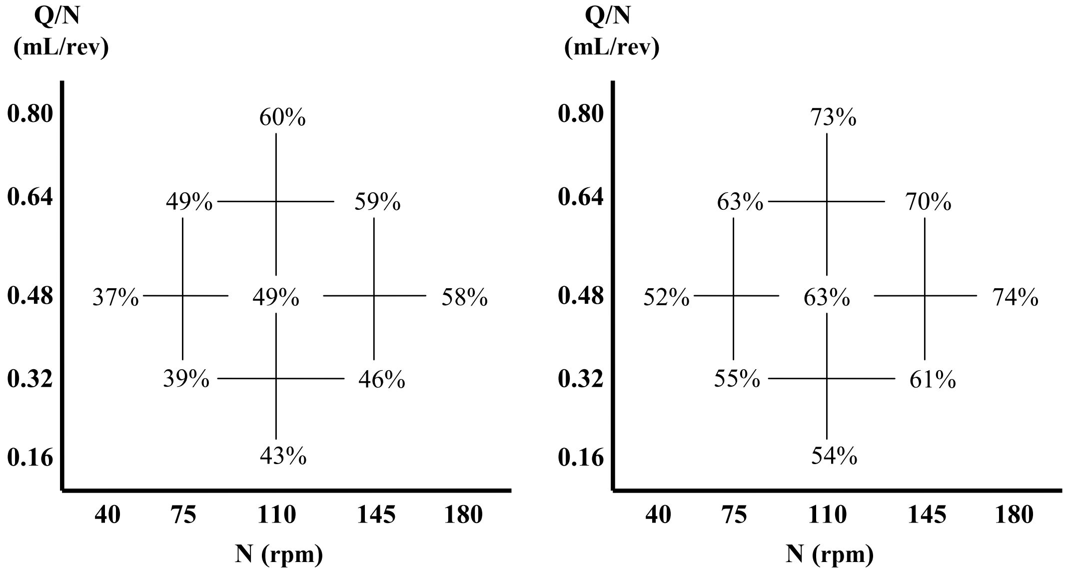

(a) (b)

Figure 5.8 - Percent breakup of 119 kPa CAMES beads using (a) narrow KBs (screw design #1) and (b) wide KBs (screw design #2) with neutral KB on 28-mm TSE

The figure above shows the average percent breakup as a function of screw speed and specific throughput using narrow kneading blocks (a) and wide kneading blocks (b). Looking at the two CCD grids, some observations were made. As the screw speed was increased for a given specific throughput, the percent breakup of beads increased for both kneading blocks. Additionally, as the specific throughput was increased for a given screw speed, the percent breakup of CAMES beads also increased for both kneading blocks. Another observation is that the constant flow rate diagonals had the same percentages of breakup, within the given error (2% for both narrow and wide kneading block grid). With increasing flow rate, the percent breakup of the CAMES beads increased (diagonal 3 has the highest percent of breakup and diagonal 2 had more breakup than diagonal 1). Comparing the two grids together, it was seen that the wide kneading blocks produced a greater percentage of bead rupture for each operating condition. The wider kneading blocks broke up on average about 13% more beads than the narrow kneading blocks.

Taking the data from the CCD grids, an equation relating important parameters to the percent breakup for the individual grids and the grids combined was generated. The equations for the grids are presented in Table 5.7.

Table 5.7 – Important parameters of prediction equations for narrow and wide KBs with neutral KB using 119 kPa CAMES beads

Predicted Grid	**Intercept**	**N**	**(Q/N)**	**KB [Narrow]**
Narrow KB	48.1	4.9	4.8	-
Wide KB	62.2	4.8	4.6	-
Narrow and Wide KB (combined)	55.2	4.8	4.7	-6.9

The table above shows the statistically important parameters from the CCD statistical analysis. For the individual CCD grids, only the screw speed and specific throughput were statistically significant. However, when the analysis was performed on the two grids simultaneously, not only was screw speed and specific throughput significant, but the size of the kneading block was also important. For example, the equation to predict percent breakup using narrow kneading blocks from the combined grids was:

$$\%\,Breakup = 55.17 + (4.83 * N) + \left(4.67 * \left({}^{Q}\!/_{N}\right)\right) - 6.94 \tag{5.1}$$

Inserting appropriate values for N and Q/N, (the corresponding screw speed and specific throughputs on the CCD grid), the percent breakup within the bounds of the two grids can be predicted accurately.

5.2.1.2 Narrow KBs vs. Wide KBs with Reverse Conveying Element Using 119 kPa CAMES Beads

The next pair of screw geometries studied was the narrow and wide kneading blocks backed by a full reverse-conveying element. These geometries were screw designs #3 and #4, as stated previously. The CAMES beads that were used had a critical stress of 119 kPa. The CCD grids for the two geometries can be seen below in Figure 5.9.

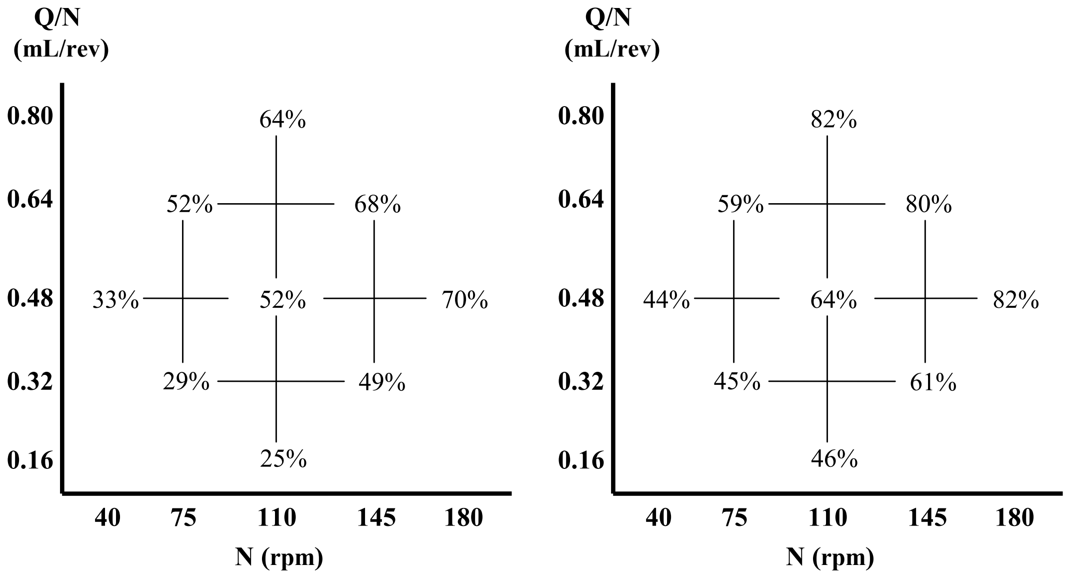

(a) (b)

Figure 5.9 - Percent breakup of 119 kPa CAMES beads using (a) narrow KBs (screw design #3) and (b) wide KBs (screw design #4) with reverse conveying on 28-mm TSE

The figure above, similar to Figure 5.8, indicates that percent breakup increased as the screw speed increased for a constant value of specific throughput. For a given screw speed, percent breakup of beads also increased as specific throughput was increased. An error of 2% was calculated using the three replicates. The diagonals on the CCD grids were also found to produce the same amount of CAMES breakup, within the error, with the exception of diagonal 1 on the narrow kneading blocks grid, which was slightly outside the error. When flow rate was increased, the percent breakup of beads also increased, as seen in both grids as diagonal 3 again had the most breakup, followed by diagonal 2 and diagonal 1 having the least amount of beads ruptured. The comparison in breakup between the wide and narrow kneading blocks again indicated that wide kneading blocks ruptured more CAMES beads for every operating condition. The average difference between the two screw geometries is approximately 12%.

Using the JMP CCD Solver, the parameters that were determined to be important for the predictive equations can be seen below in Table 5.8.

Table 5.8 - Important parameters of prediction equations for narrow and wide KBs with reverse conveying element using 119 kPa CAMES beads

Predicted Grid	Intercept	N	Q/N	$(Q/N)^2$	KB [Narrow]
Narrow KB	51.6	9.2	10.0	-1.8	-
Wide KB	61.8	9.4	8.8	-	-
Narrow and Wide KB (combined)	56.7	9.3	9.4	-	-6.7

The table above shows the parameters for the percent breakup prediction equations for the two individual grids and the concatenated grid. For the narrow kneading blocks grid, it is seen that screw speed, specific throughput, and specific throughput squared were deemed to be important for predicting percent breakup for this grid. The wide kneading blocks only had screw speed and specific throughput as important parameters. The equation that can predict both grids has N, Q/N, and the kneading blocks as important parameters, but not $(Q/N)^2$ term.

5.2.1.3 Narrow KBs vs. Wide KBs with Reverse Conveying Element Using 92 kPa CAMES Beads

The last pair of experiments run on the 28-mm utilized the same two screw geometries as the previous pair (screw design #3 and #4), but changed the strength of the CAMES beads from 119 kPa to a weaker strength of 92 kPa. The results from the experiments were plotted in the CCD grids and presented in Figure 5.10.

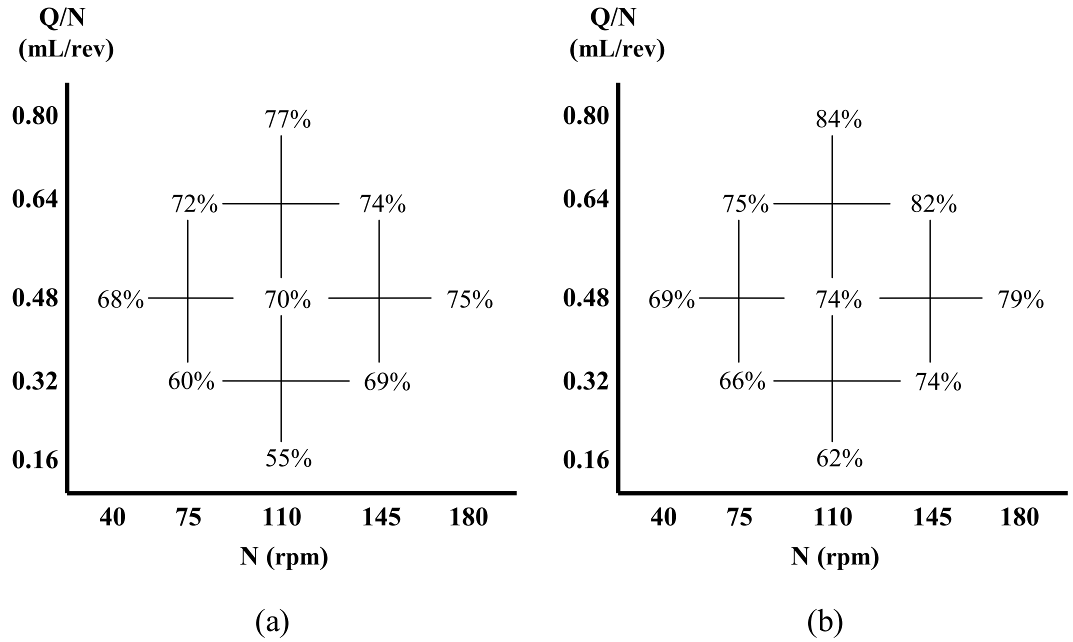

Figure 5.10 - Percent breakup of 92 kPa CAMES beads using (a) narrow KBs (screw design #3) and (b) wide KBs (screw design #4) with reverse conveying on 28-mm TSE

The figure above shows the percent breakup of narrow (a) and wide (b) kneading blocks as a function of specific throughput and screw speed. As seen in the previous two figures, for a given screw speed, the percent breakup of CAMES beads increased when the specific throughput increased. Similarly, a faster screw speed yielded a higher percentage of beads rupturing, for a constant specific throughput. Within the experimental error, which was 3% for the narrow kneading blocks and 2% for the wide kneading blocks, it was seen that wide kneading blocks again produced a higher percent breakup for every operating condition than the narrow kneading blocks. The differences between the narrow and wide kneading blocks are less than the differences between the blocks in the previous configuration. Looking at the diagonals for the two grids, the first diagonal did not yield consistent breakup;

however, diagonal 2 and 3 did result in constant breakup. The trend of increased breakup as flow rate was increased was similarly observed within these two grids.

Using the percent breakup values for each of the operating conditions, statistical analyses were performed on the data and important parameters were determined, as seen in Table 5.9.

Table 5.9 - Important parameters of prediction equations for narrow and wide kneading blocks with reverse conveying element using 92 kPa CAMES beads

Predicted Grid	Intercept	N	(Q/N)	KB [Narrow]
Narrow KB	69.4	2.1	5.1	-
Wide KB	74.4	2.9	5.1	-
Narrow and Wide KB (combined)	71.9	2.5	5.1	-2.5

The results from the analysis indicated that only screw speed and specific throughput were statistically important for the predicting equation. The negative coefficient of the narrow kneading blocks is consistent with the trends in the data tables as narrow kneading blocks produced less breakup than wide kneading blocks.

5.2.1.4 Data Set Comparisons

Comparing the results of the pairs of data that were obtained, some observations were made between the sets of data. The sets of data from Figure 5.8 and Figure 5.9 were the first to be investigated. These two sets used the same strength CAMES beads but had different elements behind the mixing section. Looking at the effects of the neutral and reverse elements with the narrow kneading blocks, it was clear that there was an impact on the differences in percent breakup due to flow rate. When the flow rate was at its lowest value (i.e. diagonal 1), the neutral kneading blocks produced higher levels of stress than the reverse element design. When the flow rate was increased to around 5 lb/hr (diagonal 2), the difference in breakup decreased, to where there was virtually no difference between the two geometries. However, when the flow rate was increased further (diagonal 3), the narrow kneading blocks with the reverse conveying element then began to break up a higher percentage of beads. Similarly, the differences in the neutral kneading block and reverse elements for the wide kneading blocks also showed a dependence on the polymer flow rate. The neutral kneading block geometry again produced more breakup than the reverse element geometry for the lowest flow rate. Diagonal 2 also had the smallest difference between the two geometries, and the differences in diagonal 3 (the highest throughput) were dominated by the reverse conveying element geometry.

Using the JMP statistical software, an equation to predict percent breakup between the pairs of data was generated and the important parameters displayed in Table 5.10.

Table 5.10 - Important parameters of prediction equation for narrow and wide KBs with neutral KB and reverse conveying element using 119 kPa CAMES beads

Predicted Grids	**Intercept**	**N**	**Q/N**	**N*BE [neutral]**	**(Q/N)*BE [neutral]**	**KB [Narrow]**
Narrow – Neutral/ Reverse	49.8	7.0	7.4	-2.1	-2.6	-
Wide – Neutral/Reverse	62	7.1	6.7	-2.3	-2.1	-
Narrow/Wide - Neutral/Reverse	55.9	7.1	7.0	-2.2	-2.4	-6.8

From the above table, it is clear that the predicting equations for percent breakup become more and more complicated as additional factors are added (i.e. the backup element). The predicting equation between the four grids (Narrow/Wide – Neutral/Reverse) was dependent on five factors, screw speed, specific throughput, screw speed and specific throughput multiplied by the coefficients of the backup element, and the kneading block size.

The other sets of CCD grids that were compared were the second and third pairs, a comparison of bead strength with identical screw geometries (Figure 5.9 and Figure 5.10). Investigating the differences in the percent breakup of the two different beads for the narrow and wide kneading blocks, it was apparent that the diagonals within the grids again yielded the most insightful results. Diagonal 1 had the highest difference in bead breakup for both narrow and wide kneading block comparisons. The differences for the narrow kneading blocks were greater than 30%, while the difference for the wide kneading blocks were around 20%. Diagonal 2 showed slightly less differences in breakup, ranging around 20% for the narrow kneading blocks and approximately 13% for the wide kneading blocks. The least amount of difference between the 92 kPa and 119 kPa stress beads occurred in diagonal 3. Only a difference between 5% and 13% existed for the narrow kneading blocks and an even smaller difference for the wide kneading blocks, between -3% and 2%. The -3% difference indicated that for that operating condition, there was more breakup for the 119 kPa beads than the 92 kPa beads. One reason for this occurrence was due to the limitations of the experimental method, which will be discussed in more detail later, as well as the experimental error within the data. Similar to the first comparison of the data sets, it was seen again that throughput seem to be related to the trends within the data.

The equations below indicate the important parameters between the differences in CAMES strength for a given screw geometry and for both geometries. Equation 5.2 shows the important parameters for the bead comparison using the narrow kneading blocks and Equation 5.3 shows the important parameters for the wide kneading blocks.

$$\begin{aligned} \%\,Breakup = {} & 137.8 + (5.6 * N) + \left(7.5 * \left(\frac{Q}{N}\right)\right) - \left(1.3 * \left(\frac{Q}{N}\right)^2\right) \\ & - \left(1.4 * N * \left(\frac{Q}{N}\right)\right) - (0.7 * BS)\,\big(0.3 * N * (BS - 105.5)\big) \\ & + \left(0.2 * \left(\frac{Q}{N}\right) * (BS - 105.5)\right) \end{aligned} \tag{5.2}$$

$$\begin{aligned} \%\,Breakup = {} & 112.4 + (6.2 * N) + \left(6.9 * \left(\frac{Q}{N}\right)\right) - (0.4 * BS) \\ & + \big(0.2 * N * (BS - 105.5)\big) + \left(0.1 * \left(\frac{Q}{N}\right) * (BS - 105.5)\right) \end{aligned} \tag{5.3}$$

Equation 5.4 below shows the prediction equation from the four CCD grids that were analyzed.

$$
\begin{aligned}
\%\,Breakup = {} & 125.1 + (5.9 * N) + \left(7.2 * \left(\frac{Q}{N}\right)\right) - \left(0.7 * \left(\frac{Q}{N}\right)^2\right) \\
& - (0.6 * BS) + \big(0.3 * N * (BS - 105.5)\big) \\
& + \left(0.2 * \left(\frac{Q}{N}\right) * (BS - 105.5)\right) - 4.6KB[narrow] \\
& - ((BS - 105.5) * KB])
\end{aligned}
\tag{5.4}
$$

The above equations display all the statistically important parameters to predict the percent breakup of CAMES with varying strengths. Compared to the other prediction equations from Table 5.10, the varying bead strength added significantly more complexity to the equations, especially to the equation generated from the four CCD grids.

5.2.1.5 28-mm Conclusions

From the three pairs of experiments and the data obtained from them, as well as the comparisons between sets of data, general conclusions regarding the data from the 28-mm twin-screw extruder were made:

1. Percent breakup increases with increasing screw speed, for a given specific throughput

In every condition, the percentage of beads that broke increased as screw speed increased, for a given specific throughput. Shear stress and elongational stress are both a function of screw speed. By increasing the screw speed, the magnitude of both induced stresses is also increased, yielding greater breakup of CAMES beads.

2. Percent breakup increases with increased specific throughput, for a given screw speed

In every condition, the percentage of broken beads increased as specific throughput increased, for a given screw speed. This observation was not an obvious result. As mentioned previously, as the specific throughput is increased, the residence-time distribution is decreased and the time the material spent inside the extruder is reduced. On the other hand, at higher specific throughput, more material experiences the elongational stress between the paddles. The results suggest that the latter phenomenon predominates.

3. Percent breakup is constant with throughput

In almost every CCD grid, the percent breakup was consistent with constant throughputs. The exceptions to this observation were the two diagonal 1's on the CCD grids were the 92 kPa CAMES beads were used. The observation that there existed a trend within with the diagonals of the grids was another unobvious result and contradicted the conclusions found previously with the Constant-Q plots in that percent breakup increased with increasing screw speed, for a constant flow rate. Furthermore, only one of the generated equations from the comparisons indicated that throughput, Q, was an important parameter. Although the CCD data suggests that flow rate is a factor, statistically, it is not significant.

4. Wide kneading blocks produce greater percentages of broken beads than narrow kneading blocks

For every operating condition, wide kneading blocks broke larger percentages of beads than narrow kneading blocks. This result was consistent with the results from the Constant-N and Constant-Q plots. The larger paddles on the wide kneading blocks produce greater magnitudes of extensional stress on the material than narrow kneading blocks, yielding higher percentages of broken beads. Furthermore, due to the wider block, more fluid experiences the higher stress.

5. Throughput influences breakup differences between elements that back up the mixing section

In the comparison of the neutral kneading block and reverse conveying element backing up the mixing section, it was found that throughput influenced the differences in percent breakup. When the flow rate was very low (diagonal 1), the percent breakup of beads was greater when the neutral kneading block was placed behind the mixing section than the reverse element. As flow rate was increased, the difference between the geometries was nonexistent (diagonal 2), and further increasing the flow rate (diagonal 3) produced a greater difference in percent breakup with the reverse element geometry generating more breakup. This is caused by a lack of axial pressure with the lower flow rates, as a result, the material remains in the channels of the neutral kneading block longer than with higher flow rates, causing more breakup of CAMES beads than the reverse conveying backup.

5.2.2 26-mm TSE

Only one comparable set of results were gathered from the 26-mm twin-screw extruder, plus an additional CCD grid.

5.2.2.1 Narrow KBs vs. Medium KBs with Reverse Conveying Element Using 92 kPa CAMES Beads

The set of results compared narrow and medium kneading blocks (screw designs #1 and #2), both with a reverse conveying element backing the mixing section. The strength of the CAMES beads used for these two geometries was 92 kPa. The results can be seen below in Figure 5.11.

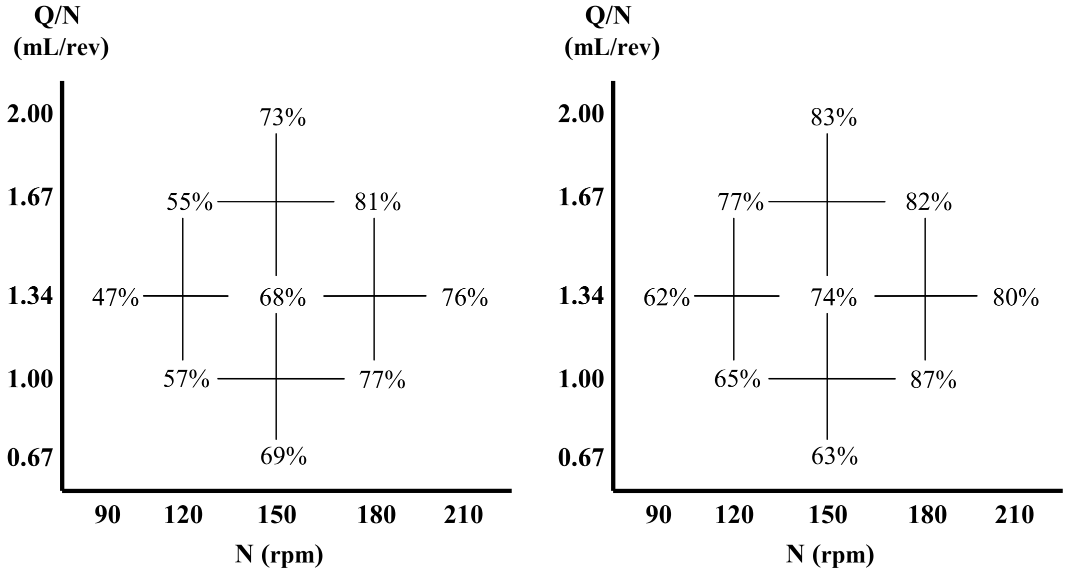

(a) (b)

Figure 5.11 - Percent breakup of 92 kPa CAMES beads using (a) narrow KBs (screw design #1) and (b) medium KBs (screw design #2) with reverse element on 26-mm TSE

The two grids in the above figure show some similar and different trends as seen earlier with the 28-mm results. A similar trend that was seen was that for a given specific throughput, increasing screw speed yielded an increase in percent breakup of beads. The only other consistent trend, with the exception of one data point (i.e. the 69% breakup using narrow kneading blocks for 150 rpm and a specific throughput of 0.67 mL/rev, which is believed to be an outlier) medium kneading blocks broke up a larger percentage of CAMES beads than the narrow kneading blocks, within the experimental error of 3% for both grids. The breakup difference between the two grids was not consistent either. Other previously stated trends, such as increasing bead rupture percentages with increasing specific throughput and consistent percent breakup along the diagonals were not seen within this data.

Using the JMP SAS CCD solver, equations from the data were generated to determine which parameters were important. The important parameters can be seen in Table 5.11.

Table 5.11 - Important parameters of prediction equations for narrow and medium KBs with reverse element using 92 kPa CAMES beads

Predicted Grid	Intercept	N	(Q/N)	KB [Medium]
Narrow KB	68.3	8.7	-	-
Medium KB	78.2	5.3	-	-
Narrow and Medium KB (combined)	73.3	7	2.4	3.9

The important parameters for the prediction equations yielded results consistent with the noted observations for the 26-mm results. For the individual grids, screw speed was the only important parameter, as stated earlier. For the combined grids, specific throughput was found to be an important parameter; however, the weight of this parameter is the least contributive of the factors.

5.2.2.2 Wide KBs with Reverse Conveying Element Using 223 kPa CAMES Beads

An additional experiment was performed using wide kneading blocks on the 26-mm extruder (screw design #3). The strength of the CAMES beads that were used were 223 kPa. Due to the short supply of this caliber stress bead, only one CCD grid (Figure 5.12) could be completed.

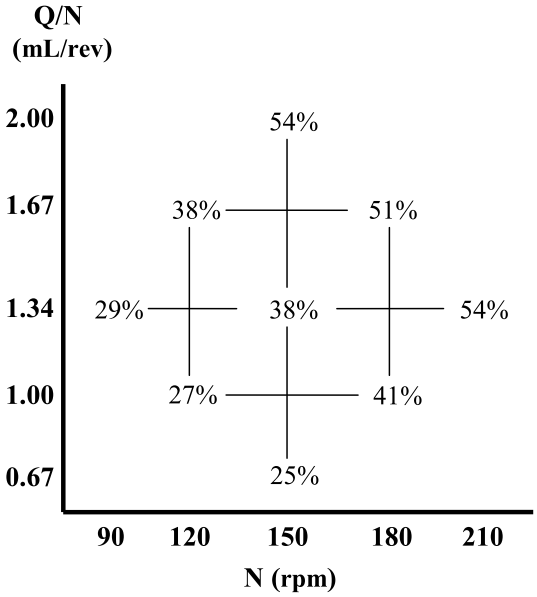

Figure 5.12 - Percent breakup of 223 kPa CAMES beads using wide KBs with reverse conveying element on 26-mm TSE

From the CCD grid shown above, all previously noted trends are observed. Percent breakup of CAMES beads increased as screw speed increases, for a given specific throughput and as specific throughput increased, for a given screw speed. Additionally, within the calculated error of 4%, the constant percent breakup along the diagonals was seen (although not statistically significant). Due to the higher strength of the CAMES beads, the percent breakup values were much lower than breakup percentages for the narrow and medium kneading blocks.

Plugging in the CCD grid from Figure 5.12 into the CCD grid solver, the prediction equation was determined, as seen in Equation 5.5.

$$\% \, Breakup = 38 + (6.4 * N) + \left(6.6 * \left(\frac{Q}{N}\right)\right) \tag{5.5}$$

As the prediction equation shows, only screw speed and throughput were found to be important parameters, which is consistent with the observations made looking at the results from the CCD grid in Section 5.2.1.

5.2.2.3 26-mm Conclusions

Using the results from the three CCD grids obtained using the 26-mm twin-screw extruder; some observations were made from this set of experiments.

1. Percent breakup increases with increasing screw speed, for a given specific throughput

As seen previously in the 28-mm results, as screw speed is increased, both extensional and shear stresses also increase, yielding higher percentages of bead breakage. Looking at the generated equations for the geometries using the 92 kPa beads, which were only dependent on screw speed, and the 223 kPa CAMES beads which was dependent on both screw speed and specific throughput, it is hypothesized that the magnitude of the critical and elongational stresses in the flow field goes higher into the flow.

2. Medium kneading blocks produce greater percentages of broken beads than narrow kneading blocks

For this set of data, this observation was seen for geometries using CAMES beads with similar critical stress levels. This is another observation previously seen in the 28-mm results. Due to the larger width of the paddles, the extensional stresses experienced by the material are greater than those induced by the narrow kneading blocks.

5.2.3 18-mm TSE

5.2.3.1 Narrow KBs vs. Medium KBs with Reverse Conveying Elements Using 158 kPa CAMES Beads

The final set of experiments were performed using narrow (screw design #1) and medium (screw design #2) kneading blocks with reverse conveying elements on the 18-mm twin-screw extruder. The results displayed in Figure 5.13 were obtained using CAMES beads with a critical stress of 158 kPa.

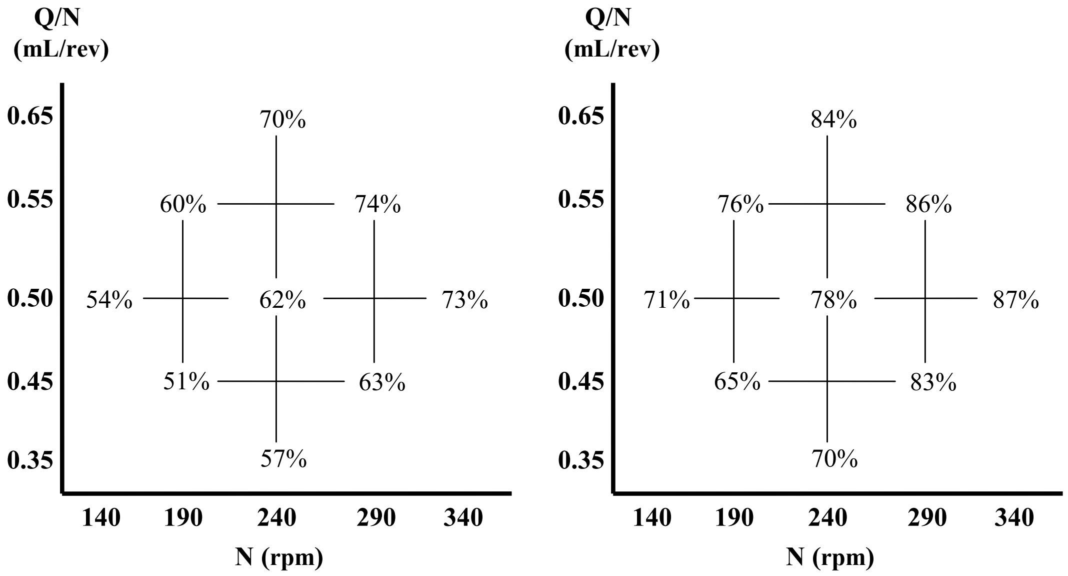

(a) (b)

Figure 5.13 - Percent breakup of 158 kPa CAMES beads using (a) narrow KBs (screw design #1) and (b) medium KBs (screw design #2) with reverse conveying elements on 18-mm TSE

The pair of CCD grids from the 18-mm extruder shows common trends previously seen in data from both 28-mm and 26-mm CCD grids. Percent breakup was again influenced by increases in screw speed and throughput. With an experimental error of 5% for the narrow kneading blocks data and 4% for the medium kneading blocks data, consistent trends in percent breakup along the three diagonals were again observed. Additionally, similar to the differences in percent breakup between narrow and wide kneading blocks on the 28-mm extruder, medium kneading blocks produced higher percentages of bead rupture than the narrow kneading blocks by an average of about 15% for every operating condition.

To confirm that the observations were consistent with the statistical calculations, a predictive equation was generated for the data set and is displayed in Table 5.12.

Table 5.12 - Important parameters of prediction equations for narrow and medium KBs with reverse conveying elements using 158 kPa CAMES beads

Predicted Grid	**Intercept**	**N**	**(Q/N)**	**KB [Medium]**
Narrow KB	61.3	5.3	3.8	-
Medium KB	78.7	5	3.5	-
Narrow and Medium KB (combined)	78.3	7.5	3.7	7.7

The table above confirms the previously stated observations. Both screw speed and specific throughput were found to be statistically important, which was similar to prediction equations in Table 5.7 and Table 5.9 from the 28-mm experiments and the prediction equation (Equation 5.5) from the 26-mm experiments.

5.2.3.2 18-mm Conclusions

From the set of results obtained using the 18-mm twin-screw extruder, conclusions were made from the trends in the data.

1. Percent breakup increases with increasing screw speed, for a given specific throughput
2. Percent breakup increases with increasing specific throughput, for a given screw speed
3. Medium kneading blocks produce greater percentages of broken beads than narrow kneading blocks

These conclusions were consistent with the observations stated for the 28-mm and 26-mm geometries.

5.3 Residence-Stress Distributions

The CCD grids in the previous sections provided insights from the average percent breakups that were collected from each of the operating conditions. Further insights were gained by investigating the generated residence distributions from the experiments, which shows the time evolution of the percent breakup of the stress beads.

A residence-stress distribution (RSD) illustrates the amount of stress the material experiences as it travels through the extruder. The RSD curves were generated by running the CAMES beads through the extruder and measuring the voltage signals from the released dye. Figure 5.14 below displays the RTD and RSD curves for an operating condition with a flow rate of 1.8 lb/hr and screw speed of 110 RPM.

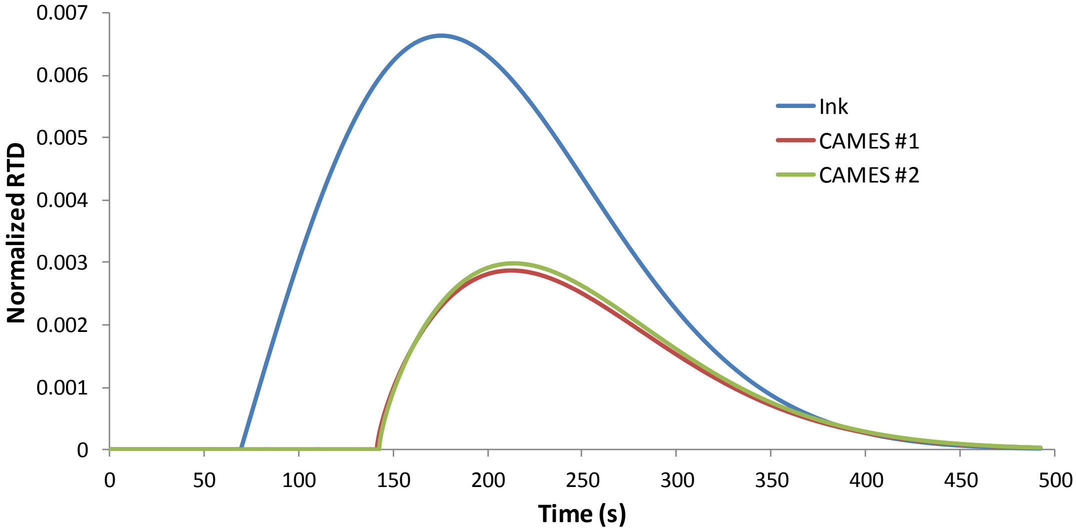

Figure 5.14 - Normalized RTD and RSD curves for 1.8/110 operating condition on 28-mm TSE

The figure shows the average of three ink RTDs generated from the experiment using screw design #4 (wide KBs with reverse conveying) from the 28-mm extruder and

119 kPa CAMES beads. This figure shows the quality of the collected data. The two RSD curves are essentially identical, demonstrating the repeatability of the experiment. The shapes of the RTD and RSD curves are very similar. This indicates that the paths taken by both the ink shots and CAMES beads were the same, validating the assumption that the CAMES are passive tracers. The percent breakup generated from this condition was 46%. The RTD and RSD curves provide further insights into the mechanisms of bead breakup.

5.3.1 Delay Time

One observation is that there exists a delay between the start of the ink RTD curve and the RSD curves. The delay can be interpreted as the beads that travel through the mixing section first traverse the least tortuous path and do not break. The least tortuous path in an extruder is in the center of the screw channel. This phenomenon is similar to what is seen for laminar flow through a pipe (Figure 5.15).

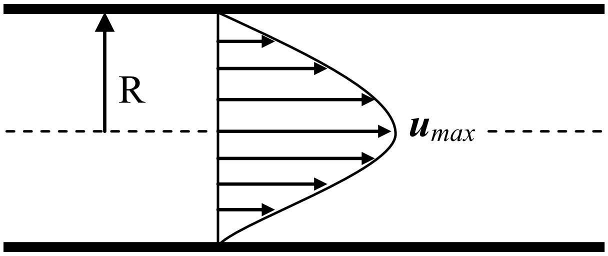

Figure 5.15 - Velocity profile of laminar flow through a pipe

The shear stress in this flow can be calculated using the following equation:

$$\tau = -\mu \frac{du}{dy} \tag{5.6}$$

where $\frac{du}{dy}$ is the velocity gradient. The velocity gradient at the center of the pipe is infinitesimally small, which is approximated as zero. Therefore, from Equation 5.1, the value of the shear stress in the center of the pipe is zero, which is the same for the shear stress in the center of the screw channel. The delay between the curves confirms this result. The fact that a percentage of the beads travel through the center of the channel and never see high levels of stress, 100% breakup cannot be achieved. The highest percentage of breakup that can be achieved is approximately 85-87%.

The delay times of the RTD and RSD curves were then investigated to determine if any relationships existed with the percent breakup. Only the experiments performed on the 28-mm extruder were investigated because multiple screw geometries and CAMES beads were used on this machine. The results from the delay time analysis can be seen in Figure 5.16.

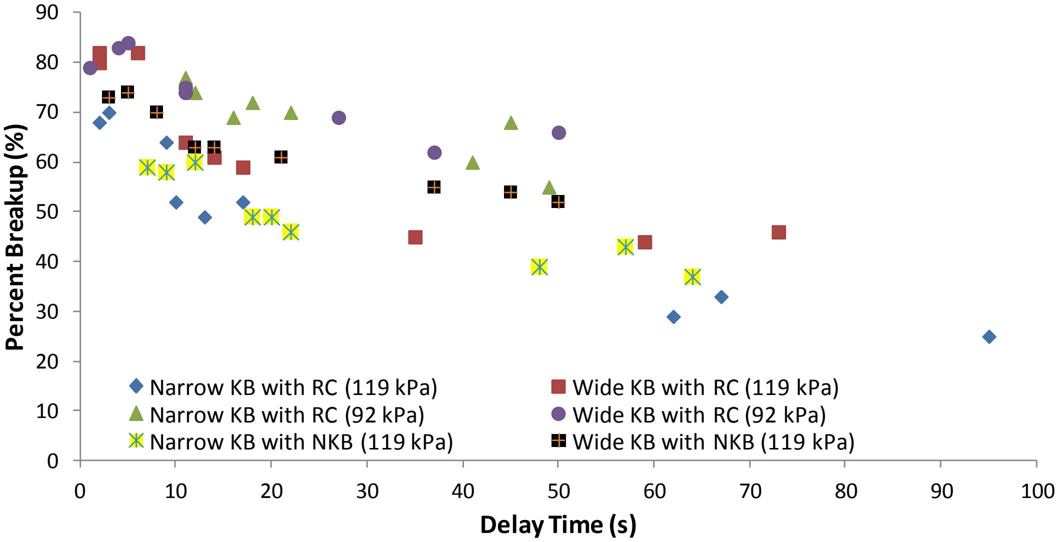

Figure 5.16 - Percent breakup as a function of delay time for 28-mm TSE

The figure above shows the percent breakup for each screw geometry and CAMES beads used on the 28-mm extruder as a function of the delay time between the ink RTD and CAMES RSD curves. Per screw geometry and CAMES beads combination, it is clear that as the delay time increases, the percent breakup of CAMES beads decreases. This result is consistent with the mechanisms at work within the extruder. As the delay time increases, this indicates that a higher percentage of CAMES beads went through the mixing section without experiencing high enough levels of stress to induce rupture. This yields low percentages of CAMES breakup. Additionally, it was observed that the delay time for wide kneading blocks was consistently less than the comparable narrow kneading blocks and the percent breakup was therefore higher in every case. This result is consistent with the previously stated conclusions. Due to the higher elongational stresses from the wide kneading blocks, more beads were rupturing; this leads to reduced delay times between the ink RTD and RSD curves. Another consistent result that is observed is that the delay times for the screw designs using 92 kPa CAMES beads compared to the 119 kPa beads were consistently smaller. This is an expected result since the 92 kPa beads require less stress for rupture. This will inherently reduce the delay time as more beads will rupture sooner with the lower critical stress than the 119 kPa beads.

The plot of percent breakup as a function of delay time for only one screw geometry (narrow kneading blocks with reverse element using 119 kPa CAMES beads) provides another insight, as seen in Figure 5.17.

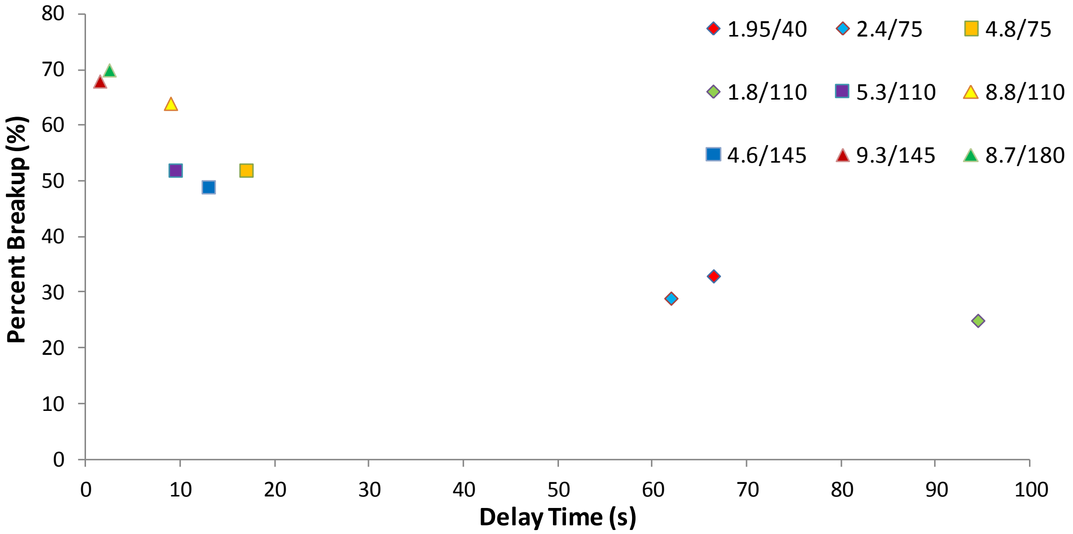

Figure 5.17 - Percent breakup vs. delay time for narrow KBs and reverse conveying element with 119 kPa CAMES beads on 28-mm TSE

The above figure shows the delay time for each operating condition. The plot indicates that operating conditions with similar flow rates (i.e. the diagonals from the CCD grids) have the approximately the same delay time. The lowest flow rates have the largest delay times and least amount of breakup. The next group of flow rates (diagonal 2 from CCD grids) has a reduced delay time and higher breakup. The operating conditions with the highest flow rates have the shortest delay time and highest percent breakup. This plot indicates that flow rate has an influence on delay time and reconfirms the observation that throughput also impacts the percent breakup of CAMES beads.

The two figures below, Figure 5.18 and Figure 5.19, display the RTD and RSD curves for two experimental operating conditions where the screw speed for both was 110 RPM and the flow rate was 5.3 and 8.8 lb/hr, respectively.

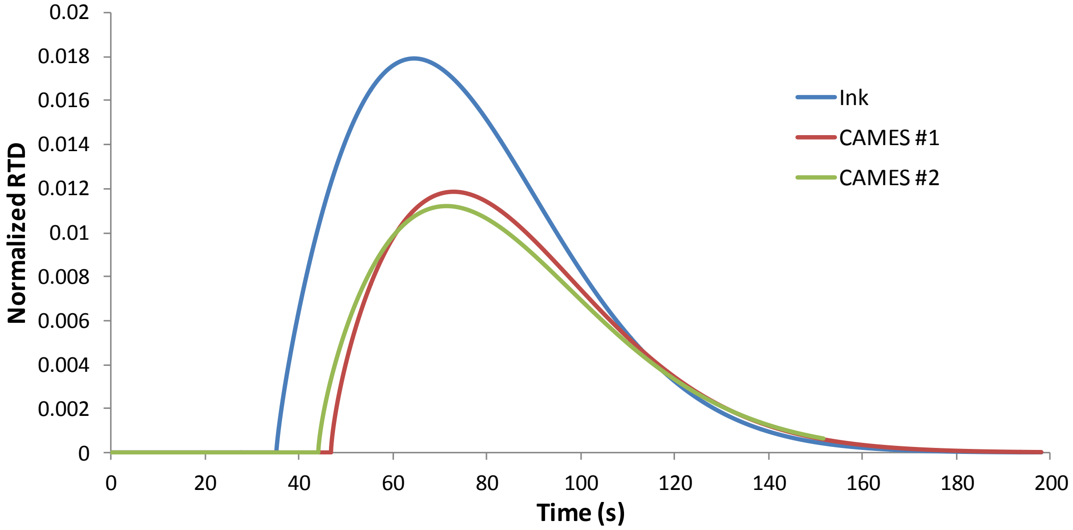

Figure 5.18 - Normalized RTD and RSD curves for 5.3/110 operating condition on 28-mm TSE

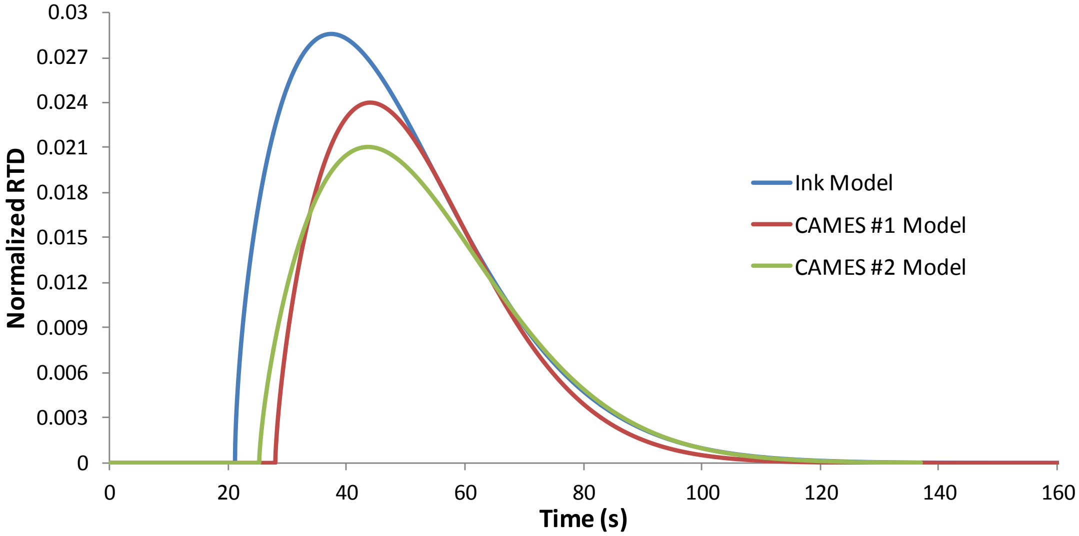

Figure 5.19 - Normalized RTD and RSD curves for 8.8/110 operating condition on 28-mm TSE

The percent breakup of CAMES beads in Figure 5.18 was calculated to be 64% and the breakup in Figure 5.19 was 82%. Using the two figures above, as well as Figure 5.14, the effect of throughput can be seen on the RTD and RSD curves. As is well understood, throughput has the greatest effect on the shape of the RTD curve. The higher the throughput, the greater the concentration of the tracer (i.e. voltage signal) and the narrow the RTD curve becomes when compared to lower flow rates. These results are also seen in these experiments. The amplitude of both the RTD and RSD curves are greatest with the 8.8 lb/hr flow rate than the 5.3 and 1.8 lb/hr flow rates. Additionally, because the screw speed was kept constant, when the throughputs were increased, the specific throughput also increased. As the machine becomes more full, the material then travels through the extruder at a faster rate, although the screw speed is kept at a constant rate. This explains why the ink RTD curve starts the earliest with the 8.8 lb/hr condition. The delay time is also the shortest for this condition because it induced the highest magnitudes of stress; therefore, the beads break sooner, reducing the delay time.

5.3.2 Distribution of CAMES breakup

Another insight obtained from the RTD and RSD plots was the location where the majority of CAMES beads break. As seen in the three previous figures (as well as every RTD and RSD curve generated from this experiment), the RSD curves overlap the RTD curve at the end or "tail." This indicates that majority of the breakup occurred during this time. The figures show that the average percent breakup is not evenly experienced over the duration of the time distribution. If the curves were to be broken into four equal sections, as seen in Figure 5.20, the distribution of the percent breakup becomes more clear.

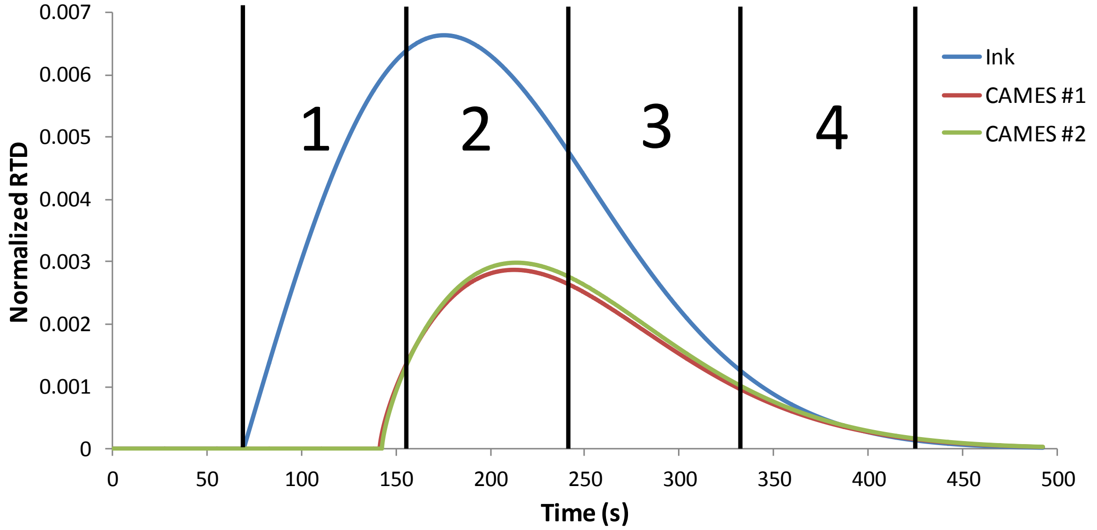

Figure 5.20 - RTD and RSD curves segmented into four equation sections

The first segment has the least amount of breakup. This again is explained by the beads travelling through the center of the channels and seeing very little stress. Segment 2 shows that the highest concentration of beads had broken; however, it is only still a relatively low percentage of breakup when compared to the RTD curve. The percentage further increases in segment 3 and is nearly 100% breakup in the last segment.

5.3.3 Effects of Different Screw Geometries

The effects of screw geometry were then investigated to see its effects on the RTD and RSD curves. The first to be investigated was the impact the back-up element after the mixing section. Figure 5.21 below shows the RTD and RSD curves using a neutral kneading block and a one-half left-handed narrow kneading blocks for an operating condition with a flow rate of 1.8 lb/hr and screw speed of 110 RPM.

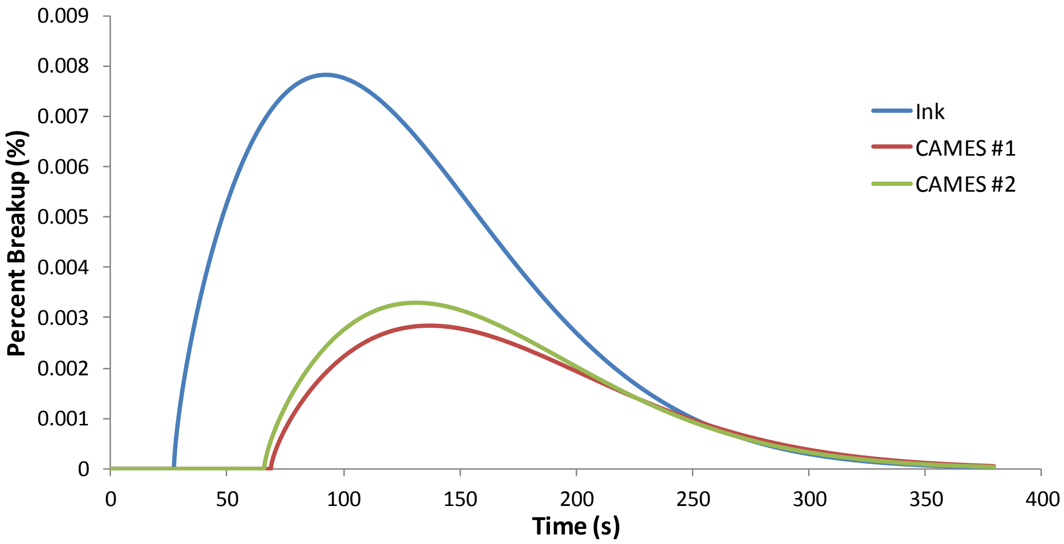

Figure 5.21 - Normalized RTD and RSD curves for 1.8/110 operating condition using neutral KB on 28-mm TSE

Comparing the above figure, which produced a percent breakup of 54%, with Figure 5.14, the effects of the different back-up elements can be seen. The start of the RTD and RSD curves occur much sooner for the neutral kneading block configuration. This is expected as the neutral kneading block and left-handed kneading block do not produce as much back-pressure as the full reverse element. In other words, the ink and CAMESs beads went through the mixing section faster. The differences in amplitude of the RTD curves are almost the same, but the duration of the curves is significantly longer using the full reverse conveying element. The duration is nearly 150 seconds longer, which is again, caused by the back-pressure. The delay time between the RTD and RSD curves is also shorter for the neutral kneading block, which is a result of the induced stress added by the neutral kneading block.

The effects of narrow and wide kneading blocks on the residence-time and residence-stress distributions were also studied. The wide kneading blocks have larger gaps between the paddles, producing more back flow than narrow kneading blocks. Additionally, the pitch of the wide kneading blocks is also much lower. This causes a later start and longer duration of the wide kneading block ink RTD than the narrow RTD curve. This result was seen throughout the experiment. Additionally, as seen in the figure with the percent breakup as a function of delay time (Figure 5.16), the delay times of the narrow kneading were longer than the wide kneading blocks due to the higher induced extensional stress of the wide kneading blocks.

5.3.4 Residence-Stress Distribution Conclusions

Studying the generated residence-stress distributions, the following insights were obtained regarding the mechanisms of bead breakup:

1. CAMES RSD curves start later than ink RTD curves

There exists a delay between the start of the ink RTD and CAMES RSD curves for every operating condition. This is due to the initial beads traveling through the center of the screw channels, were stresses are minimal. A percentage of the beads do not experience any stress regardless of operating condition and therefore do not break. This insight provides reasoning for why 100% breakup was not achieved and theoretically cannot be achieved.

2. Wide kneading blocks produced shorter delay times than narrow kneading blocks

This result was seen for every case. Wide kneading blocks induce higher magnitudes of extensional stress due to the larger paddles than narrow kneading blocks. The higher extensional stress caused beads to rupture more quickly, reducing the delay time.

3. There exists a correlation between delay time and percent breakup

As delay time between the ink residence-time distribution curve and the CAMES residence-stress distribution curves increased, the corresponding percent breakup for that operating condition decreased. This indicated that a higher percentage of CAMES beads that traveled through the mixing section first, particularly in the center of the screw channel, experienced very little stress and did not rupture.

4. The distribution of percent breakup is not evenly distributed over the time distribution

The percent breakup presented in the CCD grids provides the average CAMES breakup over the entire residence distribution. However, it was seen that the percent breakup is not evenly distributed. The initial percentage is very low, whereas, the percent breakup near the end of the distribution is nearly 100%. This can be interpreted as the initial flow through the mixing section experiences little breakup, mostly because it stays in the center of the channels. The tail of the flow followed a path that repeatedly going through the kneading block paddles, resulting in almost 100% breakup of CAMES beads.

5. Screw geometry impacts the residence-time and stress distributions

It was seen that using a neutral and left-handed kneading block produces an earlier start and end to both the RTD and RSD curves compared to a full reverse conveying element geometry. This is due to the larger back-pressure generated by the reverse conveying element. Narrow kneading blocks produced an earlier start and end to the RTD curve than wide kneading blocks because of the reduced back flow through the paddles. Wide kneading blocks produce a shorter delay time due to the higher induced stresses which break the CAMES beads sooner than narrow kneading blocks.

5.4 Other Residence Distributions

Using the residence-revolution and residence-volume distribution transformations provided earlier (Equation 2.1 and 2.2), the ink RTD and CAMES RSD curves were converted into the RRD and RVD domain. The domain transformations were performed to investigate if further insights could be obtained.

5.4.1 Residence-Revolution Distributions

The residence-revolution distribution provides information regarding the transport behavior of the extruder. It is a measure of how many screw rotations are necessary for material to travel through the extruder. Using the relationship:

$$t = \frac{n}{N} \tag{5.7}$$

Where n is the cumulative screw revolutions, the time axis from the RTD and RSDs are converted to screw revolutions. The ink and CAMES RRD curves are shown in Figure 5.22 and Figure 5.23, respectively. The presented set of data was obtained using screw design #3 on the 28-mm TSE (wide kneading blocks with reverse conveying element using 119 kPa CAMES beads).

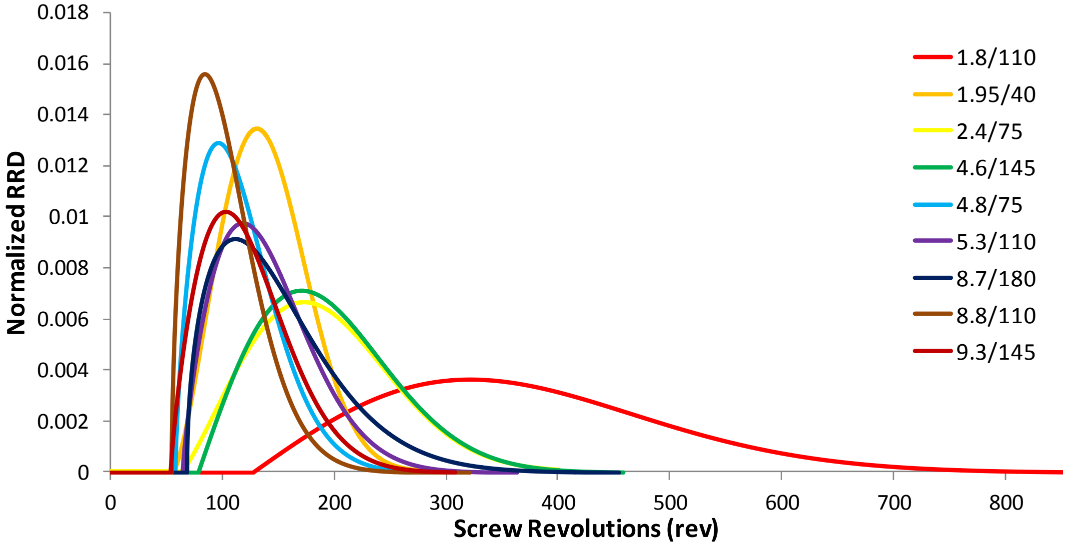

Figure 5.22 - Ink RRD curves

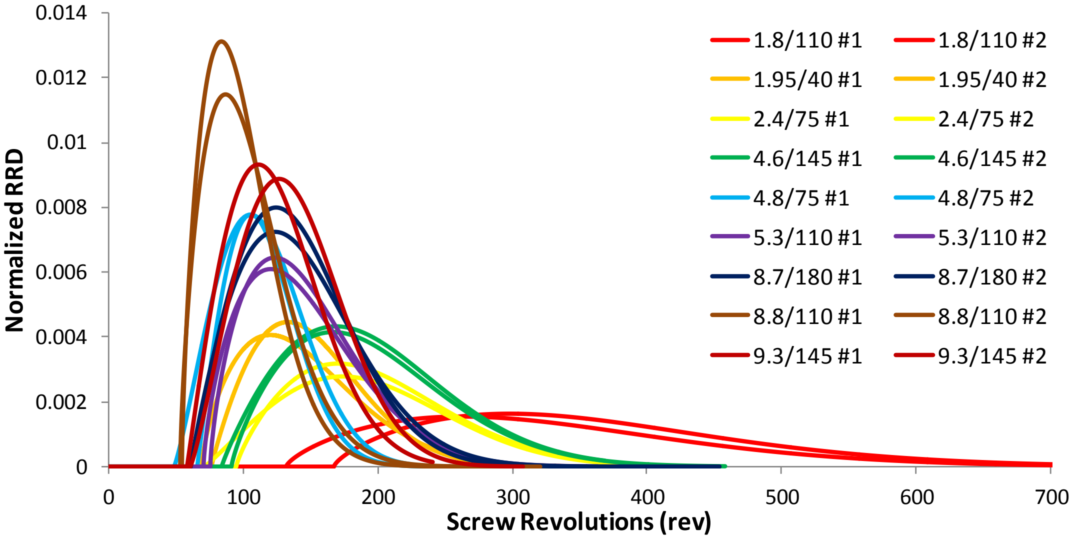

Figure 5.23 - CAMES RRD curves

The two figures above show the RRD curves where the normalized probe signal is plotted against the cumulative screw revolutions. These figures display the number of revolutions necessary to completely remove the ink and CAMES shots from the extruder. The results from both figures are consistent with the results obtained from Gao et al [53]. Operating conditions with the same specific throughputs yield nearly identical RRD curves, within some inherited experimental error. For example, the operating conditions 2.4/75 (yellow curves) and 4.6/145 (green curves), have the same specific throughput (0.32 mL/rev) and have essentially the same RRD curves. These curves start at the same amount of screw revolutions and have the same voltage response. Additionally, the operating condition with the highest specific throughput (8.8/110) has the shortest start delay and a shaper RRD shape and the lowest specific throughput (1.8/110) has the longest delay and a wider shape for both the ink and CAMES RRD curves. These observations are also consistent with Gao's findings.

5.4.2 Residence-Volume Distribution

The residence-volume distribution provides limited information into the mixing behavior of the extruder. Although it is a representation of the axial distribution of the tracer in the material, that is not enough to fully describe the mixing processes within the extruder due to numerous other factors. Using the relationship:

$$t = \frac{v}{Q} \tag{5.8}$$

Where v is the volume of extruded polymer, the time axis from the RTD and RSD curves can be transformed into volumes. The ink and CAMES RVD curves are presented in Figure 5.24 and Figure 5.25, respectively.

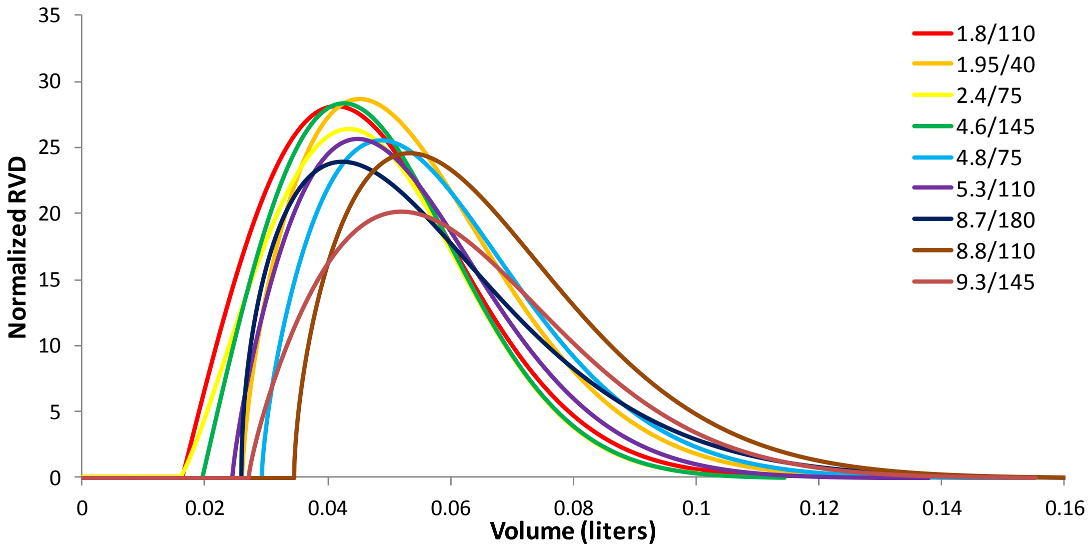

Figure 5.24 - Ink RVD curves

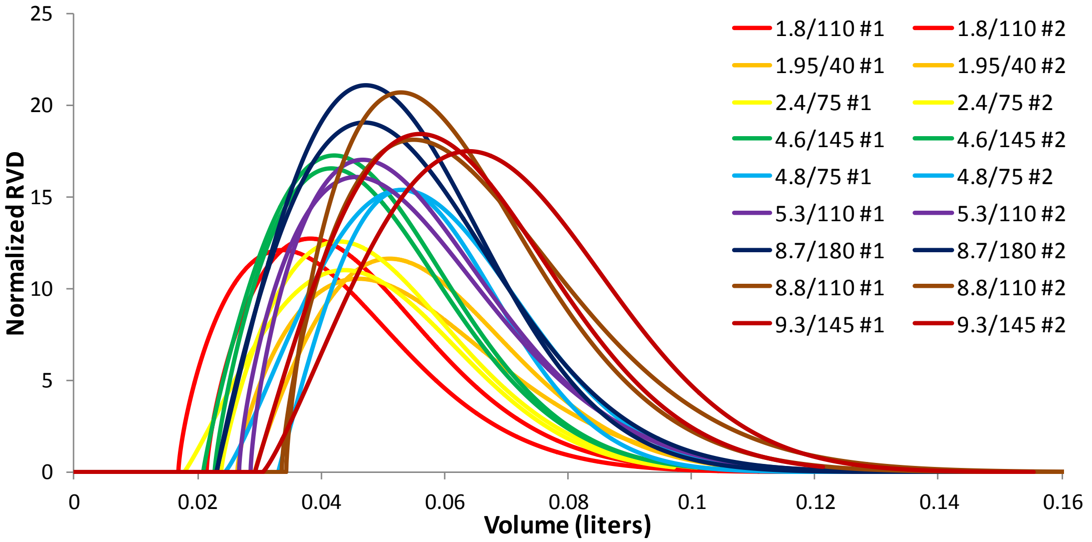

Figure 5.25 - CAMES RVD Curves

The axes of the two figures above have been converted to volumes of extrudate, in liters, and a normalized RVD probe response. The results from the transformations yield consistent results with Gao's findings [53]. The operating condition with the lowest specific throughput, 1.8/110 (red curves), have the shortest start delay and the highest specific throughput has the largest start delay. Within the inherited experimental error, it is evident that all the ink RVD curves look the same (i.e. same shape and same amplitude). However, this is not the case with the CAMES RVD curves, as seen in Figure 5.25. Due to the normalization process for the CAMES, i.e. being normalized with the area of the corresponding ink curve, the amplitudes of the curves are very different. When the delays are removed from the ink RVD curves, the resulting plot (Figure 5.26), shows that all of the ink RVD curves are essentially the same.

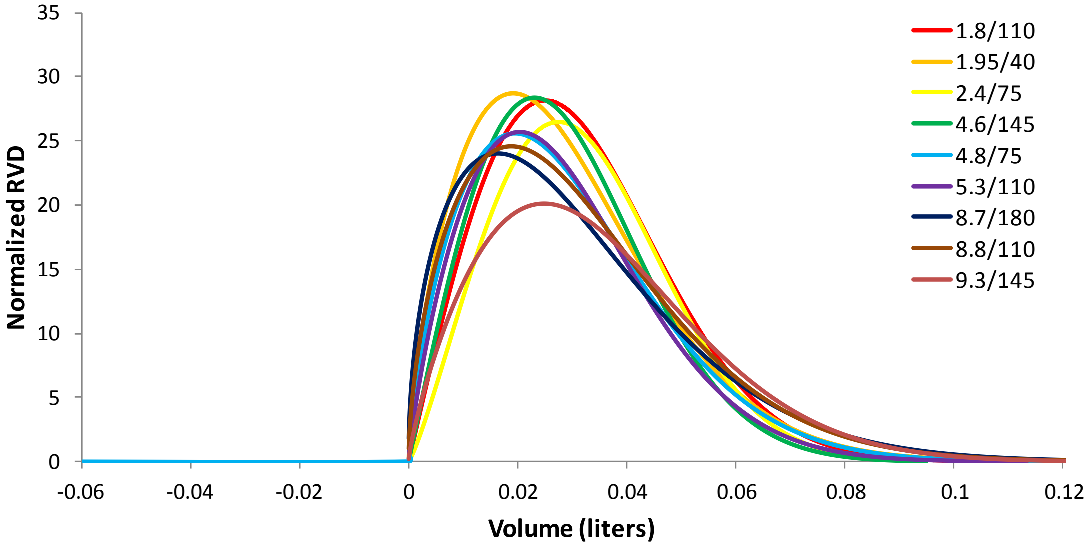

Figure 5.26 - Overlapping ink RVD curves

The shapes of the RVD curves are slightly different due to the different input parameters for the Weibull model. The plot above indicates that the axial distribution of the ink is not dependent on the operating conditions, so then it must be dependent on screw geometry.

Gao's work was the characterization of distributive mixing. This current work extends that work to also examine dispersive mixing, for systems where the polymer is dominated by viscous behavior and the stress is sufficient to break the stress beads.

The findings of this study show that the prediction of dispersive stresses follows the same normalization in both RRD and RVD domains. This provides an important physical understanding to the process.

5.4.3 Conclusions

From the plots of the ink and CAMES residence-revolution and residence-volume distribution curves, the following conclusions were made:

1. Operating conditions with the same specific throughput produce the same RRD and RVD curves

When specific throughput is the same for different operating conditions, the degree of fill within a screw section is also the same, which results in the same RRD and RVD curves. This shows that material with the same specific throughput travel the same path within the extruder, as indicated by the RRD and RVD curves.

2. Specific throughput impacts the delays of RRD and RVD curves

A larger specific throughput produces a sharper RRD curve with a shorter screw revolution delay. Yet in the RVD domain, a larger specific throughput results in a larger volume delay with very little impact on the shape of the RVD curves.

3. RVD curves are the same regardless of flow rate and screw speed, for a given screw geometry

The axial distribution of the ink is not dependent on the operating conditions, but rather the screw geometry. This shows that this approach provides insight into distributive mixing and can possibly be applied to dispersive mixing through the RVD of the CAMES.

Chapter 6 Conclusions

6.1 Intellectual Contributions and Summary of Findings

An approach has been developed to provide insights into the mechanisms of dispersive mixing within a co-rotating, fully-intermeshing twin-screw extruder. Calibrated microencapsulated sensor (CAMES) beads were found to be an effective tool for measuring the stress history within a mixing section using different screw geometries. Various-sized mixing elements (kneading blocks) were utilized on three different-sized machines to determine whether the beads can distinguish between the different geometries, as a function of the extruder operating conditions. Through theoretical calculations, it was found that the extensional stress produced by the squeezing of the polymer melt by the kneading paddles was the primary mechanism of bead breakup.

The major findings from each set of results are presented below.

6.1.1 Constant-N and Constant-Q Experiments

The first set of experiments that were performed was to investigate the individual contributions of throughput and screw speed to percent breakup of CAMES beads. Keeping the screw speed of the extruder to a constant speed and varying the flow rate yielded an increase in percent breakup with increasing flow rate. By increasing the flow rate with a constant screw speed, the specific throughput also increases. As specific throughput increases, two phenomena occur. First, it has been observed through previous visual experiments that as the degree of fill increases, the axial velocity of the polymer melt increases. This causes a higher percentage of the material to be squeezed between the paddles of the kneading blocks, causing more material to experience the induced extensional stresses. Additionally, as the specific throughput increases, the velocity profile of the material in the mixing section changes. This can result in a higher magnitude of extensional stress at the kneading block paddle, which therefore causes the critical level of stress to occur deeper within the flow field. As a result, more material experiences the critical stress yielding higher percent breakup of CAMES beads.

Feeding the polymer at a constant flow rate and increasing the screw speed also increased the percentage of broken beads. This result is commonly understood as both shear stress and elongational stress are a function of screw speed. The higher the screw speed, the greater the magnitude of the induced stresses which produce greater breakup of beads. This result was confirmed by the theoretical calculations that were performed.

Another observation made from this experiment was that wider kneading blocks produce higher percentages of breakup than narrow kneading blocks. In every experiment for all three machines, the widest kneading block produced the more bead breakup. This result confirms the common understanding that wide kneading blocks enhance dispersive mixing while narrow kneading blocks are designed for distributive mixing. Due to the larger paddle width, more material is squeezed between two paddles, causing more material to experience the high magnitudes of extensional stress. Therefore, wide kneading blocks produce greater percentages of bead breakup than narrow kneading blocks.

6.1.2 Central Composite Design of Experiment Grids

A central composite design of experiment (CCD) grid was used to lay out the percent breakup results so that visual observations could be made. Additionally, statistical analysis was performed on the sets of data generate predicting equations with statistically important parameters, such as operating conditions, and relate them to the percent breakup

From the CCD grids, it was again observed that both screw speed and specific throughput predominately influenced percent breakup. As screw speed increased, for a given specific throughput, the percent breakup of stress beads also increased. This again was found to be consistent with the understanding that increasing screw speed also increases the induced extensional stress. Additionally, the predicting equations that were generated indicated that screw speed was statistically important in every case.

Similar to the Constant-N experiment findings, specific throughput was also observed to be a function of percent breakup. Higher values of specific throughput, for a given screw speed, produced greater breakup percentages. This again is due to the change in the flow caused by increasing the degree of fill within the mixing section. Specific throughput was also found to be a statistically significant parameter in the predicting equations from Section 5.2, confirming the observation.

The size of the kneading blocks was again observed to have an impact on the percent breakup of CAMES beads. For each machine, it was found that increasing the size of the kneading paddles also increased the percentage of broken beads. This is again due to the larger width of the paddles, causing more material to experience the extensional stress.

6.1.3 Residence-Stress Distributions

Plotting the generated ink residence-time distributions and CAMES residence-stress distributions provided further insights into the mechanisms of bead breakup. For each experimental run, it was found that there is a delay between the start of the ink RTD and CAMES RSD curves. This is due to the flow coming through initially travels in the center of the channel and experiences minimal elongational stresses. Therefore, the beads that go through the mixing section first do not break. This provides explanation for the maximum achievable breakup percentage to be around 85 to 87%. It was also found that there was a correlation between the start time of the ink RTD and start of the CAMES RSD curves and the percent breakup. The shorter the delay time, the higher percentage of beads that broke The RTD and RSD curves also indicate that the average bead breakup is not distributed evenly across the ink RTD. The initial breakup was found to always be the lowest, whereas the tail of the distribution saw nearly 100% breakup.

6.1.4 Residence-Revolution and Residence-Volume Distributions

The ink RTD and CAMES RSD curves were then transformed to both residence-revolution and residence-volume distributions. Operating conditions with the same specific throughput produce the same RRD and RVD curves for a given screw geometry. Additionally, a higher specific throughput produces a sharper RRD curve and a shorter screw-revolution delay. The opposite happens in the RVD domain where a greater specific throughput produces a greater volume delay than small specific throughputs. In the RVD domain, regardless of operating conditions and specific throughput, the distributions had essentially the same shape and size. This indicates that the axial distribution of the ink concentrate is independent of operating conditions. The results from these transformations again confirm that specific throughput cannot be ignored from consideration when predicting bead breakup. The RVD and RRD approach worked for the distributive mixing mechanism, as seen with the ink concentrations, as well as the dispersive mixing as seen with the CAMES RVD and RRD curves.

6.2 Future Work

The presented work has significantly enhanced the understanding of the stress history within twin-screw extruders; future work can provide even further insights.

- The investigated range of operating conditions is only a small portion of total operating conditions that an extruder is capable of. By investigating higher specific throughputs and screw speeds in conjunction with different CAMES beads with higher critical stress levels, a greater understanding of the stresses induced by kneading blocks will be gained.

- Investigating different types of extruders, such as non-intermeshing or counter-rotating twin-screw extruders will further advance the understanding of the stress mechanisms. Other investigations could also include the use of other mixing elements, such as gear mixers, or the use of other polymers with different viscosities.

- The applications of this approach are endless. One example of an application of this approach could be to relate percent breakup of CAMES beads to achieved properties of a composite material. For instance, good dispersion of carbon fiber agglomerates is crucial to producing a high quality composite. Mechanical and thermal properties are dependent on the dispersion of agglomerates. The more equally distributed the carbon fibers, the better the composite properties. The percent breakup of CAMES beads is a direct indication of the magnitude of induced stresses. Therefore, a correlation can be determined between the percent breakup and the achieved mechanical and thermal properties.

- Another area of study could be in the pharmaceutical area. It is critical to evenly distribute the active pharmaceutical ingredients into the polymer matrix while remaining below the stress limits of the ingredients. This approach would provide a quantitative technique for comparing screw configurations and creating an expression for mixing as a function of important parameters.

Appendix A: MATLAB Code

```
%Modeling RTD of the Ink Curve

%Read File and get file size
      A = xlsread('C:\Users\David Bigio\Desktop\Neutral Wide\
            1.95_40_CAMES_1.xlsx');
      [M,N]=size(A(:, 1));
%Find delay point
      [x]=find((A(1:M, 3)>[1e-4;]));
      shift1=min(x)
%Initialize error values
      errorprev =1000000;
      error=0;
 %Find Values of C,K,L for Weibull Model
      for C=0:.005:.2
       for K=1:.1:4;
        for L=20:2:150;
         for iii=14:100:(M-shift1)/2.5
             model(shift1+iii,1) = (C).*((A(iii,1)./L).^(K-
                  1)).*exp(-1.*((A(iii,1)./L).^K)));

              error=error + sqrt( (model(shift1+iii,1) -
                  A(shift1+iii,3))^2 );
          end
           if (error<errorprev)
                 k1=K;
                 l1=L;
                 c1=C;
                 errorprev=error;
                 error=0;
           else
                error=0;
           end
        end
       end
      end
%Name Conversion
      Ink(14:M,3) = A(14:M,3);
%Generate Full Model curve using found C,K,L
      for iii=14:1:(M-shift1)
            inkmodel(shift1+iii,1)=((c1).*((A(iii,1)./l1).^(k1-
                  1)).*exp(-1.*((A(iii,1)./l1).^k1)));
      end
%Plotting RTD and RSD
      figure(1)
      plot(A(14:M,1),  inkmodel(14:M,1),'b-','LineWidth',2);hold on
      plot(A(14:M,1), Ink(14:M,3),'k-','LineWidth',2);
      xlabel('time');
%RVD MODELING and RVD Domain Transformation
      rate=.000256;
      Volume(14:M,1)=A(14:M,1)*rate;
      RVD_Raw_Data_Curve(14:M,3)=A(14:M,3)/rate;
      RVDmodel(14:M,1)=inkmodel(14:M,1)/rate;
```

```
%Plotting RVDs
      figure(2)
      plot(Volume(14:M,1), RVD_Raw_Data_Curve(14:M,3),'k-',
            'Linewidth',2); hold on
      plot(Volume(14:M,1), RVDmodel(14:M,1), 'b-', 'Linewidth',2);
      xlabel('Volumes');
%RRD MODELING and RRD Domain Transformation
      screwspeed=40;
      Revolution(14:M,1)=A(14:M,1)*(screwspeed/60);
      RRD_Raw_Data_Curve(14:M,3)=A(14:M,3)/(screwspeed/60);
      RRDModel(14:M,1)=inkmodel(14:M,1)/(screwspeed/60);
%Plotting RRDs
      figure(3)
      plot(Revolution(14:M,1), RRD_Raw_Data_Curve(14:M,3), 'k-',
            'Linewidth',2); hold on
      plot(Revolution(14:M,1), RRDModel(14:M,1), 'b-',
      'Linewidth',2);
      xlabel('Revolutions')

%Modeling of CAMES Curve

%Read File and get file size
      A = xlsread('C:\Users\David Bigio\Desktop\Neutral
            Wide\1.95_40_CAMES_1.xlsx');
      [M,N]=size(A(:, 1));
%Find delay point and end of file
      [x]=find((A(1:M, 6)>[1e-4;]));
      shift2=min(x)
      [yy]=find((A(1:M, 6)<[1e-6;]));
      Mt=max(yy);
%Initialize error values
      errorprev = 1000;
      error=0;
 %Calculates percent breakup to adjust model curve
      percent1=A(9,2)/A(8,2);
 %Find Values of C,K,L for Weibull Model
      for C=0:.005:.2
       for K=1:.1:3;
        for L=20:1:150;
         for iii=14:100:(Mt-shift2)
                  model(shift2+iii,1)=((C).*((A(iii,1)./L).^(K-
                        1)).*exp(-1.*((A(iii,1)./L).^K)))*percent1;
                  error = error + sqrt( (model(shift2+iii,1) -
                              A(shift2+iii,6))^2
         end
           if (error<errorprev)
                 k2=K;
                 l2=L;
                 c2=C;
                 errorprev=error;
                 error=0;
           else
                error=0;
           end
         end
       end
      end
```

```
%Name Conversion
      Cames1(14:M,6)  = A(14:M,6);
%Generate Full Model curve using found C,K,L
      for iii=14:1:(M-shift2)
            cames1model(shift2+iii,1)=((c2).*((A(iii,1)./l2).^(k2-
                  1)).*exp(-1.*((A(iii,1)./l2).^k2)))*percent1;
      end
%Plotting CAMES RSD
      figure (1)
      hold on;
      plot(A(14:M,1), cames1model(14:M,1),'r-','LineWidth',2);hold
            on
      plot(A(14:M,1), Cames1(14:M,6),'k-','LineWidth',2);
 %RVD MODELING and RVD Domain Transformation
      Volume(14:M,1)=A(14:M,1)*rate;
      CAMES_1_RVD_Raw_Data_Curve(14:M,6)=A(14:M,6)/rate;
      CAMES_1_RVDmodel(14:M,1)=cames1model(14:M,1)/rate;
%Plotting RVD
      figure(2)
      hold on
      plot(Volume(14:M,1), CAMES_1_RVD_Raw_Data_Curve(14:M,6),'k-',
            'Linewidth',2);
      plot(Volume(14:M,1), CAMES_1_RVDmodel(14:M,1), 'r-',
            'Linewidth',2);
      xlabel('Volumes');
%RRD MODELING and RRD Domain Transformation
      Revolution(14:M,1)=A(14:M,1)*(screwspeed/60);
      CAMES_1_RRD_Raw_Data_Curve(14:M,6)=A(14:M,6)/(screwspeed/60);
      CAMES_1_RRDModel(14:M,1)=cames1model(14:M,1)/(screwspeed/60);
%Plotting RRD
      figure(3)
      hold on
      plot(Revolution(14:M,1), CAMES_1_RRD_Raw_Data_Curve(14:M,6),
            'k-', 'Linewidth',2); hold on
      plot(Revolution(14:M,1), CAMES_1_RRDModel(14:M,1), 'r-',
            'Linewidth',2);
      xlabel('Revolutions')
```

Bibliography

[1] S. Levy and J. F. Carley, *Plastics extrusion technology handbook*. Industrial Press Inc., 1989.

[2] D. V. Rosato, *Extruding plastics: a practical processing handbook*. Springer, 1998.

[3] C. I. Chung, *Extrusion of polymers: theory and practice*. Hanser Verlag, 2000.

[4] J. L. White, H. Potente, and U. Berghaus, *Screw extrusion: science and technology*. Hanser Gardner Publications, 2003.

[5] C. Rauwendaal, *Polymer extrusion*. Hanser Verlag, 2001.

[6] I. Ghebre-Selassie, C. Martin, C. M. (M.B.A.), and M. D. (Firma comercial), *Pharmaceutical Extrusion Technology*. CRC Press, 2003.

[7] Y. Wang, *Compounding in Co-Rotating Twin-Screw Extruders*. iSmithers Rapra Publishing, 2000.

[8] K. Kohlgrüber and M. Bierdel, *Co-rotating twin-screw extruders: fundamentals, technology, and applications*. Hanser Verlag, 2008.

[9] C. Rauwendaal, *Mixing in polymer processing*. CRC Press, 1991.

[10] U. Berghaus, *Plastics extrusion technology*. Hanser Verlag, 1997.

[11] E. L. Paul, V. A. Atiemo-Obeng, and S. M. Kresta, *Handbook of industrial mixing: science and practice*. Wiley-IEEE, 2004.

[12] L. Erwin, “Mixing: Basic Concepts of Polymer Processing,” Encyclopedia of Materials Science and Engineering, 1982.

[13] N. P. Cheremisinoff, *Polymer mixing and extrusion technology*, vol. 16. CRC, 1987.

[14] H. F. Giles, J. R. Wagner, and E. M. Mount, *Extrusion: the definitive processing guide and handbook*. William Andrew, 2005.

[15] P. J. Cullen, *Food Mixing: Principles and Applications*. John Wiley and Sons, 2009.

[16] J. F. Funt, *Mixing of Rubber*. iSmithers Rapra Publishing, 2009.

[17] O. Levenspiel, *Chemical reaction engineering*. Wiley, 1972.

[18] O. S. Carneiro, J. A. Covas, J. A. Ferreira, and M. F. Cerqueira, “On-line Monitoring of the Residence Time Distribution Along a Kneading Block of a Twin-Screw Extruder,” *Polymer Testing 23*, pp. 925-937, 2004.

[19] Z. Tadmor and C. G. Gogos, *Principles of Polymer Processing*, 1st ed. John Wiley & Sons, 1979.

[20] G. C. Papanicolaou, A. F. Koutsomitopoulou, and A. Sfakianakis, “Effect of thermal fatigue on the mechanical properties of epoxy matrix composites reinforced with olive pits powder,” *Journal of Applied Polymer Science*.

[21] I. Manas-Zloczower, *Mixing and compounding of polymers: theory and practice*. Hanser Verlag, 2009.

[22] J. Curry and A. Kiani, “Experimental Identification of the Distribution of Fluid Stresses in Continuous Melt Compounders - Part 2,” in *SPE-ANTEC Tech Papers*, 1991, vol. 37, pp. 114-118.

[23] J. Curry and A. Kiani, “Measurement of Stress Level in Continuous Melt Compounders,” in *SPE-ANTEC Tech. Papers*, 1990, vol. 36, pp. 1599-1602.

[24] I. Manas-Zloczower, A. Nir, and Z. Tadmor, "Dispersive Mixing in Internal Mixers—A Theoretical Model Based on Agglomerate Rupture," *Rubber Chemistry and Technology*, vol. 55, p. 1250, 1982.

[25] E. Canedo and L. Valsamis, in *SPE ANTEC Proceedings*, 1989, p. 116.

[26] W. Szydlowski, K. Min, M. H. Kim, and J. L. White, "Technology and Analysis of Flow," *Advances in Polymer Technology*, vol. 7, p. 177, 1987.

[27] A. C. Rios, P. J. Gramann, and T. A. Osswald, "Comparative study of mixing in corotating twin screw extruders using computer simulation," *Advances in Polymer Technology*, vol. 17, no. 2, pp. 107-113, Jun. 1998.

[28] L. Zhu, K. A. Narh, and K. S. Hyun, "Investigation of mixing mechanisms and energy balance in reactive extrusion using three-dimensional numerical simulation method," *International Journal of Heat and Mass Transfer*, vol. 48, no. 16, pp. 3411-3422, Jul. 2005.

[29] T. Kajiwara, Y. Nagashima, Y. Nakano, and K. Funatsu, "Numerical study of twin-screw extruders by three-dimensional flow analysis—development of analysis technique and evaluation of mixing performance for full flight screws," *Polymer Engineering & Science*, vol. 36, no. 16, pp. 2142-2152, Aug. 1996.

[30] H. Cheng and I. Manas-Zloczower, "Distributive mixing in conveying elements of a ZSK-53 co-rotating twin screw extruder," *Polymer Engineering & Science*, vol. 38, no. 6, pp. 926-935, Jun. 1998.

[31] T. Ishikawa, S. Kihara, and K. Funatsu, "3-D non-isothermal flow field analysis and mixing performance evaluation of kneading blocks in a co-rotating twin srew extruder," *Polymer Engineering & Science*, vol. 41, no. 5, pp. 840-849, May 2001.

[32] T. Ishikawa, T. Amano, S. Kihara, and K. Funatsu, "Flow patterns and mixing mechanisms in the screw mixing element of a co-rotating twin-screw extruder," *Polymer Engineering & Science*, vol. 42, no. 5, pp. 925-939, May 2002.

[33] X. Zhang, L. Feng, W. Chen, and G. Hu, "Numerical simulation and experimental validation of mixing performance of kneading discs in a twin screw extruder," *Polymer Engineering & Science*, vol. 49, no. 9, pp. 1772-1783, Sep. 2009.

[34] A. Lawal, D. M. Kalyon, and Z. Ji, "Computational study of chaotic mixing in co-rotating two-tipped kneading paddles: Two-dimensional approach," *Polymer Engineering & Science*, vol. 33, no. 3, pp. 140-148, Feb. 1993.

[35] K. Funatsu, S. Kihara, M. Miyazaki, S. Katsuki, and T. Kajiwara, "3-D numerical analysis on the mixing performance for assemblies with filled zone of right-handed and left-handed double-flighted screws and kneading blocks in twin-screw extruders," *Polymer Engineering & Science*, vol. 42, no. 4, pp. 707-723, Apr. 2002.

[36] V. L. Bravo, A. N. Hrymak, and J. D. Wright, "Study of particle trajectories, residence times and flow behavior in kneading discs of intermeshing co-rotating twin-screw extruders," *Polymer Engineering & Science*, vol. 44, no. 4, pp. 779-793, Apr. 2004.

[37] M. A. Huneault, M. F. Champagne, and A. Luciani, “Polymer blend mixing and dispersion in the kneading section of a twin-screw extruder,” *Polymer Engineering & Science*, vol. 36, no. 12, pp. 1694-1706, Jun. 1996.

[38] D. Strutt, C. Tzoganakis, and T. A. Duever, “Mixing analysis of reactive polymer flow in conveying elements of a co-rotating twin screw extruder,” *Advances in Polymer Technology*, vol. 19, no. 1, pp. 22-33, Jan. 2000.

[39] M. Yoshinaga, S. Katsuki, M. Miyazaki, L. Liu, S. Kihara, and K. Funatsu, “Mixing mechanism of three-tip kneading block in twin screw extruders,” *Polymer Engineering & Science*, vol. 40, no. 1, pp. 168-178, Jan. 2000.

[40] H. Cheng and I. Manas-Zloczower, “Study of mixing efficiency in kneading discs of co-rotating twin-screw extruders,” *Polymer Engineering & Science*, vol. 37, no. 6, pp. 1082-1090, Jun. 1997.

[41] G. Shearer and C. Tzoganakis, “The effects of kneading block design and operating conditions on distributive mixing in twin screw extruders,” *Polymer Engineering & Science*, vol. 40, no. 5, pp. 1095-1106, May 2000.

[42] G. Shearer and C. Tzoganakis, “Distributive mixing profiles for co-rotating twin-screw extruders,” *Advances in Polymer Technology*, vol. 20, no. 3, pp. 169-190, Sep. 2001.

[43] G. Shearer and C. Tzoganakis, “Relationship between local residence time and distributive mixing in sections of a twin-screw extruder,” *Polymer Engineering & Science*, vol. 41, no. 12, pp. 2206-2215, Dec. 2001.

[44] J. Cheng, Y. Xie, and D. Bigio, “Characterization of Kneading Block Performance in Co-Rotating Twin Screw Extruders,” in *SPE-ANTEC Tech. Papers*, 1998, pp. 198-202.

[45] D. B. Todd, “Residence time distribution in twin-screw extruders,” *Polymer Engineering & Science*, vol. 15, no. 6, pp. 437-443, Jun. 1975.

[46] Z. Tadmor and C. G. Gogos, *Principles of polymer processing*. John Wiley and Sons, 2006.

[47] P. Cassagnau, M. Courmont, F. Melis, and J. Puaux, “Study of mixing of liquid/polymer in twin screw extruder by residence time distribution,” *Polymer engineering and science*, vol. 45, no. 7, pp. 926–934, 2005.

[48] J. . Puaux, G. Bozga, and A. Ainser, “Residence time distribution in a corotating twin-screw extruder,” *Chemical Engineering Science*, vol. 55, no. 9, pp. 1641-1651, May 2000.

[49] G. E. Gasner, D. Bigio, C. Marks, F. Magnus, and C. Kiehl, “A new approach to analyzing residence time and mixing in a co-rotating twin screw extruder,” *Polymer Engineering & Science*, vol. 39, no. 2, pp. 286-298, Feb. 1999.

[50] G. Pinto and Z. Tadmor, “Mixing and residence time distribution in melt screw extruders,” *Polymer Engineering & Science*, vol. 10, no. 5, pp. 279-288, Sep. 1970.

[51] Z. Sun, C. -K Jen, C. -K Shih, and D. A. Denelsbeck, “Application of ultrasound in the determination of fundamental extrusion performance: Residence time distribution measurement,” *Polymer Engineering & Science*, vol. 43, no. 1, pp. 102-111, Jan. 2003.

[52] R. M. van den Einde, P. Kroon, A. J. van der Goot, and R. M. Boom, “Local mixing effects of screw elements during extrusion,” *Polymer Engineering & Science*, vol. 45, no. 3, pp. 271-278, Mar. 2005.

[53] J. Gao, G. C. Walsh, D. Bigio, R. M. Briber, and M. D. Wetzel, “Residence-time distribution model for twin-screw extruders,” *AIChE Journal*, vol. 45, no. 12, pp. 2541-2549, Dec. 1999.

[54] J. Gao, G. C. Walsh, D. Bigio, R. M. Briber, and M. D. Wetzel, “Mean residence time analysis for twin screw extruders,” *Polymer Engineering & Science*, vol. 40, no. 1, pp. 227-237, Jan. 2000.

[55] X. Zhang, L. Feng, S. Hoppe, and G. Hu, “Local residence time, residence revolution, and residence volume distributions in twin-screw extruders,” *Polymer Engineering & Science*, vol. 48, no. 1, pp. 19-28, Jan. 2008.

[56] “LyondellBasell Alathon H6018 High Density Polyethylene (Extrusion Grade).” .

[57] “CAMES Sensors Report.” Internal Report .

[58] “CAMES Technology Report.” Internal Report .

[59] “DuPont Ti-Pure R-105 Titanium Dioxide.” 2007.

[60] A. C. Cohen, “Maximum Likelihood Estimation in the Weibull Distribution Based on Complete and on Censored Samples,” *Technometrics*, vol. 7, no. 4, pp. 579-588, Nov. 1965.

[61] C. D. Denson and B. K. Hwang Jr., “The influence of the axial pressure gradient on flow rate for Newtonian liquids in a self wiping, co-rotating twin screw extruder,” *Polymer Engineering & Science*, vol. 20, no. 14, pp. 965-971, Sep. 1980.

[62] M. L. Booy, “Geometry of fully wiped twin-screw equipment,” *Polymer Engineering & Science*, vol. 18, no. 12, pp. 973-984, Sep. 1978.

[63] D. Bigio, R. Briber, J. Cheng, and Y. Xie, “Model Development to Caclulate the Critical Stress for CAMES.” Internal Report, 1996.